



Cite this: *Chem. Soc. Rev.*, 2015,  
44, 1526

Received 26th May 2014

DOI: 10.1039/c4cs00186a

[www.rsc.org/csr](http://www.rsc.org/csr)

## Surface modification and characterization of photon-upconverting nanoparticles for bioanalytical applications

Andreas Sedlmeier and Hans H. Gorris\*

Photon-upconverting nanoparticles (UCNPs) can be excited by near-infrared light and emit visible light (anti-Stokes emission) which prevents autofluorescence and light scattering of biological samples. The potential for background-free imaging has attracted wide interest in UCNPs in recent years. Small and homogeneous lanthanide-doped UCNPs that display high upconversion efficiency have typically been synthesized in organic solvents. Bioanalytical applications, however, require a subsequent phase transfer to aqueous solutions. Hence, the surface properties of UCNPs must be well designed and characterized to grant both a stable aqueous colloidal dispersion and the ability to conjugate biomolecules and other ligands on the nanoparticle surface. In this review, we introduce various routes for the surface modification of UCNPs and critically discuss their advantages and disadvantages. The last part covers various analytical methods that enable a thorough examination of the progress and success of the surface functionalization.

### 1. Introduction

Luminescent labels and probes are indispensable tools in bioanalysis. Organic fluorophores, however, are prone to photo-bleaching and quantum dots contain toxic heavy metals. Furthermore, almost all luminescent labels follow a conventional downconversion mode: the excitation with UV or visible light of

higher energy results in the emission of lower energy photons. High energy light, however, can lead to photodamage and auto-fluorescence of biomolecules and thus a low signal-to-noise ratio. By contrast, the emission of upconverting nanoparticles (UCNPs) is based on an anti-Stokes process, *i.e.* on the conversion of low-energy photons into photons of higher energy. While other anti-Stokes processes such as second harmonic generation, two photon excitation, or anti-Stokes Raman scattering include at least one virtual energy state, photon-upconversion is based on real and long-lived energy states in the inner *f*-orbitals of certain lanthanide ions.<sup>1</sup> Therefore, photon-upconversion can

*Institute of Analytical Chemistry, Chemo- und Biosensors, University of Regensburg, Universitätsstr. 31, 93040 Regensburg, Germany. E-mail: hans-heiner.gorris@ur.de; Fax: +49-941-943-4064; Tel: +49-941-943-4015*



Andreas Sedlmeier studied chemistry and graduated with a MSc from the University of Regensburg in 2011. He is currently pursuing his PhD at the Institute of Analytical Chemistry, Chemo- and Biosensors under the supervision of Dr Hans-Heiner Gorris. His research topic is the surface modification of upconverting nanoparticles for bioanalytical applications.

Andreas Sedlmeier



Hans H. Gorris

Hans-Heiner Gorris studied biology at the University of Münster, Germany, and the University of York, UK. He received his PhD with Dr Andreas Frey from the University of Lübeck in 2005. After working on single enzyme molecule kinetics in optical-fiber bundle arrays with Prof. David Walt at Tufts University, USA he joined the Faculty of Chemistry and Pharmacy at the University of Regensburg (2009) and established his research group "Bioanalysis on the Micro- and Nanometer scale". His research is focused on ultrasensitive detection methods for bioanalysis.



be generated by using low energy excitation<sup>2</sup> and yields a higher quantum efficiency<sup>1</sup> compared to other anti-Stokes processes. Photon-upconversion is a non-linear optical process and the quantum yield depends on the excitation laser power density,<sup>3</sup> but also on the material and size of the nanoparticles and their surface structure.<sup>4,5</sup> Quantum yields in the range of  $10^{-5}$  to 1%<sup>3-8</sup> have been measured. Photon-upconverting materials consist of a crystalline host matrix doped with certain lanthanide ions, which determine the excitation and emission wavelengths. For example, ytterbium ( $\text{Yb}^{3+}$ ) can be used as an efficient sensitizer ion that absorbs near-infrared light of 980 nm and transfers the energy to activator ions such as erbium ( $\text{Er}^{3+}$ ) or thulium ( $\text{Tm}^{3+}$ ). Depending on the type of activator ions, distinct emission bands can be obtained as shown in Fig. 1.

Using NIR light for excitation avoids photodamage, background fluorescence in biological systems and enables a higher penetration depth into biological tissue. Compared to the broad emission bands of most fluorophores, UCNPs display several narrow emission bands that can be adjusted, *e.g.* by the lanthanide dopant composition and enable new options for multiplexed encoding.<sup>9</sup> All these unique photophysical properties of UCNPs provide many advantages for biomedical as well as diagnostic applications such as cell imaging,<sup>10-27</sup> cell targeting,<sup>12,15,18,23,25,26</sup> *in vivo* imaging,<sup>6,11,13,25,26</sup> LRET-based assays,<sup>28-32</sup> bioassays,<sup>33,34</sup> or biosensors.<sup>35-39</sup>

Many different routes for the synthesis of UCNPs have been described and they are covered by many excellent reviews.<sup>8,40-44</sup> For example coprecipitation,<sup>36,45,46</sup> thermal decomposition,<sup>16,47-50</sup> solvothermal synthesis,<sup>51-54</sup> and high-temperature coprecipitation<sup>55</sup>

are typically carried out in organic solvents. Some synthetic routes such as hydrothermal synthesis,<sup>56-60</sup> and sol-gel processes<sup>61,62</sup> can also be performed in aqueous media. Chemical vapor deposition is a less common route that does not belong to either category.<sup>63</sup> Highly monodisperse UCNPs of uniform size and shape are mainly synthesized in high-boiling organic solvents. For example, oleic acid serves as a solvent and also controls the crystal growth by coordinating to the nanoparticle surface and forms a hydrophobic layer of surface ligands. Usually, a subsequent surface modification is necessary to yield a hydrophilic surface composition before these UCNPs can be employed in bioanalytical applications (Fig. 2).

In special cases, an additional surface modification step can be circumvented if the hydrophobic ligands are replaced by hydrophilic ligands as the growth-controlling reagent. Surface passivation by coating with a shell of (un)doped host material is commonly used to enhance the overall upconversion efficiency but does not allow for a direct functionalization. In contrast, the growth of a silica shell creates an easily accessible platform for introducing various functional groups *via* silanization. Furthermore, the binding of gold or silver nanoparticles on the UCNPs surface can enhance the upconversion emission intensity by localized plasmon resonance and also provides an anchoring site for thiol-containing ligands. Other surface modifications rely on non-covalent intermolecular interactions of new ligands with the UCNPs surface. For example, the hydrophobic surface ligands can be replaced by hydrophilic ligands during a ligand exchange reaction. Alternatively, the hydrophobic surface ligands can be partially oxidized to obtain a hydrophilic surface functionalization. A subsequent modification step is commonly performed for binding biomolecules to the surface of UCNPs.

As every surface functionalization step can change several features of UCNPs, it is not only important to confirm the successful surface functionalization but also that the modification has no negative impact on the upconversion efficiency or the colloidal stability in aqueous dispersions. Depending on the type of functionalization, several methods can be used for analyzing the functionalization, changes in the size and shape of UCNPs and their dispersibility in aqueous systems.

While there are numerous reviews on the synthesis of UCNPs, only a few specifically cover the surface functionalization of UCNPs.<sup>40,41,43,44</sup> This review provides a comprehensive account of the most important methods for the surface modification and characterization of UCNPs. It critically discusses which advantages and disadvantages are conferred by each type of modification regarding high upconversion efficiency, the formation of long-term stable colloids, and an efficient functionalization with biomolecules. A careful design and optimization of these aspects is essential before UCNPs can be used for bioanalytical applications.

## 2. Increasing the luminescence of UCNPs by a core–shell design

The emission intensity of an upconverting material depends on its dimension. Decreasing the size from the bulk over

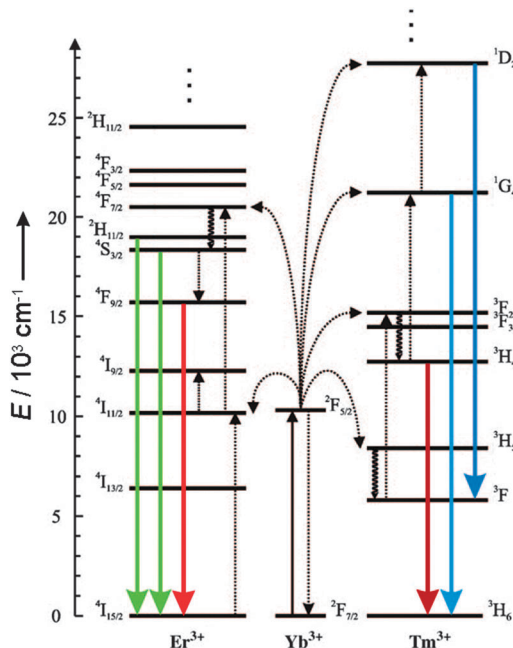
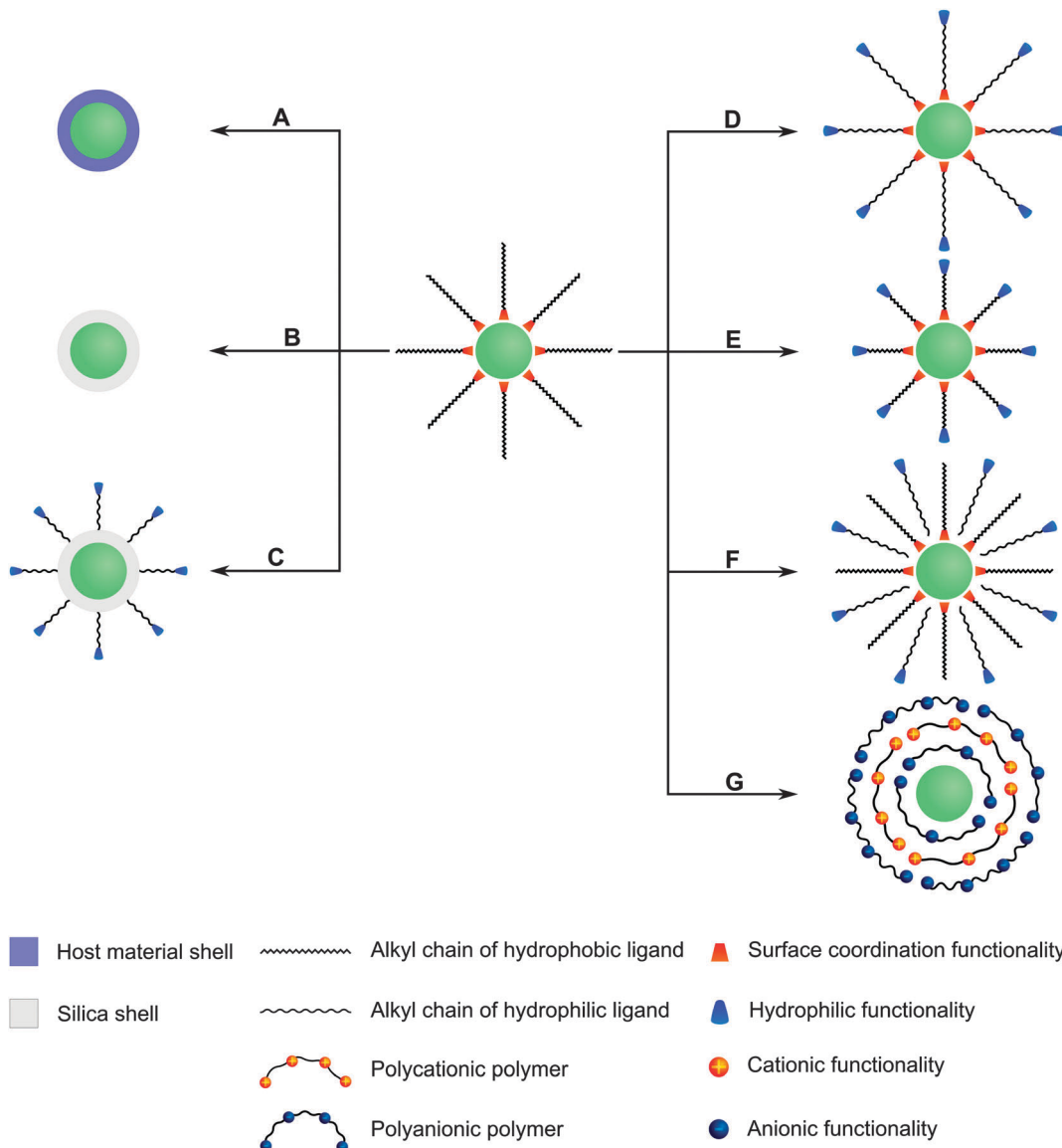


Fig. 1 Energy-level diagram of anti-Stokes processes in UCNPs ( $\text{NaYF}_4$ :  $\text{Yb},\text{Er}/\text{Tm}$ ). The sensitizer ion  $\text{Yb}^{3+}$  absorbs NIR light, and the activator ions  $\text{Er}^{3+}$  or  $\text{Tm}^{3+}$  emit visible or NIR light. Sensitizer and activator ions are embedded in a hexagonal nanocrystal of  $\text{NaYF}_4$ . Full arrows: radiative transitions, dotted arrows: non-radiative energy transfer, curled arrows: multiphonon relaxation. Adapted from ref. 2 with permission.





**Fig. 2** Common routes for the surface modification of oleic acid-coated UCNPs: (A) Surface passivation enhances the upconversion efficiency. (B) A silica shell is chemically inert and confers water dispersibility. (C) Functional groups can be bound covalently to the silica shell by silanization. Oleic acid can be replaced by a ligand exchange reaction (D) or oxidized (E) to yield a hydrophilic surface functionalization. (F) Ligand interactions are exploited to insert further layers of ligands on the surface of UCNPs. (G) Polyanions and polycations can be deposited on the UCNPs surface by the layer-by-layer (LbL) technique.

microparticle to nanoparticle dimensions leads to an increase of the surface-to-volume ratio of the material and thus surface effects become more pronounced. For example, energy migration from the center of the nanocrystal to the surface<sup>64,65</sup> *via* neighboring lanthanide ions reduces the emission intensity. In particular, the sensitizer  $\text{Yb}^{3+}$  is involved in the energy transfer due to its high doping concentration in many upconversion materials.<sup>5,66</sup> Additionally, dopant ions near the nanoparticle surface result in point defects of the crystal structure of the host material and may further decrease the luminescence intensity.<sup>67,68</sup> Molecules close to the UCNPs surface can also reduce the intensity, since the vibrational states of chemical bonds like O–H, C–H or N–H match the phonon states of the host material resulting in non-radiative

relaxation of the excited lanthanide ions.<sup>66,69</sup> This quenching effect can originate from both organic and aqueous solvents or from surface ligands.<sup>67</sup> Oleic acid, which is frequently used for surface coordination during synthesis, shows high vibrational states that cause non-radiative transitions.<sup>64,70</sup> The quenching effect of water is even stronger compared to organic ligands due to the high vibrational states of hydroxyl groups.<sup>71,72</sup> This phenomenon is detrimental for bioanalytical applications of core-only particles. These quenching effects are much lower in larger UCNPs with a lower surface-to-volume ratio. Many bioanalytical applications, however, require small nanoparticles such that the optimal size is a compromise of brightness and bio-applicability.



The design of core–shell structures can minimize the surface quenching effects mentioned above and thus strongly enhances the luminescence intensity.<sup>5,73</sup> Growing a shell on the surface of the nanoparticles both increases the distance between lanthanide ions and surface ligands of high vibrational states and reduces the non-radiative energy transfer of the dopants from the core to the nanoparticle surface. Typically, UCNPs showing hydrophobic surface ligands such as oleic acid<sup>64,72,74–77</sup> after synthesis are used for the design of core–shell structures.

Most shells that passivate the surface of UCNPs against quenching effects consist of the same host material as the core but without dopants. However, other crystalline materials are also applicable as long as (A) the crystal lattice has a low phonon energy to avoid non-radiative processes, (B) the shell material is chemically stable, and (C) the lattice of core and shell have similar crystal structures to minimize non-radiative processes due to crystal defects.<sup>78,79</sup> Some material combinations for the design of core–shell nanoparticles are summarized in Table 1.

Table 1 Material combinations for active core–passive shell UCNPs

Core	Shell		
Host material	Dopant(s)	Material	Ref.
NaGdF <sub>4</sub>	Er <sup>3+</sup>	NaGdF <sub>4</sub>	73
NaGdF <sub>4</sub>	Yb <sup>3+</sup> , Tm <sup>3+</sup>	NaYF <sub>4</sub>	75
NaGdF <sub>4</sub>	Yb <sup>3+</sup> , Tm <sup>3+</sup>	NaGdF <sub>4</sub>	72
NaGdF <sub>4</sub>	Yb <sup>3+</sup> , Er <sup>3+</sup>	NaGdF <sub>4</sub>	74
NaYF <sub>4</sub>	Yb <sup>3+</sup> , Er <sup>3+</sup>	NaGdF <sub>4</sub>	77
NaYF <sub>4</sub>	Yb <sup>3+</sup> , Er <sup>3+</sup>	NaYF <sub>4</sub>	5, 10, 64–66, 70, 71, 80
NaYF <sub>4</sub>	Yb <sup>3+</sup> , Tm <sup>3+</sup>	NaYF <sub>4</sub>	10, 37, 70, 75, 80, 81
NaYbF <sub>4</sub>	Tm <sup>3+</sup>	CaF <sub>2</sub>	82
BaF <sub>2</sub>	Yb <sup>3+</sup> , Tm <sup>3+</sup>	SrF <sub>2</sub>	68
BaF <sub>2</sub>	Yb <sup>3+</sup> , Tm <sup>3+</sup> , Nd <sup>3+</sup>	SrF <sub>2</sub>	
KYF <sub>4</sub>	Yb <sup>3+</sup> , Er <sup>3+</sup>	KYF <sub>4</sub>	83
BaGdF <sub>5</sub>	Yb <sup>3+</sup> , Er <sup>3+</sup>	BaGdF <sub>5</sub>	76

Active core–passive shell UCNPs generally show an enhanced emission intensity compared to the respective core-only nanoparticles (Fig. 3A). A comparison between core–shell and core-only UCNPs of the same size verifies that the intensity increase can be attributed to the growth of a passive shell on the nanoparticle surface and is not just a result of the larger particle diameter. It is also possible that core–shell UCNPs smaller than the core-only nanoparticles have an even higher emission intensity (Fig. 3B).<sup>5</sup> The luminescence enhancement also depends on the lanthanide dopants. Using the same host material of NaYF<sub>4</sub> and chloroform as the dispersant, doping with Yb<sup>3+</sup> and Er<sup>3+</sup> leads to a 7.4-fold higher emission intensity in core–shell UCNPs compared to core-only UCNPs.<sup>70</sup> Doping with Yb<sup>3+</sup> and Tm<sup>3+</sup> increases the luminescence by a factor of 29.6. The emission intensity of NaYF<sub>4</sub>:Yb<sup>3+</sup>,Er<sup>3+</sup>@NaYF<sub>4</sub> dispersed in hexane is 50 times higher compared to respective core-only nanoparticles.<sup>5</sup> The increase of the overall emission intensity and thus the UCNPs brightness is of great advantage for all applications, because UCNPs can then be excited under milder conditions.

While the passivating shells described so far are designed to prevent surface quenching effects and are not directly involved in the upconversion process, the host material of the shell can also be doped with sensitizers and/or activators resulting in an active shell. This can further enhance the emission intensity (doping with sensitizers),<sup>74,76</sup> enable multicolor tuning of the emission (doping with activators),<sup>73</sup> or lead both to an increase in the emission intensity and an introduction of new emission wavelengths (doping with sensitizers and activators).<sup>84</sup> The design of differently doped shell architectures provides a flexible way for generating additional emission wavelengths.<sup>75</sup> Examples of active core–passive shell UCNPs are shown in Table 2.

For example, if the host material of the shell is doped with the sensitizer Yb<sup>3+</sup> but without activators, the upconversion efficiency is increased compared to a passive shell consisting only of the host material.<sup>74,76</sup> It is well known that the emission intensity of UCNPs depends on the sensitizer concentration.<sup>86,87</sup> The dopant concentration of the sensitizer, however, is ultimately

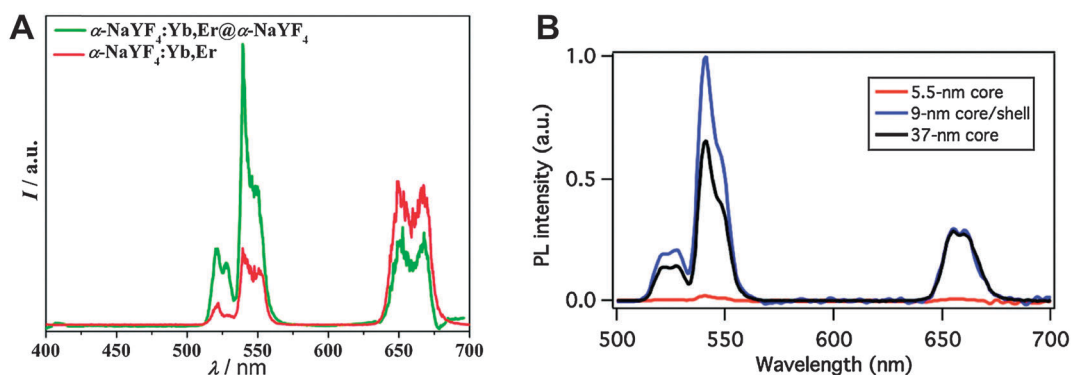


Fig. 3 Influence of a core–shell design on the upconversion luminescence of NaYF<sub>4</sub>:Yb,Er nanocrystals under 980 nm excitation. (A) The intensity of the green emission of  $\alpha$ -NaYF<sub>4</sub>:Yb<sup>3+</sup>,Er<sup>3+</sup>@ $\alpha$ -NaYF<sub>4</sub> core–shell nanoparticles increases by a factor of two compared to core-only  $\alpha$ -NaYF<sub>4</sub>:Yb<sup>3+</sup>,Er<sup>3+</sup>. (B) A core–shell design of  $\beta$ -NaYF<sub>4</sub>:Yb<sup>3+</sup>,Er<sup>3+</sup>@NaYF<sub>4</sub> leads to an even stronger luminescence enhancement compared to core-only  $\beta$ -NaYF<sub>4</sub>:Yb<sup>3+</sup>,Er<sup>3+</sup>. Adapted with permission from ref. 65 and 5. Copyright © 2007 and Copyright © 2012, American Chemical Society.



Table 2 Material combinations for active core–active shell UCNPs

Core	1st shell		2nd shell		Ref.	
Host material	Dopant(s)	Host material	Dopant(s)	Host material	Dopant(s)	
NaGdF <sub>4</sub>	Er <sup>3+</sup>	NaGdF <sub>4</sub>	Ho <sup>3+</sup>	—	—	73
NaGdF <sub>4</sub>	Er <sup>3+</sup>	NaGdF <sub>4</sub>	Ho <sup>3+</sup>	NaGdF <sub>4</sub>	—	—
NaGdF <sub>4</sub>	Yb <sup>3+</sup> , Tm <sup>3+</sup>	NaGdF <sub>4</sub>	Tb <sup>3+</sup>	—	—	75
NaGdF <sub>4</sub>	Yb <sup>3+</sup> , Tm <sup>3+</sup>	NaGdF <sub>4</sub>	Eu <sup>3+</sup>	—	—	—
NaGdF <sub>4</sub>	Yb <sup>3+</sup> , Tm <sup>3+</sup>	NaGdF <sub>4</sub>	Dy <sup>3+</sup>	—	—	—
NaGdF <sub>4</sub>	Yb <sup>3+</sup> , Tm <sup>3+</sup>	NaGdF <sub>4</sub>	Sm <sup>3+</sup>	—	—	—
NaGdF <sub>4</sub>	Yb <sup>3+</sup> , Tm <sup>3+</sup> , Y <sup>3+</sup>	NaGdF <sub>4</sub>	Tb <sup>3+</sup>	—	—	—
NaGdF <sub>4</sub>	Yb <sup>3+</sup> , Tm <sup>3+</sup>	NaGdF <sub>4</sub>	Tb <sup>3+</sup>	NaGdF <sub>4</sub>	—	—
NaGdF <sub>4</sub>	Yb <sup>3+</sup> , Er <sup>3+</sup>	NaGdF <sub>4</sub>	Yb <sup>3+</sup>	—	—	74
NaYF <sub>4</sub>	Yb <sup>3+</sup> , Er <sup>3+</sup>	NaYF <sub>4</sub>	Gd <sup>3+</sup>	—	—	77
NaYF <sub>4</sub>	Yb <sup>3+</sup> , Er <sup>3+</sup>	NaGdF <sub>4</sub>	Y <sup>3+</sup>	—	—	—
NaYF <sub>4</sub>	Yb <sup>3+</sup> , Er <sup>3+</sup>	NaYF <sub>4</sub>	Yb <sup>3+</sup> , Tm <sup>3+</sup>	—	—	85
NaYF <sub>4</sub>	Yb <sup>3+</sup> , Tm <sup>3+</sup>	NaYF <sub>4</sub>	Yb <sup>3+</sup> , Er <sup>3+</sup>	—	—	84, 85
NaYF <sub>4</sub>	Yb <sup>3+</sup> , Tm <sup>3+</sup>	NaYF <sub>4</sub>	Yb <sup>3+</sup> , Er <sup>3+</sup>	NaYF <sub>4</sub>	Yb <sup>3+</sup> , Tm <sup>3+</sup>	84
BaF <sub>2</sub>	Yb <sup>3+</sup> , Tm <sup>3+</sup>	SrF <sub>2</sub>	Nd <sup>3+</sup>	—	—	68
BaF <sub>2</sub>	Yb <sup>3+</sup> , Tm <sup>3+</sup>	SrF <sub>2</sub>	Gd <sup>3+</sup>	—	—	—
BaF <sub>2</sub>	Yb <sup>3+</sup> , Tm <sup>3+</sup>	SrF <sub>2</sub>	Nd <sup>3+</sup> , Gd <sup>3+</sup>	—	—	—
BaGdF <sub>5</sub>	Yb <sup>3+</sup> , Er <sup>3+</sup>	BaGdF <sub>5</sub>	Yb <sup>3+</sup>	—	—	76
BaGdF <sub>5</sub>	Yb <sup>3+</sup> , Er <sup>3+</sup>	BaGdF <sub>5</sub>	Yb <sup>3+</sup>	BaGdF <sub>5</sub>	Yb <sup>3+</sup>	—

limited by cross relaxation. The distribution of the sensitizer ions in both the core and the shell circumvents this concentration limitation and leads to an enhanced upconversion efficiency.<sup>74</sup>

The absorption maximum of Yb<sup>3+</sup> at 980 nm largely overlaps with the absorption band of water molecules, which attenuate the excitation light while passing through biological materials and may lead to overheating of cells or tissues.<sup>18,88,89</sup> A 915 nm laser was shown to be efficient for exciting Yb<sup>3+</sup>-doped UCNPs and avoiding heating effects since the absorption of water is lower at this wavelength.<sup>90</sup> When neodymium (Nd<sup>3+</sup>) was used as a sensitizer and Yb<sup>3+</sup> as an energy mediator, the excitation wavelength could be shifted even further from 980 nm to 800 nm resulting in a high upconversion luminescence without heating effects due to low absorption of water at this wavelength (Fig. 4).<sup>89</sup> For an optimal energy transfer, both core and shell were doped with Nd<sup>3+</sup> to avoid the concentration limit where cross relaxation becomes dominant. But only the core was doped with Yb<sup>3+</sup> and activator ions to avoid surface quenching effects.<sup>88</sup>

For some bioanalytical applications such as multiplexing, it is necessary to yield several bright emission bands that can be well separated.<sup>52,91,92</sup> Doping of core-only or active core–passive shell UCNPs with more than one activator in the core, however, leads to enhanced cross relaxation between these emitting lanthanide ions and thus to a strongly decreasing upconversion efficiency.<sup>73,85</sup> The spatial separation of the activator ions avoids this detrimental effect (Fig. 5).<sup>84</sup> The separation also enables a nearly selective excitation of one type of activator by adjusting the power density of the excitation source.<sup>85</sup> The UV and blue emission of Tm<sup>3+</sup> require the absorption of 4 or 5 low-energy photons, while only 2 photons are necessary to induce the green and red emission of Er<sup>3+</sup>. Therefore, higher excitation power densities can be employed

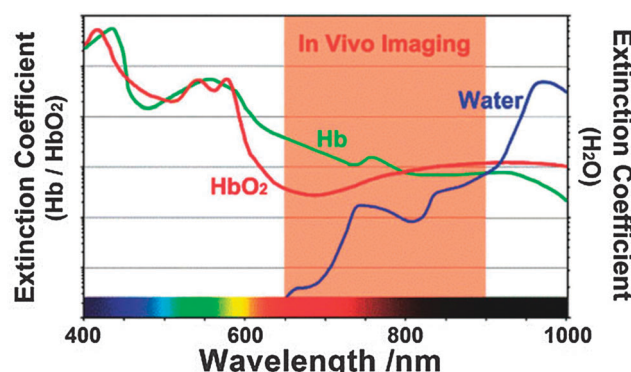


Fig. 4 Optimal spectral range for tissue imaging. The absorption of water is 20-fold lower at 800 nm compared to 980 nm. Light absorption of hemoglobin (Hb) and oxyhemoglobin (HbO<sub>2</sub>) can be avoided by using long-wavelength light. Reprinted with permission from ref. 89 Copyright © 2013, Wiley.

to selectively increase the UV and blue luminescence relative to the green and red emission.

The emission spectra of UCNPs can be tuned by various combinations of lanthanide ions. The combination of downconversion and upconversion in a single UCNPs enables spectral tuning in the near infrared range but typically requires two excitation wavelengths. For example, Tm<sup>3+</sup> shows emission at 802 nm under excitation at 975 nm, while Nd<sup>3+</sup> is excited at 796 nm and emits 890 nm and 1054 nm light.<sup>68</sup> In contrast, energy migration *via* a gadolinium sublattice in active-core–active-shell UCNPs opens the way for color tuning over the whole visible range with only a single-wavelength excitation.<sup>75</sup> In these upconversion systems also the downconversion luminescence of the lanthanides terbium, europium, dysprosium, and samarium can be generated under 980 nm irradiation.



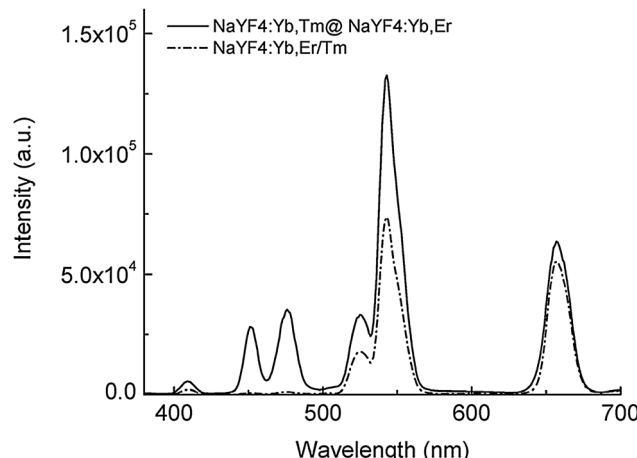


Fig. 5 Luminescence spectra of active-core-active-shell  $\text{NaYF}_4$  UCNPs (emission bands of  $\text{Tm}^{3+}$ : 409 nm, 450 nm and 475 nm; emission bands of  $\text{Er}^{3+}$ : 520 nm, 541 nm and 653 nm). The spatial separation of the two activators in  $\text{NaYF}_4:\text{Yb,Tm}@\text{NaYF}_4:\text{Yb,Er}$  avoids quenching of the activators compared to co-doped  $\text{NaYF}_4:\text{Yb,Er/Tm}$  UCNPs. Reprinted with permission from ref. 84. Copyright © 2008, American Chemical Society.

### 3. Generating a hydrophilic surface on UCNPs

Since most core and core-shell UCNPs are covered by hydrophobic ligands after synthesis,<sup>17,22,47,48,64</sup> a surface modification is required to obtain UCNPs that form stable aqueous dispersions. Many functional groups are amenable to improving the dispersibility of UCNPs in water or aqueous buffers such as hydroxyl groups, primary or secondary amines, maleimides, epoxides, carboxylic acids, or phosphonates. Each functionality improves the hydrophilicity to a different extent and especially ionic groups exert a particularly strong influence on the dispersibility. Moreover, the nanoparticle dispersions must be long-term stable in aqueous media to avoid aggregation and precipitation during storage or applications. In addition to the introduction of a hydrophilic surface, the surface ligands can also prevent aggregation by exploiting steric<sup>93–98</sup> or electrostatic<sup>70,95</sup> repulsion. Furthermore, most bioanalytical applications require a modification of the UCNPs surface by antibodies,<sup>15,16,23,31,45</sup> oligonucleotides,<sup>15,21,28–30,35</sup> proteins,<sup>16,26,39</sup> or lectins/carbohydrates<sup>19,32,34</sup> to specifically bind cellular target structures or other analytes. These modification steps should be feasible under mild reaction conditions that do not alter the structure or functionality of the biomolecule and do not lead to nanoparticle aggregation.

The transfer from an organic solvent to water or aqueous buffers typically leads to quenching of the upconversion luminescence because the surface of the UCNPs is only insufficiently shielded from the aqueous medium.<sup>10</sup> As a consequence of the higher phonon energy of water compared to organic solvents, non-radiative transitions of the UCNPs are enhanced. The degree of quenching can differ depending on the emission wavelength and the lanthanide dopant composition.<sup>32,99,100</sup> Holmium-doped UCNPs, for example, show a shift from green

to yellow due to a higher quenching susceptibility of the green emission compared to the red emission. Also the hydrophilic ligand employed influences the quenching because the ability to shield the activator ions from water molecules is more distinct for larger and bulkier ligands such as polyacrylic acid than for smaller and/or linear ligands such as azelaic acid (Fig. 6).<sup>99</sup> This luminescence decrease is one of the major challenges for the application of UCNPs in bioanalysis.

#### 3.1 Synthetic routes resulting in a hydrophilic surface

While most routes for the synthesis of UCNPs result in a hydrophobic surface, combinations of hydrophobic and hydrophilic ligands can also be used in coprecipitation,<sup>45,101</sup> hydrothermal<sup>25,38,102,103</sup> or solvothermal<sup>92</sup> techniques. Similar to hydrophobic ligands, the hydrophilic ligands coordinate either *via* carboxylic groups or *via* amines (including primary, secondary, and tertiary amines) to the lanthanide ions and the UCNPs surface. They also serve to control the growth of UCNPs during the synthesis and thus determine their size and shape. Such UCNPs are readily dispersible in aqueous media and in some cases additionally in organic solvents.

**3.1.1 Acidic ligands.** When citrate serves as the growth-controlling agent during hydrothermal synthesis, the resulting UCNPs are dispersible in aqueous solutions.<sup>104</sup> Depending on the ratio of citrate to lanthanide ions added during the synthesis, the UCNPs can be spherical nanoparticles, nanorods or submicroplates. However, the presence of citrate on the UCNPs surface after synthesis leads to quenching of the upconversion emission due to the high-energy vibrational modes of the hydroxyl groups.<sup>104</sup> Annealing of the UCNPs at elevated temperatures can avoid these detrimental effects because citrate and residual water is removed from the surface of the UCNPs.<sup>7,104</sup> Without citrate coordinated to the surface, however, the UCNPs tend to aggregate in aqueous dispersions.

6-Aminohexanoic acid can be used in combination with hydrophobic capping agents like oleic acid<sup>102</sup> or bis(2-ethylhexyl)sulfosuccinate (AOT)<sup>25</sup> to control the particle growth and render the particles hydrophilic. The dispersibility in aqueous systems can be tuned by adjusting the ratio between 6-aminohexanoic acid and the hydrophobic compound. The nanoparticles form stable dispersions in polar as well as non-polar solvents if both surface ligands are present in equal amounts on the nanoparticle surface. Additionally, the particle shape is influenced by the ratio of hydrophobic–hydrophilic surface components. Pure oleic acid leads to hexagonal, a ratio of 1:1 to cylinder-like, and pure 6-aminohexanoic acid to irregularly shaped UCNPs.<sup>102</sup> The amine group of 6-aminohexanoic acid also allows a direct functionalization with biomolecules *via* established methods.

Chelating agents are also capable of controlling the nanoparticle growth. One of the best known chelators is the hexadentate ethylenediaminetetraacetic acid (EDTA).<sup>21,101,103,105</sup> The chelation constant of EDTA is high for all rare earth ions and, hence, the size of the synthesized nanoparticles can be tuned by the ratio of EDTA to trivalent rare earth ions.<sup>106,107</sup> EDTA stabilizes the lanthanide ions in solution by chelation and coordinates to the nanoparticle surface.

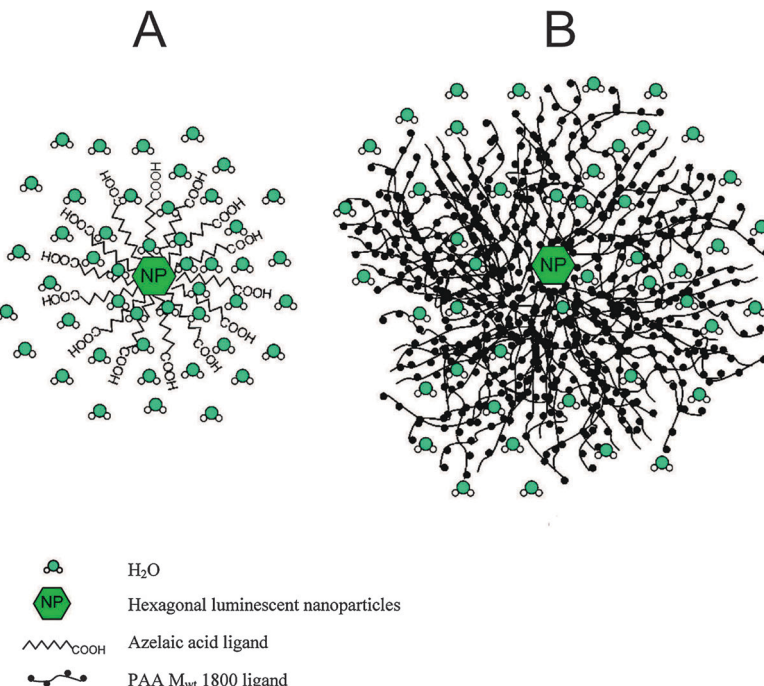


**Fig. 6** Shielding effect from water molecules of (A) azelaic acid (small/linear ligand) and (B) polyacrylic acid ( $M_w = 1800$ , large/bulky) resulting in differing quenching factors of the upconversion luminescence by water. Reprinted with permission from ref. 99. Copyright © 2009, American Chemical Society.

While these UCNP are highly dispersible in DMSO<sup>57</sup> and ethanol,<sup>108</sup> their colloidal stability in water is strongly pH-dependent because deprotonated EDTA<sup>4-</sup>, which has the highest chelating capacity, is only present under alkaline conditions.<sup>46</sup> In physiological buffers,<sup>109</sup> EDTA is partially protonated and desorbs from the UCNP surface which leads to aggregation of the UCNP. A heat treatment to enhance the upconversion efficiency by a phase change of the host material can result in pyrolysis of the surface ligands and thus in a decreased dispersibility.<sup>91</sup> The lack of functional groups necessary for binding biomolecules is an additional drawback of EDTA-modified nanoparticles.<sup>109</sup>

Similarly, ethylene-bis(oxyethylene) tetraacetic acid (EGTA)<sup>29</sup> or diethylenetriamine pentaacetic acid (DTPA)<sup>35</sup> are suitable to control the particle growth and the surface coordination. UCNP prepared in presence of DTPA display free carboxylic groups on the surface, are well dispersible in aqueous solutions and enable the direct surface modification with biomolecules.<sup>110</sup>

**3.1.2 Polymers.** Polymers with carboxylic or amine/imine groups have an even greater chelating potential than EDTA since each monomer functionality can coordinate lanthanide ions. During a solvothermal synthesis, polyacrylic acid (PAA) typically with an average molecular weight ( $M_w$ ) of 1800<sup>38,111</sup> can control the particle growth by decreasing the reactivity of the rare earth ions with fluoride and leads to nanoparticles that are small and uniform in shape.<sup>111</sup> The carboxylic groups of PAA also coordinate to the lanthanide ions on the UCNP surface resulting in a high dispersibility of the UCNP in water.<sup>38,60</sup> However, these carboxylic groups possess high vibrational states that decrease the upconversion luminescence intensity.<sup>111</sup> PAA is

not cytotoxic and the non-coordinated carboxylic groups of PAA are available for subsequent bioconjugation.<sup>111</sup>

The synthesis in presence of the amphiphilic polymer polyvinylpyrrolidone (PVP, average  $M_w = 40\,000$ )<sup>107</sup> results in PVP-coated nanoparticles with a size down to 30 nm<sup>100</sup> that are well dispersible in water and in many organic solvents. The stability of UCNP dispersions in nonpolar solvents such as hexane, however, is lower compared to polar solvents. Aggregation of UCNP can be prevented by using a mixture of polar and nonpolar solvents, *e.g.* hexane and ethanol.<sup>107</sup> Similar to the carboxylic groups of PAA, the pyrrolidone moieties of PVP control the particle growth by coordinating to rare earth ions during synthesis. This chelation occurs also on the nanoparticle surface after synthesis. Since the functionalities of PVP are not easily accessible for binding biomolecules, a subsequent surface modification is crucial before these nanoparticles can be used for bioanalytical applications.<sup>11</sup>

The polymer polyethylenimine (PEI) can also be added during the synthesis to obtain hydrophilic UCNP. This branched macromolecule with its primary, secondary and tertiary amino groups can easily coordinate to the lanthanide ions and thus influence the nanoparticle growth.<sup>11,92,112</sup> However, the nanoparticle size does not only depend on the presence of PEI during the synthesis but also on the molecular weight of the polymer, typically 25 000<sup>92,109</sup> or 10 000.<sup>112,113</sup> High molecular weight PEI ( $M_w = 25\,000$ ) leads to spherical and uniform nanoparticles whereas UCNP prepared in presence of low molecular weight PEI ( $M_w = 800$ )<sup>109</sup> result in an irregular shape and varying sizes. The high number of chelating groups in high molecular weight



PEI coordinates more efficiently to the nanoparticle surface and thus exerts a stronger influence on the particle size and form during synthesis.<sup>109</sup> The high cytotoxicity of PEI that affects among other things the adhesion and proliferation of cells<sup>114</sup> is avoided if the polymer is coordinated to the nanoparticle surface, as shown for mammalian cells.<sup>109</sup> The attachment of PEI on the surface also results in good water dispersibility due to the positively charged amines.<sup>39,109</sup> Additionally they form stable dispersions in polar organic solvents like dimethylformamide (DMF) or dimethyl sulfoxide (DMSO).<sup>92</sup> The secondary amines of PEI provide reaction sites for subsequent functionalization with biomolecules.<sup>109,113</sup>

### 3.2 Ligand exchange

The use of hydrophilic surface ligands during synthesis is an easy way to obtain UCNPs dispersible in water or polar solvents without the necessity of subsequent modifications. However, the synthesis of UCNPs in organic solvents employing only hydrophobic ligands to control the nanoparticle growth typically results in highly monodisperse UCNPs, improved long-term dispersibility, and a better control of the nanoparticle size and shape. There are several methods including ligand exchange, ligand modification, ligand interactions, and layer-by-layer deposition that enable a modification of the hydrophobic UCNPs surface to obtain nanoparticles dispersible in water or buffers.

The hydrophobic ligands bound to the UCNPs surface can be exchanged by more hydrophilic ligands to form stable aqueous dispersions and introduce functional groups for a subsequent functionalization with (bio)molecules. A complete exchange of the hydrophobic by a hydrophilic ligand can be ensured by elevated temperatures, an excess of the new ligand, and a suitable solvent.<sup>115</sup> The choice of solvent depends on the dynamic solvability of the hydrophobic and the new surface ligand. Also the number and type of coordination sites in both ligands influences the ligand exchange. For example, multidentate ligands are preferred over monodentate ligands and carboxylate groups are preferred compared to amines due to a higher coordination ability.<sup>115</sup> Applicable ligands include acids, mostly derivatives of a carboxylic acid or phosphoric acid, and polymers binding with several coordination sites to the nanoparticle surface. The ligand exchange can also be performed repeatedly. Alternatively the hydrophobic ligands can be removed from the surface without introducing new ligands. This technique

is based on pH changes and yields water dispersible UCNPs due to the positively charged nanoparticle surface.<sup>75,116</sup>

**3.2.1 Acidic ligands.** Acidic ligands typically consist of carboxylate or phosphonate groups that coordinate to the positively charged surface of UCNPs by electrostatic interactions and a second hydrophilic group that improves the dispersibility in aqueous media and enables subsequent modification steps. The length of the alkyl chain between the coordinating group and the second functionality determines the distance between the nanoparticle surface and the surrounding and thus the shielding efficiency of the nanoparticle surface from water by the ligand. Some representative examples are shown in Table 3.

UCNPs coated with citrate after ligand exchange are dispersible in water.<sup>24,117,118</sup> The ligand exchange has no effect on the size or morphology of the UCNPs<sup>118</sup> but the hydrodynamic diameter increases due to the new hydrophilic ligand and the resulting additional layer of water molecules on the nanoparticle surface.<sup>117</sup> Also the emission intensity is reduced after coating with citrate.<sup>24,120</sup> The cytotoxicity of such UCNPs tested by a MTT assay is relatively low, even for higher nanoparticle concentrations (up to 500 µg mL<sup>-1</sup>).<sup>117</sup>

Hexanedioic acid shows similar binding characteristics as citrate. Compared to shorter dicarboxylic acids, the length of the alkyl chain reduces the risk that both carboxylic groups bind back to the nanoparticle surface and also ensures a good dispersibility in water compared to longer dicarboxylic acids.<sup>115</sup> Typically, elevated temperatures and an excess of the new ligand are applied to ensure a complete exchange of oleic acid by hexanedioic acid. Since binding of both carboxylate groups of hexanedioic acid to the nanoparticle surface is still possible but less distinct than for smaller diacids, a large excess of the diacid added during the ligand exchange reaction can diminish these effects even further. Most optical properties of the UCNPs are nearly the same before and after the exchange, only the luminescence intensity ratio of the emission bands may change.<sup>115</sup>

A ligand exchange reaction does not have to replace all hydrophobic surface ligands with a hydrophilic compound but only a certain percentage. However, the newly introduced ligands need to have a minimal length in order to render their surface functionality accessible for subsequent modifications. For example, 1,10-decanedicarboxylic acid<sup>121</sup> only partially replaces the hydrophobic surface ligands in a ligand exchange and thus avoids aggregation due to crosslinking of two UCNPs by the two carboxylic groups on the opposite ends of the ligand.

Table 3 Ligand exchange reactions with acidic ligands

Compound	Coordinating functionality	Surface exposed functionality	Ref.
Citric acid	Carboxylic acid/hydroxyl group	Carboxylic acid	24, 117–120
Hexanedioic acid	Carboxylic acid	Carboxylic acid	115
1,10-Decanedicarboxylic acid	Carboxylic acid	Carboxylic acid	121
11-Mercaptoundecanoic acid	Carboxylic acid	Thiol	121
6-Aminohexanoic acid	Carboxylic acid	Amine	122
Thioglycolic acid	Thiol	Carboxylic acid	68, 123
3-Mercaptopropionic acid	Thiol	Carboxylic acid	16
1-Hydroxyethane-1,1-diphosphonic acid	Phosphonate	Phosphonate	69



The ratio of the diacid to the hydrophobic surface ligands has to be chosen carefully to obtain both functionalized and stable UCNPs.<sup>121</sup> Crosslinking can be further reduced by replacing one carboxylic acid of the diacid by a functional group of lower affinity to the UCNP surface such as a thiol. The use of 11-mercaptopundecanoic acid instead of 1,10-decanedicarboxylic acid results in a lower aggregation tendency and stable dispersions of smaller UCNPs.<sup>121</sup>

In contrast to 11-mercaptopundecanoic acid, thioglycolic acid and 3-mercaptopropionic acid bind *via* their thiols instead of the carboxylic group to the UCNP surface<sup>16,68,123</sup> as evidenced by the missing infrared absorption peak of the thiol group at 2600 cm<sup>-1</sup>.<sup>123</sup> The different binding mode does not affect the nanoparticle size<sup>16</sup> and yields hydrophilic nanoparticles that form highly stable aqueous dispersions.<sup>68,123</sup> It has been reported, however, that it is necessary to further functionalize such UCNPs with biomolecules before they are internalized efficiently by cells and are suitable for intracellular bioimaging under NIR excitation.<sup>16</sup>

The introduction of amine functionalities on the UCNP surface can be realized by a ligand exchange reaction with 6-aminohexanoic acid.<sup>122</sup> This new surface ligand decreases the luminescence intensity only marginally and results in stable aqueous dispersions for at least two days which is long enough for most bioimaging applications in cells or small animals. The combined ligand exchange of 6-aminohexanoic acid and folic acid extends the applicability of these UCNPs to targeted bioimaging of tumor cells.<sup>122</sup>

1-Hydroxyethane-1,1-diphosphonic acid coordinates only with one phosphonate group to the UCNP surface while the second group forms a hydrophilic surface.<sup>69</sup> Since 1-hydroxyethane-1,1-diphosphonic acid is soluble and hydrophobic UCNPs dispersible in *N*-(2-hydroxyethyl)ethylenediamine, it is not necessary to work with solvent mixtures. The phosphonate-modified UCNPs are well dispersible in water and aqueous buffers. They are also 45 times brighter compared to unmodified nanoparticles.<sup>69</sup>

**3.2.2 Linear polymers as multidentate ligands.** Compared to acidic ligands polymers can contain several functionalities to coordinate to the nanoparticle surface and to define the new surface composition. The multiple coordinating sites of polymers lead to a higher coating density of the UCNP surface area. Polymers can be synthesized over a wide range of molecular weights without losing their characteristic properties. Additionally, the polymers can be equipped with new properties by synthesizing block copolymers. Some polymers typically used for ligand exchange on UCNPs are shown in Table 4.

Polyacrylic acid is one of the most frequently used polymers in ligand exchange reactions.<sup>125,128</sup> This polydentate polymer attaches to the UCNP surface and the remaining uncoordinated carboxylic groups enable subsequent conjugation steps with biomolecules or other polymers.<sup>124</sup> PAA-modified nanoparticles form stable dispersions in water for several months due to a strong electrical repulsion of the negative surface charge provided by PAA.<sup>93,99,129</sup> Since PAA is a polydentate ligand, some aggregation may result from crosslinking of two UCNP surfaces with one polymer molecule.<sup>129</sup> The formation of a stable dispersion of the nanoparticles in buffer rather depends on the buffer type. The stability reduces to less than 24 h in PBS (pH = 7.4),<sup>99</sup> to 10 days for certain physiological buffers (pH = 7.2),<sup>127</sup> or to a few weeks in Tris-HCl buffer (pH = 7.4)<sup>64</sup> because buffer salts interfere with the electrostatic repulsion of the negatively charged surface ligands.<sup>129</sup> The colloidal stability in serum depends on the type of serum. For example, while the UCNPs show no aggregation in fetal bovine serum,<sup>124</sup> other serum types may lead to aggregation<sup>129</sup> caused by protein adsorption and cross-linking. When evaluating these different results, however, differences in experimental conditions have to be taken into account.

Additionally, PAA can act as a binding site for the block copolymer  $\alpha$ -acetal-polyethylene glycol-*b*-poly(2-(*N,N*-dimethylamino)ethyl methacrylate) (acetal-PEG-*b*-PAMA).<sup>93</sup> The positive charge of the PAMA moiety binds the copolymer electrostatically to the UCNP surface, while the acetal group which is easily converted to an aldehyde group can be employed for attaching biomolecules.

Polyvinylpyrrolidone (PVP), a polymer with a high biocompatibility and low toxicity,<sup>100</sup> attaches to the surface of UCNPs *via* its carbonyl groups. The preparation of hydrophobic UCNPs with oleic acid on the surface and subsequent ligand exchange with PVP in a solvent mixture of toluene, dimethylformamide, and dichloromethane at elevated temperatures yields water dispersible nanoparticles with a diameter of 20 nm or lower, which are advantageous for bioanalytical applications.<sup>100</sup> The PVP-coated UCNPs are also dispersible in various organic solvents including ethanol, chloroform, and dimethyl sulfoxide. The multidentate PVP shows only a slight tendency to crosslinking and thus aggregation of UCNPs. The polymer provides several advantages such as a long circulation time in blood and low accumulation in organs which are important for biodistribution or bioimaging studies.<sup>100</sup>

**3.2.3 Dendrimers as multidentate ligands.** In contrast to linear polymers, the repetitive subunits of dendrimers form branched macromolecules. For example, poly(amidoamine)

Table 4 Polymers applicable for ligand exchange reactions

Polymer	Molecular weight	Coordinating functionality	Surface exposed functionality	Ref.
Polyacrylic acid (PAA)	1800, 5000, 15 000	Carboxylic acid	Carboxylic acid	64, 93, 99, 124–129
Polyvinylpyrrolidone (PVP)	10 000	Pyrrolidone	Pyrrolidone	100
Poly(amidoamine) (PAMAM)	n.d.	Amine	Amine	32
Polyethylene glycol diacid	600	Carboxylic acid	Carboxylic acid	71, 130
Polyethylene glycol phosphate ester	n.d.	Phosphoric acid	Polyethylene glycol	10
Polyethylene glycol maleimide acid	2000	Carboxylic acid	Maleimide	71



(PAMAM, G0 generation) is a highly hydrophilic and well biocompatible dendrimer.<sup>32</sup> The terminal amines of PAMAM coordinate to the UCNP surface and the remaining amines are available for subsequent functionalization with (bio)molecules. The multiple binding sites of PAMAM also yield a high loading capacity of probe molecules on the UCNP surface, which is particularly important if the interaction of probe and analyte is weak. UCNPs coated by PAMAM are well dispersible in water and applicable for biological applications.<sup>32</sup>

Another dendrimer consisting of polyglutamic acid with a porphyrin core unit can be used to generate a hydrophilic surface on UCNPs.<sup>131</sup> Since the increased dispersibility in aqueous systems depends on the amount of unbound carboxylic groups exposed to the dispersant, the control of the ratio of coordinating to free carboxylate groups is crucial. The UCNPs are well dispersible over a wide pH range and are suitable for bioanalytical applications.<sup>131</sup>

**3.2.4 Polyethylene glycol (PEG).** PEG is a polymer that has found many applications ranging from the preparation of cosmetics, pharmaceutical and medicinal research and production, medicinal applications and research. PEG provides many advantages for biological applications such as low toxicity, no immunogenicity and no metabolic degradation during clearance from the body.<sup>132</sup> Nanoparticles coated with PEG form stable colloids in pure water as well as in aqueous buffers.<sup>133</sup> PEG also reduces the non-specific binding of PEG-modified nanoparticles to proteins or cell surfaces.<sup>134</sup> A ligand exchange reaction can be performed with either simple linear PEG carrying terminal acidic functionalities or PEG as a part of a block copolymer.

Polyethylene glycol diacid (average  $M_w = 600$ ) has two terminal carboxylic acids. After ligand exchange, the nanoparticles are dispersible in deionized water and are stable for at least two weeks but crosslinking *via* the two acidic functionalities has also been reported.<sup>71</sup> Additionally, this ligand exchange has no effect on the optical properties of UCNPs.<sup>130</sup>

Polyethylene glycol phosphate (PEG-phosphate,  $M_w = 2000$  or 750), a PEG esterified with phosphate at one end, is also a promising compound for ligand exchange reactions

(Fig. 7), that result in a good water dispersibility at acidic and neutral pH for several months.<sup>10</sup> The dispersibility is essentially independent of the PEG chain length. Increasing the pH, however, leads to a replacement of the PEG phosphate ligands by hydroxyl ions and ensuing aggregation.<sup>10</sup> It is also crucial to remove excess PEG phosphate by dialysis because only purified PEG-phosphate-coated UCNPs are stable in cell growth media without aggregation. Interestingly, the opposite aggregation behavior can be observed in PBS. Here, PEG-phosphate free in solution is necessary to rebind to the surface when the phosphate ions in PBS displace the surface attached ligands.<sup>10</sup>

Heterobifunctional PEG with a molecular weight of 2000 carrying on one end a carboxylic group for surface coordination and on the opposite end maleimide for protein conjugation are also suitable for ligand exchange reactions. Although such UCNPs are only dispersible in aqueous systems for one day, the storage time can be prolonged in ethanol under rotation.<sup>71</sup> The limited stability is likely a result of the dissociation of the large PEG which is coordinated to the surface by a single carboxylic group only.

A better anchoring can be achieved if PEG is combined with polymers that have multiple coordination sites for the UCNP surface. The block copolymer polyethylene glycol-*b*-polyacrylic acid (PEG-*b*-PAA) anchors to the nanoparticle surface through the polydentate PAA and PEG affords an excellent dispersibility in aqueous dispersants.<sup>33</sup> After the ligand exchange reaction, excess amounts of unbound ligands can be removed by centrifugation. The UCNP surface is coated completely during the ligand exchange reaction when PEG-*b*-PAA is applied in at least a fivefold excess compared to the amount of UCNPs as shown by zeta potential measurements.<sup>33</sup> In contrast to UCNPs coated only by PAA, the block copolymer avoids crosslinking and aggregation. Furthermore, the presence of PEG on the outer surface covers the anionic polymer and such UCNPs are less susceptible to changes in pH and ionic strength of physiological buffers. Therefore, nanoparticles coated with PEG-*b*-PAA are better suitable for bioanalytical applications than UCNPs coated with PAA alone.<sup>33</sup>

UCNPs coated with PAA can also be subsequently modified with PEG, either covalently<sup>128</sup> or electrostatically,<sup>93</sup> by using the carboxylic groups of PAA as the binding sites. Such UCNPs are well dispersible in water and provide advantages for bioanalytical applications<sup>93,126</sup> such as a reduced non-specific binding to proteins.<sup>128</sup> *In vivo* techniques benefit from the subsequent polymer modification of UCNPs that leads to an improved circulation in blood.<sup>26</sup>

**3.2.5 Ligand-free UCNPs.** In a variation of the ligand exchange reaction, ligand-free UCNPs can be generated by treating oleic acid-coated UCNPs with strong acids.<sup>75,116</sup> At low pH, the oleate ligands are protonated and thus detach from the UCNP surface. While the upconversion luminescence strongly depends on the pH with maximum signal intensity at pH 4, it is less affected by the acid composition that provides the counter anion for the positively charged lanthanide ions.<sup>116</sup> The dispersion stability of these “naked” UCNPs depends on their surface charge that can be adjusted by the pH. The

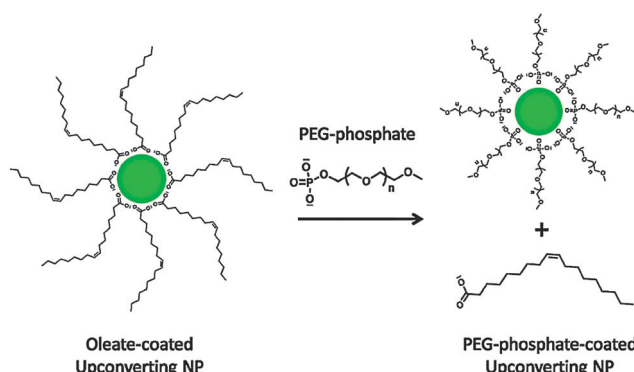
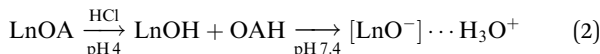
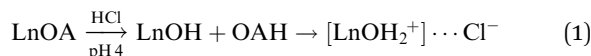


Fig. 7 Scheme of the ligand exchange reaction of oleate-coated UCNPs with PEG-phosphate. The hydrophilic PEG-phosphate ligand replaces the hydrophobic oleate ligand by coordinating to the UCNP surface with its phosphate group. Reprinted with permission from ref. 10. Copyright © 2010 American Chemical Society.



positive surface charge at low pH gradually changes over a less charged surface at the isoelectric point (pH = 5.8) to negative values at pH  $\geq 7$ . This process can be attributed to the stepwise deprotonation of adsorbed water on the UCNP surface.<sup>116</sup>



with Ln as the lanthanide on the UCNP surface; OA as oleate on the UCNP surface, OAH as oleic acid. Since strong electrostatic repulsion of nanoparticles with the same surface charge promotes the formation of stable colloidal systems, “naked” UCNPs show high dispersion stability at pH  $\leq 4$  and  $\geq 7$ , respectively. This phenomenon can be explained by the DLVO-theory that describes the stability of colloidal dispersions.

Alternatively, the oleate ligand can be removed by nitrosonium tetrafluoroborate ( $\text{NOBF}_4$ ).<sup>135</sup> The  $\text{BF}_4^-$  anion attaches weakly to the positively charged UCNP surface and creates UCNPs that are easily dispersible in several polar aprotic solvents such as *N,N*-dimethylformamide (DMF), dimethyl sulfoxide (DMSO), and acetonitrile but not well dispersible in water. The dispersibility in water can be improved by adding a small amount of DMF. In a solvent mixture of DMF/water (1 : 20)  $\text{BF}_4^-$ -coated UCNPs can be stored for several years. In this way, even larger UCNPs are storable that are otherwise not stable as oleic acid-coated UCNPs in hexane. The potential storage period of  $\text{BF}_4^-$ -coated UCNPs dispersed in DMF is several months without any signs of aggregation.<sup>135</sup> A subsequent ligand exchange can be performed either with hydrophobic ligands such as hexylamine or tetradecylphosphonic acid, or with hydrophilic polymers such as polyvinylpyrrolidone (PVP) (Fig. 8). The reaction can be easily performed in less than one minute by mixing the  $\text{BF}_4^-$ -coated UCNPs dispersed in DMF with the new ligand.<sup>135</sup>

### 3.3 Ligand oxidation

Hydrophobic surface ligands present on the UCNP surface after most syntheses can also be modified instead of performing a ligand exchange reaction. The double bond between C<sub>9</sub> and C<sub>10</sub> in the monounsaturated oleic acid can be oxidized with the Lemieux-von Rudloff reagent to yield azelaic acid and nonanoic acid (Fig. 9). The surface attached azelaic acid renders the UCNP surface hydrophilic and enables further conjugation steps.<sup>26,99</sup>

The Lemieux-von Rudloff reagent is a mixture of permanganate ( $\text{MnO}_4^-$ ) in catalytic amounts and periodate ( $\text{IO}_4^-$ ) in stoichiometric amounts. Both reagents are needed for the three-step conversion of the double bond to two carboxylic groups because permanganate first oxidizes the double bond and is then reoxidized by periodate. The reaction time should not exceed two hours to avoid the formation of  $\text{MnO}_2$  which cannot be easily separated from the UCNPs and strongly reduces the upconversion luminescence.<sup>99</sup> Azelaic acid-coated UCNPs form stable dispersions in water for one week but also in some other polar solvents such as DMSO or DMF.<sup>28,53,99</sup> Additionally, the

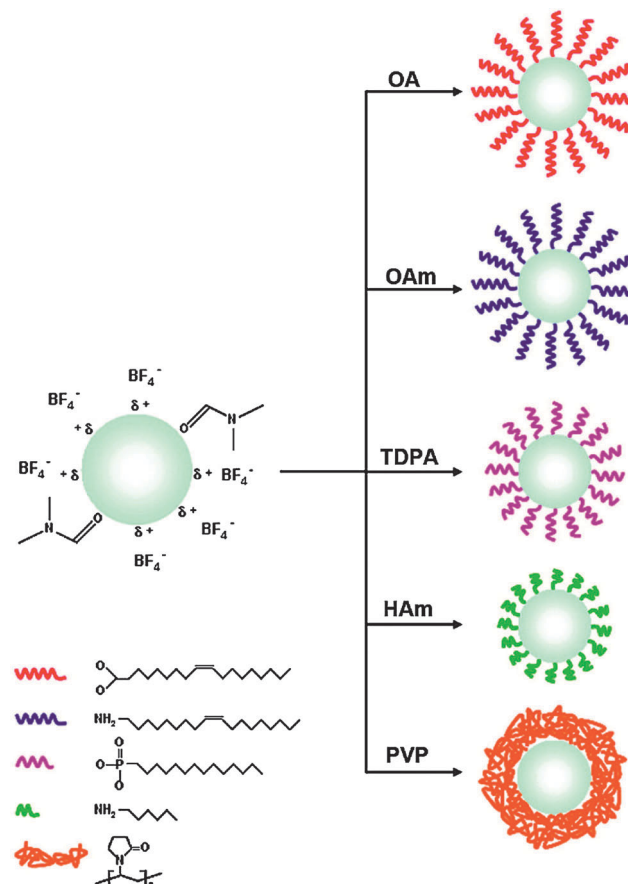
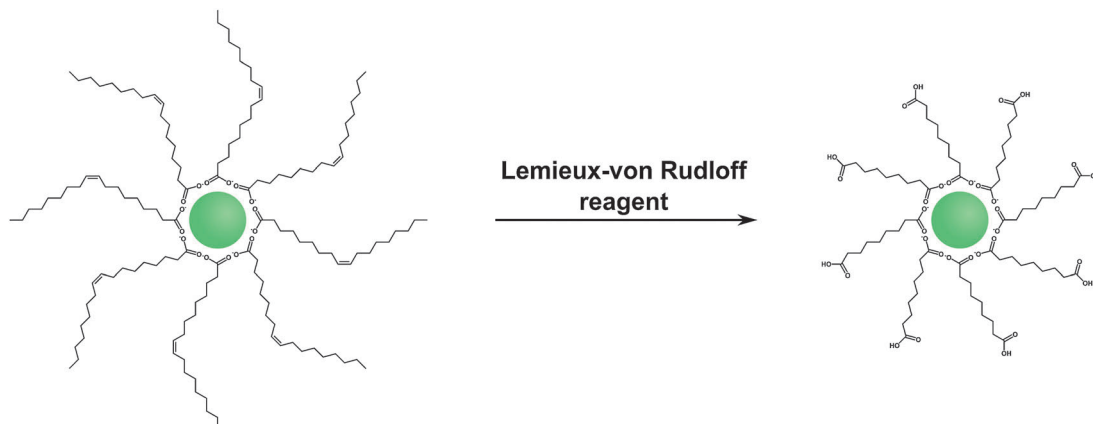


Fig. 8 Subsequent ligand exchange reactions of  $\text{BF}_4^-$ -coated UCNPs in dimethylformamide (DMF). The use of oleic acid (OA), oleylamine (OAm), tetradecylphosphonic acid (TDPA), or hexylamine (HAm) yields hydrophobic UCNPs dispersible in hexane, while the use of polyvinylpyrrolidone (PVP) results in UCNPs dispersible in aqueous media. Adapted with permission from ref. 135. Copyright © 2011, American Chemical Society.

modification has no influence on the size, shape, or crystal phase of the UCNPs.<sup>28,53</sup> The formation of azelaic acid and the following transfer to aqueous systems, however, decrease the luminescence intensity of the UCNPs<sup>28,53</sup> because the relatively short azelaic acid is only insufficiently able to shield the surface from the quenching effects of water.<sup>99</sup> The newly formed carboxylic acid can be used for further bioconjugation steps, *e.g.* with streptavidin, but UCNPs coated with azelaic acid are also taken up by endocytosis without the need of further modifications.<sup>27,28</sup>

Alternatively, azelaic acid-coated UCNP can be generated by ozonolysis.<sup>121,136</sup> Compared to the Lemieux-von Rudloff reagent, the oxidation of the double bond with ozone can also lead to the formation of aldehydes on the nanoparticle surface instead of a carboxylic acid.<sup>136</sup> The intermediate of the ozonolysis can be homogeneously oxidized to carboxylic acids by using a second oxidant such as a mixture of hydrogen peroxide and acetic acid, or homogeneously reduced to aldehydes *e.g.* by using dimethyl sulfide.<sup>136</sup> The UCNPs modified with carboxylic acids<sup>121,136</sup> or aldehydes<sup>136</sup> are well dispersible in water or ethanol and show the same size, shape, and emission properties as before the ozonolysis. On the other hand, the reduction to aldehydes by





**Fig. 9** Scheme of the oxidation of oleic acid with the Lemieux–von Rudloff reagent ( $\text{MnO}_4^-/\text{IO}_4^-$ ). The oxidation of the double bond leads to the formation of hydrophilic carboxylate groups on the UCNPs surface which are accessible for subsequent conjugation steps. Adapted with permission from ref. 28. Copyright © 2008, American Chemical Society.

dimethyl sulfide enables a straightforward conjugation of amine-containing compounds such as many biomolecules *via* the formation of imines.<sup>136</sup>

### 3.4 Ligand interaction

The hydrophobic surface ligands on UCNPs can also be used as an attachment site for a second layer of amphiphilic molecules. This ligand interaction in an aqueous environment is driven by van-der-Waals interactions between the hydrophobic alkyl chains of the surface ligands and of the amphiphilic compounds such as modified polymers or detergents (Fig. 10).

Amphiphilic polymers consist of both hydrophobic units such as alkyl chains and hydrophilic parts.<sup>24,70</sup> The alkyl chains

of amphiphilic polymers can interact with the hydrophobic surface ligands of UCNPs such as oleic acid or oleylamine. Amphiphilic polymers can be prepared for example by the formation of amide bonds between PAA and octylamine<sup>24</sup> or a mixture of octylamine-isopropylamine.<sup>70</sup> The ratio of modified to unmodified acid groups in PAA has to be well adjusted to provide stable attachment sites *via* hydrophobic interactions and to keep the hydrophilic character of PAA for the generation of water dispersible UCNPs. A mixture of octylamine/isopropylamine (5 : 8) results in a modification of 65% of carboxylic groups while 35% remain unmodified.<sup>70,137</sup> UCNPs coated with this modified polymer form stable dispersion in water, ethanol, PBS (pH = 7.4), or Tris-borate-EDTA (TBE, pH = 9.3) buffer. No aggregation was

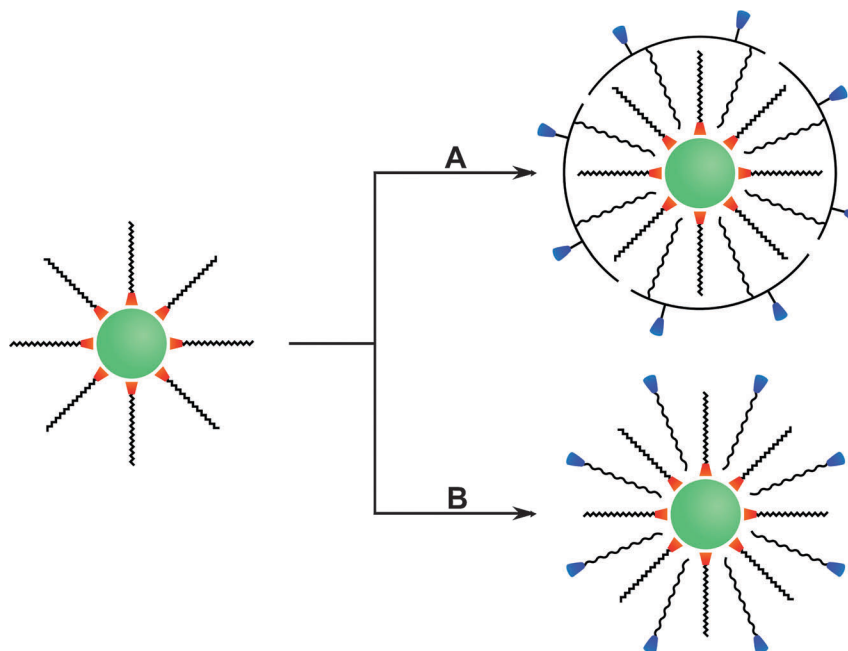


**Fig. 10** Preparation of functionalized UCNPs by ligand interaction using (A) (modified) polymers with multiple hydrophobic chains to interact with hydrophobic surface and (B) detergents with a single hydrophobic chain.



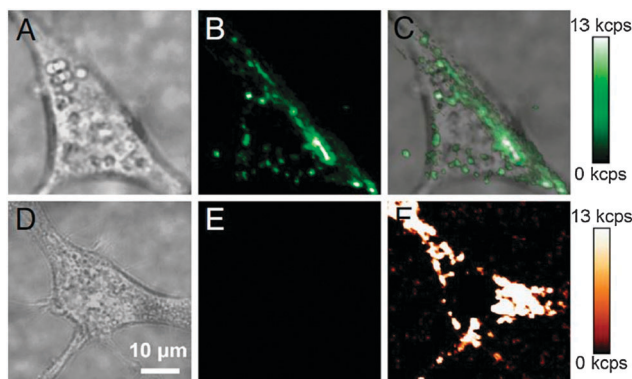


Fig. 11 Endocytosis of PAA-coated UCNPs by murine fibroblasts (NIH 3T3). (A) Brightfield image of a cell with endocytosed UCNPs, (B) upconverting luminescence under 980 nm excitation, and (C) overlay. (D) Brightfield image of a cell without UCNPs, (E) upconverted luminescence under 980 nm excitation, and (F) cellular autofluorescence under 532 nm excitation. Reprinted with permission from ref. 24 Copyright © 2009, PNAS.

observed in aqueous systems for two weeks and after a month, small amounts of aggregates are formed in water or PBS only but not in TBE.<sup>70</sup> The higher colloidal stability in TBE buffer can be attributed to the strong negative surface charge of the nanoparticles at alkaline pH. Compared to oleic acid-coated UCNPs, the second surface layer of PAA decreases the upconversion luminescence by approximately 60%. Since the excitation light is not affected by the PAA coating, the reduced signal results from the quenching effect of the polymer.<sup>70</sup> In bioimaging studies with murine fibroblasts, such PAA-modified UCNPs are readily taken up by endocytosis and background-free images can be recorded under NIR excitation (Fig. 11).<sup>24</sup>

Hydrophobic polymers can also be modified with hydrophilic compounds to form amphiphilic polymers. For example, hydrophobic poly(maleic anhydride-*alt*-1-octadecene) (PMHC<sub>18</sub>) readily reacts with hydrophilic amine-functionalized PEG. The amphiphilic polymer can then be bound to oleic acid-coated UCNPs by hydrophobic interaction and yields stable aqueous dispersions.<sup>138</sup> Additionally, hydrophobic dyes can be embedded into the hydrophobic layer of PMHC<sub>18</sub>. For example, rhodamine B, rhodamine 6G, and Tide Quencher 1 can be immobilized to create a LRET system because their absorption spectra overlap with the emission bands of the UCNPs.<sup>138</sup>

Poloxamers are amphiphilic triblock copolymers consisting of a central hydrophobic chain of polypropylene glycol (PPG) framed by two hydrophilic chains of PEG. The hydrophobic PPG chains of the poloxamers Pluronic F127 (PEG length: 100 monomer units, PPG length: 65 monomer units) and Pluronic P123 (PEG length: 20 monomer units, PPG length: 70 monomer units) can interact with oleic acid on the UCNPs surface while the PEG chains form a hydrophilic outer surface.<sup>139</sup> The resulting UCNPs are dispersible in water and in conventional culture media. While the UCNPs coated with Pluronic F127 are stable in cell culture media for over a week, aggregation is observed for Pluronic P123-coated UCNPs. Since the hydrophobic PPG chains are not packed densely in the oleic acid layer, the PEG

chains have to be long enough to shield the nanoparticle surface and the hydrophobic alkyl chains of oleic acid efficiently from the aqueous environment. The upconversion luminescence is decreased by 57% for Pluronic F127 but by 84% for Pluronic P123 as a result of different chain lengths of PEG and PPG.<sup>139</sup> By comparing the two poloxamers with the low molecular weight surfactant polyethylene glycol *tert*-octylphenyl ether (C<sub>8</sub>PhE<sub>10</sub>), the dependence of the preservation of luminescence intensity on the molecular weight and on the ratio of hydrophilic-to-hydrophobic blocks can be studied. Despite its comparatively low molecular weight, C<sub>8</sub>PhE<sub>10</sub> can shield the hydrophobic UCNPs surface from water molecules more efficiently than Pluronic P123. Due to a higher ratio of hydrophilic-to-hydrophobic blocks and thus a more compact packing of the PEG chains, C<sub>8</sub>PhE<sub>10</sub> decreases the luminescence only by 72% compared to 84% by Pluronic P123. A higher molecular weight leads to the formation of a thicker hydrophilic layer and reduced quenching effects such that C<sub>8</sub>PhE<sub>10</sub> can preserve 28% and Pluronic F127 43% of the original luminescence. The ratio of hydrophilic-to-hydrophobic blocks, however, has a higher impact on the upconversion luminescence than the molecular weight.<sup>139</sup>

Block copolymers of PEG can also be attached to the surface of UCNPs by the so-called Flash NanoPrecipitation (FNP) method.<sup>96,129,140</sup> This technique is fast and suitable to encapsulate hydrophobic compounds including drugs or nanoparticles by a amphiphilic polymer such as polyethylene glycol-*b*-polycaprolactone (PEG-*b*-PCL) or polyethylene glycol-*b*-poly(lactic-*co*-glycolic acid) or a polyelectrolyte such as  $\epsilon$ -polylysine or chitosan.<sup>141-143</sup> For the preparation of a hydrophilic surface of UCNPs, the hydrophobic UCNPs and the respective amphiphilic block copolymers are dispersed in an organic solvent that is miscible with water.<sup>129,140</sup> The organic solvent is mixed at high speed with water to induce a supersaturation of the copolymer. Under these conditions, the copolymers start to deposit on the nanoparticle surface. The formation of block copolymer-coated nanoparticles with a uniform size depends on (1) the nucleation and growth time of the nanoparticles, (2) the self-assembly time of the copolymer, and (3) the overall mixing time.<sup>129,141</sup> The optimization of these parameters is crucial. If the self-assembly time is too short empty micelles of block copolymers can form, and if the nucleation and growth times are too fast the UCNPs can aggregate.

UCNPs can be coated with polyethylene glycol-*b*-polycaprolactone (PEG-*b*-PCL) by this method. Depending on the amount of copolymer the optical properties are affected differently. When the ratio of polymer to UCNPs is changed from 0.1 : 1 to 6 : 1, the luminescence of the UCNPs decreases from 50% to 10%.<sup>140</sup> Compared to other block copolymers, the modification with PEG-*b*-PCL leads to aggregation of UCNPs in serum.<sup>96,129</sup> This high aggregation tendency can be attributed to the low glass transition temperature and high mobility of PCL chains. The copolymers can rearrange and either form domains on the UCNPs surface leaving the hydrophobic parts in contact with the aqueous surroundings or form lamellar structures, *i.e.* a layer of hydrophobic polymer part between two layers of hydrophilic polymer parts. In both cases aggregation is strongly enhanced.<sup>129</sup>



In contrast, the block copolymer polyethylene glycol-*b*-poly(lactic acid) (PEG-*b*-PLA) on the surface of UCNPs results in stable dispersions at 4 °C in water, PBS buffer (pH = 7.4, 10 mM) as well as protein-containing culture medium for at least 3 months without any signs of aggregation.<sup>96</sup> Under physiological more relevant conditions, at 37 °C and in serum, UCNPs dispersions are stable for at least 25 hours which is sufficient for most bioanalytical applications. The PEG-*b*-PLA-coated UCNPs also show a low cytotoxicity as demonstrated by a sulforhodamine B assay.<sup>96</sup> The triblock copolymer methoxy polyethylene glycol-*b*-poly(lactic-*co*-glycolic acid) (PEG-*b*-PLGA) essentially imparts the same surface properties to UCNPs that are well dispersible in water, PBS buffer, and culture media for at least one week.<sup>129</sup>

In general, surfactants are amenable to tune the hydrophilic surface properties of UCNPs. Since the aqueous dispersibility of UCNPs depends on electrostatic or steric repulsion, surfactants with charged or bulky groups enable the design of hydrophilic UCNPs that are long-term stable without aggregation. The surface modification of hydrophobic UCNPs *via* ligand interaction with either anionic sodium dodecyl sulfate (SDS), cationic cetyltrimethylammonium bromide (CTAB), or bulky PEG *tert*-octylphenyl ether (C<sub>8</sub>PhE<sub>10</sub>) resulted in aqueous dispersions that were stable for at least one week.<sup>95</sup> While the size and monodispersity is not affected by the surfactant layer, the upconversion luminescence intensity decreases to approximately 30% in water. The most decisive factor for yielding stable hydrophilic UCNPs coated by SDS, CTAB, or C<sub>8</sub>PhE<sub>10</sub> is the surfactant concentration that defines the inner diameter of the micelles in microemulsion. For high concentrations, the micelles have the appropriate size to enclose a single UCNPs only. Lower surfactant concentrations lead to larger micelles containing several UCNPs. Very low surfactant concentrations result in large superstructures of UCNPs that are not a result of aggregation but rather the formation of larger surfactant structures since the size and shape of UCNPs is not affected.<sup>95</sup> SDS adsorbed to the oleate-coated UCNPs has also been used for binding cationic pyrrole by electrostatic interactions. Pyrrole was then polymerized on the UCNPs surface to yield a covalently linked network of the conductive polymer polypyrrole.<sup>95</sup>

Phospholipids are biological surfactants that can bind to the hydrophobic surface of UCNPs by ligand interaction and mimic the outer surface of cells.<sup>18</sup> They are highly biocompatible and can also be conjugated to PEG *via* the phosphate containing head group.<sup>144,145</sup> PEG avoids biodegradation and prolongs the typically short lifetimes of phospholipids during *in vivo* imaging. The phospholipids are anchored to the oleic acid-coated UCNPs by two fatty acids while the hydrophilic phosphate group is in contact with the aqueous environment.<sup>18</sup> Phospholipid-coated UCNPs form stable aqueous dispersions without aggregation. Importantly, the upconversion luminescence is only slightly decreased compared to the emission intensities of the UCNPs in cyclohexane which indicates an efficient shielding of the UCNPs surface by the phospholipids from water.<sup>18</sup> Since the phosphate group with its attached PEG chain can easily be modified *e.g.* by dyes, maleimide or carboxylic groups, the UCNPs can be readily used for various bioanalytical applications.

A fluorescent dye such as rhodamine B, for example, can be linked to the PEG chain to enable LRET or folic acid can be attached to create a probe for tumor targeting.<sup>18</sup>

### 3.5 Layer-by-layer deposition

Polymer-modified UCNPs can also be used for a so-called layer-by-layer (LbL) deposition. Alternating layers of polyanions and polycations can be deposited on a charged surface by electrostatic interactions.<sup>146</sup> Since polyions like polymers or biomolecules have a flexible structure and the LbL process is mainly performed in solution, LbL can be performed on all types of surfaces including glass slides and nanoparticles.<sup>93,125,146</sup> The size of UCNPs can be adjusted by repeated deposition of polyions with alternating charges of each layer.<sup>36</sup> The change of the surface charge or functionalities is crucial for bioanalytical applications. For example, amine-functionalized UCNPs can be generated by depositing alternating layers of poly(allylamine hydrochloride) and poly(styrene sulfonate) on UCNPs.<sup>36</sup> Amine groups can then serve as an attachment site for biomolecules.

### 3.6 Growing a silica shell and silanization

**3.6.1 Growth of a silica shell.** Silica is one of the most commonly used materials for growing a shell on the surface of UCNPs. The influence of a silica shell on the luminescence properties of UCNPs is in most cases very low or undetectable.<sup>17,73,97</sup> A slightly decreasing luminescence can be attributed to scattering of the excitation light and emission light by silica.<sup>147,148</sup> The transparent, biocompatible and non-toxic silica shell provides several advantages for optical bioanalytical applications and is commonly used to modify the surface of nanomaterials such as quantum dots, metal oxide nanoparticles and UCNPs.<sup>12–14,149–152</sup> NIR-transparency is especially important for the excitation of UCNPs with 980 nm light.<sup>19</sup> Silica is also chemically inert and hydrophilic resulting in highly stable silica-coated nanoparticles that are well dispersible in aqueous buffers.<sup>13,45,97,103,153</sup> Furthermore, the shell can be further modified with various functional groups by well-established silanization techniques.<sup>152,154</sup>

UCNPs that have a hydrophilic surface after synthesis are typically coated with a silica shell by using a modified Stöber process while hydrophobic UCNPs are coated by the micro-emulsion technique. The initial Stöber process<sup>155</sup> which yielded pure silica particles by hydrolyzing tetraalkyl orthosilicates in alcoholic solvents in presence of ammonia can be modified for coating UCNPs with a silica shell. The UCNPs are dispersed in an alcohol of low molecular weight, mostly ethanol, or in a mixture of ethanol and water.<sup>101,151,154</sup> The thickness of the shell can be adjusted by varying the amount of the tetraalkyl orthosilicate,<sup>64,101,107,156</sup> usually tetraethyl orthosilicate, but also by changing the sonication time.<sup>151</sup> The functionalization of UCNPs can either be performed during the growth of the silica shell or the silica-coated UCNPs can be used for a subsequent silanization reaction.<sup>101</sup> PVP interacts strongly with silica and thus can be applied to control the growth of a silica shell on the UCNPs surface.<sup>100</sup> PVP can either be used as a chelator during UCNPs synthesis<sup>107</sup> or added after synthesis to bind to the UCNPs surface before the silica shell growth.<sup>156</sup>



Since the most efficient syntheses yield UCNPs covered with a hydrophobic surface, however, a microemulsion technique is typically used to grow a silica shell on UCNPs. Reverse micelles serve as nanoreactors for the growth of the silica shell during the hydrolysis of a tetraalkyl orthosilicate. A detergent is applied to form these micelles in a nonpolar solvent, *e.g.* cyclohexane, enclosing a small aqueous compartment. The growth of a silica shell is initiated by adding ammonia. The size of the micelles should be adjusted to encapsulate a single UCNP only. Depending on the amount of detergent added, the micelles have a spherical form or a more rod-like shape that can lead to the encapsulation of several UCNPs.<sup>157</sup> A silanization reaction can also be performed either during or after the growth of the silica shell.<sup>17,30,52,77</sup>

A mesoporous silica shell with pore sizes in the nanometer range can be generated, for example, by adding the micelle-forming detergent cetyltrimethylammonium bromide during the synthesis of the silica shell.<sup>20,154</sup> These micelles are incorporated during the growth of the silica shell. The micelles inside the silica shell can be removed either by washing with a solvent of suitable pH or by calcination that leads to pore sizes of 2 to 50 nm in diameter. The mesoporous shell has a larger surface area compared to a plain silica shell and thus more reagents such as drugs or photosensitizers<sup>20</sup> can be loaded to the UCNPs surface. For example, a higher amount of photosensitizer results in an increased production of singlet oxygen and thus in a more efficient photodynamic therapy.<sup>20</sup> Zinc(II) phthalocyanine and Merocyanine 540 are photosensitizing dyes that produce singlet oxygen under excitation and can be used for the treatment of cancer cells.<sup>20,158</sup>

Since certain surface ligands show a high affinity to silica, the prior surface modification with certain polymers or detergents is useful to obtain a silica coating of the UCNPs. In addition to the polymer polyvinylpyrrolidone (PVP),<sup>100,156</sup> the surfactant cetyltrimethylammonium bromide (CTAB)<sup>95</sup> can adsorb the silica precursors like TEOS and thus a uniform layer of silica is gradually grown on the nanoparticle surface whose thickness depends on the amount of TEOS added. Compared to UCNPs coated with CTAB, dispersions of silica-coated UCNPs are more stable without any observable aggregation.<sup>95</sup>

Although the flexible growth of a silica shell provides many advantages for bioanalytical and biomedical applications, there are some limitations. For example, more than a single nanoparticle can be enclosed in a common silica shell.<sup>28,150,157,159</sup> This multicore incorporation can lead to a high degree of polydispersity in UCNPs dispersions that originally were monodisperse.<sup>160</sup> Depending on the buffer system, pH and ionic strength, silica-coated UCNPs can form aggregates in dispersion<sup>100,116</sup> because they have a large surface area and large hydrodynamic radius.<sup>96,161</sup> The buffer conditions have to be optimized for each size of silica nanoparticles<sup>162</sup> that show similar surface properties as silica-coated UCNPs of the same size, and their dispersion stability can last from a few hours to several months depending on the growth conditions of the silica shell.<sup>64,77,100,101,129</sup> Finally, the silica shell on UCNPs can lead to enhanced non-specific binding of biomolecules like proteins or cells which is detrimental for bioanalytical application.<sup>161</sup>

**3.6.2 Silanization of a silica shell.** Silanization is a method to further modify the surface of silica-coated UCNPs with functional groups (Table 5). This modification can be performed either during or after the growth of the silica shell (Fig. 12).

A functionalization of silica-coated UCNPs with amines is well established and most commonly applied for binding small molecules, biomolecules or other nanoparticles to the UCNPs surface. 3-aminopropyltri(m)ethoxysilane – or, less commonly, *N*-[3-(trimethoxysilyl)propyl]ethylenediamine<sup>15,166</sup> – are short primary amines that can be added for growing an amine-modified silica shell during a Stöber process or the microemulsion technique.<sup>30,91,163,167</sup> Amine-functionalized UCNPs are typically conjugated to biomolecules *via* active ester formation in the presence of *N*-hydroxysuccinimide (NHS) and 1-ethyl-3-(3-dimethylaminopropyl)carbodiimide (EDC).<sup>12,15,165,167,168</sup> Isothiocyanate groups can be directly employed for binding to the amine functionality.<sup>91</sup> Heterobifunctional linkers with or without a spacer unit attach with one end to an amine on the UCNPs surface and on the other end provide a second functional group like aldehydes or carboxylic acids that can be coupled to biomolecules.<sup>30,31,160,164</sup> Silica-coated UCNPs modified with amines, however, are susceptible to aggregation because the positively charged amines and the negatively charged silicate surface lead to electrostatic attraction at physiological pH (Fig. 13A).<sup>19</sup> An additional functionalization with methyl phosphonate is suitable to reduce this electrostatically induced aggregation (Fig. 13B).<sup>161</sup>

Since carboxylic acids increase the negative surface charge of UCNPs compared to silanol groups at physiological pH, the use of carboxyl silanes such as carboxyethylsilanetriol for the silanization reaction is favorable compared to amines.<sup>10,89</sup> In this case, the carboxylic acids on the UCNPs surface have a dual function: they avoid aggregation due to electrostatic repulsion and can be activated by NHS and EDC for the conjugation to amine groups of biomolecules.<sup>169</sup> Alternatively, previously activated carboxylic acids such as succinimidyl ester can be directly introduced during silanization<sup>152</sup> but only have limited stability in an aqueous environment.

Cyanogen bromide can form cyanates with the silanol groups on the silica shell.<sup>29</sup> These activated silanol groups can then be conjugated to a primary amine *via* the formation of an isourea group. Cyanogen bromide, however, is acute toxic and highly volatile. UCNPs can be modified by thiol-containing silanes, *e.g.* 3-mercaptopropyl-triethoxysilane, and linked to maleimide-activated compounds.<sup>170,171</sup> Maleimide can also be attached to the nanoparticle surface using suitable silanes. UCNPs activated with maleimide provide advantages for site specific labeling because thiols are less common in biomolecules than amines.<sup>71</sup> The silanization with *e.g.* (3-glycidyloxypropyl)-trimethoxysilane results in epoxides on the surface that reacts readily with different nucleophiles such as amines, hydroxyls or thiols, commonly found in biomolecules.<sup>105</sup>

Amines, carboxylic acids and thiols are omnipresent in biological systems and cannot be labeled specifically in complex biological systems. So-called bioorthogonal groups are particularly useful for *in vitro* and *in vivo* labeling because



Table 5 Functionalized silanes employed for the silanization of silica-coated UCNPs

Functional group of silane	Application	Binding partner	Complementary functional group	Ref.
Amine	Binding of biomolecules	Antibody	Carboxylic acid	15, 23, 163
		RNA	Aldehyde <sup>a</sup>	31, 164, 165
		Folic acid	Carboxylic acid	30
		Protein	Non-covalent	15, 166
		Biotin	Carboxylic acid	12, 15
	Binding of nanoparticles	Streptavidin	Carboxylic acid	167
		Quantum dot	Aldehyde <sup>a</sup>	168
	Binding of dyes	Fe <sub>3</sub> O <sub>4</sub> nanoparticle	Carboxylic acid	160
		Fluorescein	Isothiocyanate	—
		Tetramethyl-rhodamine	Isothiocyanate	17
		Rhodamine B	Isothiocyanate	12, 17, 91
Carboxylic acid	Reduction of aggregation	—	Carboxylic acid	17
	Binding of biomolecules	Lectin	Amine	167
		Antibody	Amine	19
Thiol	Binding of nanoparticles	Silver nanoparticle	Elementary silver	169
	Binding of photocaged bioluminescent probes	d-Luciferin	Maleimide	170
Maleimide	Binding of biomolecules	Antibody	Thiol	171
N-Succinimidyl ester	Binding of biomolecules	Streptavidin	Amine	71
		Protein	Amine	152
Epoxide	Binding of biomolecules	Avidin	Amine	105
Alkyne/azide	Binding of biomolecules <i>via</i> click chemistry	Biotin	Azide/alkyne	101
	Binding of dyes <i>via</i> click chemistry	DNA	Alkyne	21
		BODIPY derivative	Alkyne	101
		Phenoxazine derivative	Alkyne	—
Heptadentate ligand	Complexation of paramagnetic gadolinium	Diethylenetriamine-pentaacetic acid derivate	Trivalent gadolinium	147

<sup>a</sup> Functionality of a homobifunctional crosslinker.

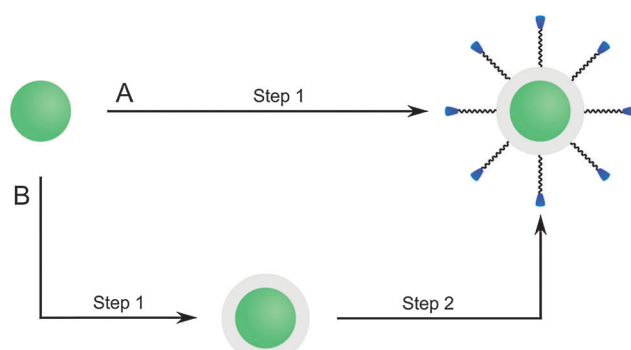


Fig. 12 Silanization by (A) growing a silica shell in presence of a functionalized silane (one-step silanization) or (B) growing a silica shell and subsequent silanization with a functionalized silane (two-step silanization).

they do not interact or interfere with biological materials or processes.<sup>172</sup> The copper(i)-catalyzed Huisgen cycloaddition of organic azides and terminal alkynes is one of the best known bioorthogonal reaction. As a possible application of the “click chemistry” concept, the Huisgen cycloaddition result in high selectivity, high yields and simple reaction conditions

in biocompatible solvents such as water.<sup>173,174</sup> Either the azide or the terminal alkyne can be introduced into the silica shell of UCNPs using respective silanes. Since the low dispersion stability of alkyne-modified UCNPs in aqueous media can lead to aggregation, it is more common to employ azide-functionalized UCNPs that result in more stable dispersions.<sup>21,101</sup>

The silanization of silica-coated UCNPs also enables the generation of nanoparticles that – in addition to the upconversion luminescence – allow a multimodal readout. The silane 3-aminopropyl (trimethoxysilyl)diethylenetriamine tetraacetic acid, for example, forms a multidentate ligand on the nanoparticle surface that strongly chelates Gd<sup>3+</sup> ions.<sup>147</sup> Since almost no toxic Gd<sup>3+</sup> is released from the complex, such Gd<sup>3+</sup>-complex modified nanoparticles can be used as luminescent and MRI-active probes that show higher magnetic resonance relaxivities than free Gd<sup>3+</sup> complexes in solution. This increase can be attributed to the slower tumbling rate of the nanoparticle-bound complexes.<sup>175,176</sup>

Organic fluorophores or quantum dots can be inserted into the silica shell to expand the emission spectrum beyond the intrinsic upconversion luminescence of UCNPs (Fig. 14).

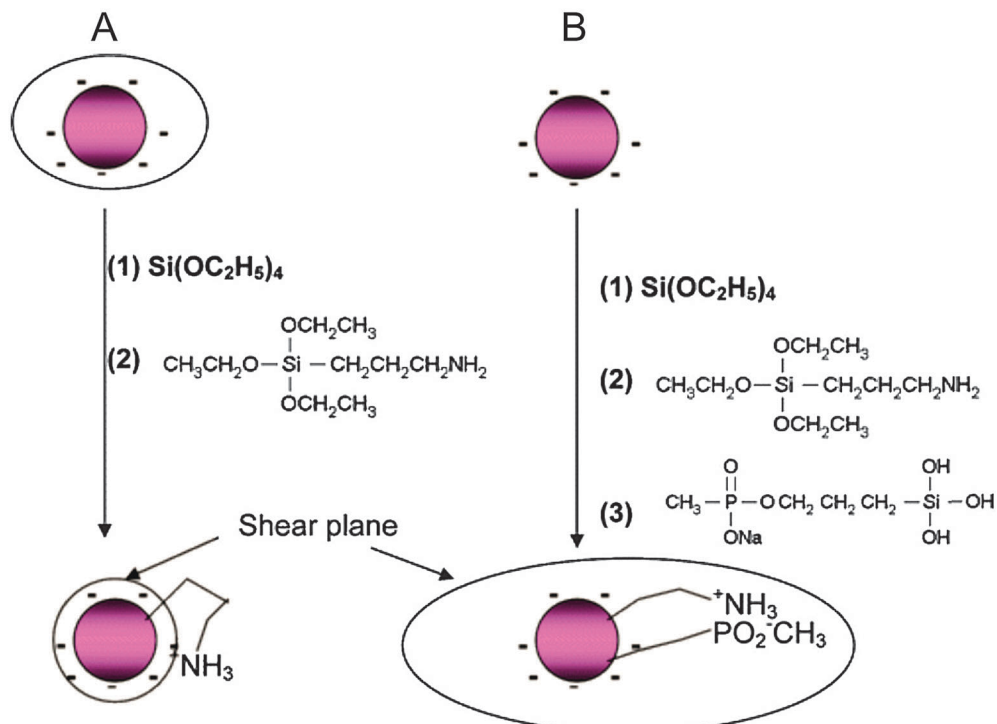


**Fig. 13** Scheme of the back bonding mechanism of amine-functionalized silica nanoparticles on the same nanoparticle (A) and the potential avoidance by a silanization with methyl phosphonate (B). The simultaneous modification with amines, positively charged at physiological pH, and methyl phosphonate, negatively charged at physiological pH, results in an increased shear plane and electrostatic repulsion. Reprinted with permission from ref. 161. Copyright © 2006, American Chemical Society.

Binding fluorophore-modified silanes to the silica shell of UCNPs allows the parallel detection of upconverting and down-converting emission.<sup>12,17</sup> Furthermore, a tuning of the emission spectra of UCNPs can be obtained by a functionalization

with organic fluorophores. The fluorescence of a fluorophore can also be used if the upconversion emission cannot be detected directly due to a lack of instruments for the upconversion readout.<sup>177</sup>

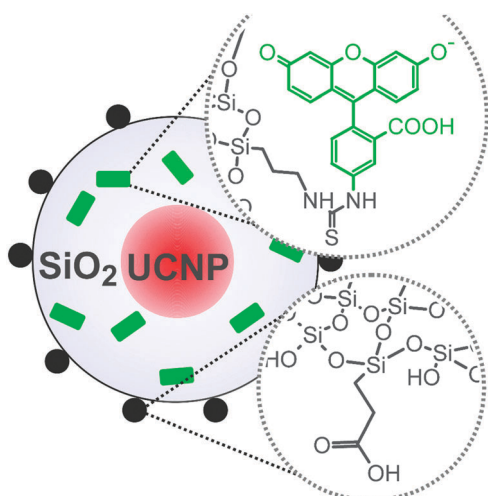


**Fig. 14** Scheme of silica-coated UCNPs. Fluorescein (green) added during silanization enables the detection in the conventional down-conversion mode. Further functionalities (e.g. carboxylic acids) on the surface can be used to improve the water dispersibility of the UCNPs. Reprinted with permission from ref. 177 Copyright © 2014, American Chemical Society.

## 4. Bioconjugation

For numerous bioanalytical applications it is necessary to modify the surface of UCNPs with a biomolecule that serves as a specific recognition element (Table 6).

The bioconjugation step depends on the previous surface modification. For example, organic silanes such as 3-amino-propyltri(m)ethoxysilane can be added during the silanization reaction as described in Section 3.6.2. These functional groups can then be used as a conjugation site for biomolecules. Amine-modified silica shells, however, typically do not form stable dispersions because the amines are partially protonated and can electrostatically interact with deprotonated silanol groups over a wide pH range. Thus, in many cases it is favorable to introduce a linker for the attachment of biomolecules as shown in Fig. 15.

Furthermore, many ligand exchange reactions do not directly yield a conjugation site for biomolecules. In this case, it is necessary to modify the surface ligands such that a functional group for bioconjugation is generated. The surface modification also allows for a modular surface design or the



Table 6 Bioconjugation of UCNPs

Biomolecule	Application	Type of UCNPs	Ref.
Antibody	<i>In vitro</i> imaging	NaYF <sub>4</sub> :Yb,Er	15, 23, 158
	LRET system	NaYF <sub>4</sub> :Yb,Er,Gd	16
	Photodynamic therapy	NaYbF <sub>4</sub> :Er/NaYbF <sub>4</sub> :Tm/NaYbF <sub>4</sub> :Ho	163
	Proof of principle	NaYF <sub>4</sub> :Yb,Er	31
DNA/RNA	LRET system	NaYF <sub>4</sub> :Yb,Er	28–30, 38, 166
	Delivery and transfection of siRNA	NaYbF <sub>4</sub> :Yb,Tm	35
	Specific binding site	NaYF <sub>4</sub> :Yb,Er	15, 166
	Proof of principle	NaYF <sub>4</sub> :Yb,Er	18, 178
Protein/peptide	LRET system	NaYF <sub>4</sub> :Yb,Er	21
	<i>In vivo</i> imaging	NaYF <sub>4</sub> :Yb,Er,Tm	26
	LRET system	NaYF <sub>4</sub> :Yb,Er	167
	Proof of principle	NaYF <sub>4</sub> :Yb,Er	26
Carbohydrate	LRET system	NaYF <sub>4</sub> :Yb,Er	39
	Assay application	NaYF <sub>4</sub> :Yb,Er/NaYF <sub>4</sub> :Yb,Er,Gd	152
Lectin	LRET system	NaYF <sub>4</sub> :Yb,Er	32
	<i>In vitro</i> imaging	NaYF <sub>4</sub> :Yb,Er	19
Folic acid	Tumor targeting/imaging	NaYF <sub>4</sub> :Yb,Er	60
		NaYF <sub>4</sub> :Yb,Tm	122
		LaF <sub>3</sub> :Yb,Ho/LaF <sub>3</sub> :Yb,Tm	102
Biotin	LRET system	NaYF <sub>4</sub> :Yb,Er	36
	Assay application	Y <sub>2</sub> O <sub>2</sub> S:Yb,Er	168
	Proof of principle	NaYF <sub>4</sub> :Yb,Er	101
(Strept)avidin	LRET system	NaYF <sub>4</sub> :Yb,Er	105
	Assay application	NaYF <sub>4</sub> :Yb,Er	28, 60
	Proof of principle	NaYF <sub>4</sub> :Yb,Er/NaYF <sub>4</sub> :Yb,Tm	115

introduction of a flexible spacer. There are only few examples where biomolecules have been directly bound to the surface of UCNPs during a ligand exchange reaction at ambient temperatures.<sup>33,122</sup> Typically, a complete ligand exchange can only be achieved at elevated temperatures, which is deleterious for most biomolecules.

#### 4.1 Direct binding of biomolecules to the surface of UCNPs

The exceptionally high affinity of streptavidin and biotin<sup>179</sup> has led to a widespread use of this modular labeling system in many bioanalytical applications. Since streptavidin is a negatively charged protein, it can coordinate to the UCNPs surface.<sup>33</sup> Coating with streptavidin only, however, leads to nanoparticle aggregation. By coimmobilizing PEG-*b*-PAA and streptavidin on the nanoparticle surface (Fig. 16), non-specific binding is reduced and usually at least one of the four binding sites of streptavidin is accessible for biotin binding. Such UCNPs are readily dispersible in physiological buffers. The structural integrity of streptavidin attached to a UCNPs surface was studied on a microtiter plate coated with biotinylated antibodies. Since the upconversion luminescence increased with increasing amounts of coating antibody, the structure of streptavidin was not affected by the attachment to the surface of UCNPs.<sup>33</sup>

Folic acid is widely used for targeting tumor cells because the folic acid receptor is overexpressed on the surface of some tumor cells. The two carboxylic groups of folic acid can coordinate to the UCNPs surface during a ligand exchange reaction while the unit that binds to the folic acid receptor remains accessible. A ligand exchange reaction with 9 parts of 6-aminohexanoic acid and 1 part of folic acid yielded hydrophilic UCNPs dispersible in aqueous media.<sup>122</sup> A MTT assay revealed low cytotoxicity in a concentration range of 100 to 800 µg UCNPs per mL after an exposure time of 10 h. Tumor targeting and imaging with folic acid-modified UCNPs were tested by using KB cell lines that express the folic acid receptor. The folic acid receptor-negative MCF-7 cell line served as a control. The upconversion luminescence was only detectable on the surface of the KB cells but not on the control cell line, which demonstrates a high selectivity of folic acid-modified UCNPs for the folic acid receptor on cell surfaces with low non-specific binding.<sup>122</sup>

Oleate-coated UCNPs can also be used for a ligand exchange reaction with DNA. The negatively charged phosphate groups of DNA can directly coordinate to the surface exposed lanthanide ions. Such UCNPs are well dispersible in water and the DNA retains its ability to bind to target structures. For example, aptamers on the surface of UCNPs could be used for targeting and imaging of tumor cells. UCNPs modified with aptamers



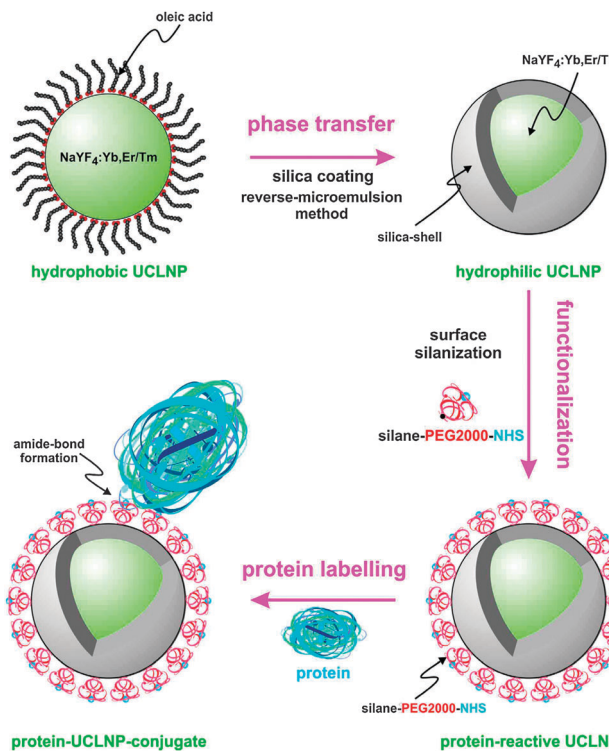


Fig. 15 Surface engineering of UC(L)NPs. Silica-coating renders UC(L)NPs water dispersible and provides an attachment site for silanization that can then be used for the covalent attachment of proteins or other biomolecules. Reprinted with permission from ref. 152 Copyright © 2013, Theranostics.

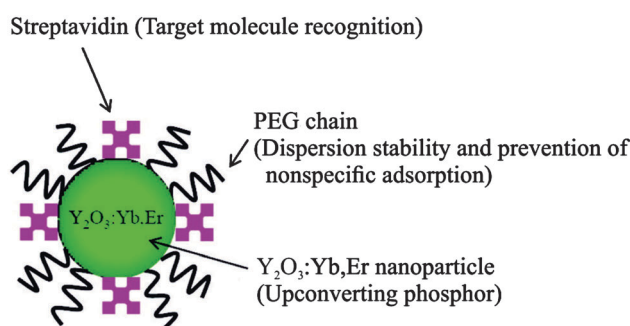


Fig. 16 Scheme of UCNPs coated by PEG-PAA and streptavidin by ligand exchange reaction. The polymer increases the dispersion stability and prevents non-specific binding, while streptavidin serves as a binding site for target molecules. Reprinted with permission from ref. 33. Copyright © 2008, American Chemical Society.

that recognize nucleolin, a protein that is overexpressed on MCF-7 cells, specifically bound to MCF-7 cells and were subsequently endocytosed. In contrast, no binding was observed on the nucleolin-negative control cell line NIH-3T3.<sup>178</sup>

#### 4.2 Indirect binding of biomolecules to the surface of UCNPs

The surface ligands on UCNPs can be converted to new functional groups that enable subsequent bioconjugation steps. Maleimide, thiol, carboxylic, aldehyde, and amine groups are commonly used for the attachment of biomolecules. Compared to amine

or carboxylic groups, thiol groups are less common in proteins and specifically react with maleimides (site specific labeling). Small molecules like cyclic peptides can also be modified with thiol groups for maleimide-binding on UCNPs.<sup>26,71</sup> Maleimide-activated spacers can be attached to thiol-functionalized UCNPs without any side reactions. Amine groups on the UCNPs surface can be converted to a carboxylic group by the ring opening reaction of succinic anhydride or glutaric anhydride.<sup>30</sup> The exposed carboxylic groups can then be activated by the formation of *N*-hydroxysuccinimide esters. Amine-modified UCNPs can also be linked to amine groups in biomolecules *via* a homobifunctional linker with terminal aldehydes for imine formation.<sup>31</sup> The labeling protocol has to carefully chosen to avoid crosslinking of nanoparticles. For example, homobifunctional linkers can also bind to two nanoparticles and lead to aggregation.

Antibodies are usually attached to the surface of UCNPs *via* their amine or carboxylic groups after EDC/NHS activation<sup>15,16,23,158,163</sup> or *via* thiol groups, which typically requires disulfide reduction.<sup>71</sup> Also short spacer molecules functionalized with aldehydes were used to attach antibodies to the UCNPs surface.<sup>31</sup> Since antibodies are highly specific for their respective target epitope, they are predestined for directed cellular studies such as *in vitro* imaging of cancer cells, delivery of small interfering RNA (siRNA) into cells, or photodynamic therapy. This excellent specificity is also the reason for the vast amount of homogeneous and heterogeneous assays based on antibody-antigen binding. The assay sensitivity is strongly improved if UCNPs serve as optical labels.

Most LRET-based assays with UCNPs are used to analyze DNA or RNA. Three types of LRET-based assays have been described: first, a short capture oligonucleotide and complementary reporter oligonucleotide are bound to the donor and the acceptor, respectively. After hybridization, donor and acceptor are located in close proximity resulting in LRET.<sup>28–30</sup> Second, an intercalating dye serves as the acceptor and indicates either the binding of the target oligonucleotide to the capture strand on the UCNPs surface or

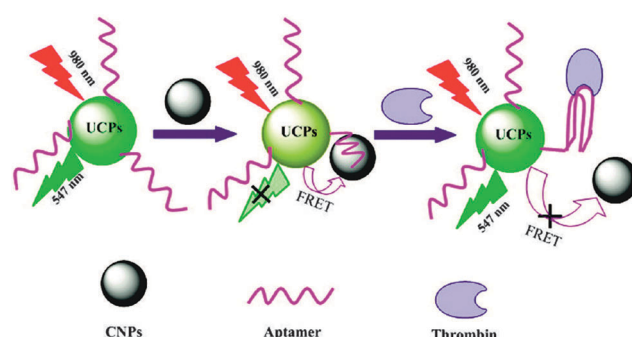


Fig. 17 Scheme of the design and function of a thrombin sensor based on UCNPs. An aptamer on the UCNPs surface binds to a carbon nanoparticle (CNP) *via* weak  $\pi$ - $\pi$  interactions. The CNP quenches the upconversion emission by LRET. Thrombin changes the structure of the aptamer, releases the CNP from the UCNPs surface and thus restores the upconversion emission. Reprinted with permission from ref. 38. Copyright © 2011, American Chemical Society.

the presence of double stranded oligonucleotides.<sup>35,166</sup> Third, if the surface-bound oligonucleotide is an aptamer it can change its structure by the influence of an enzyme, *e.g.* by thrombin, and the acceptor is released from the LRET system resulting in luminescence changes (Fig. 17).<sup>38</sup>

UCNPs can also be modified with siRNA for transfection of cellular DNA. These UCNPs are additionally functionalized with an antibody for cell delivery. A successful transfection can then be verified for example by the silencing of genes by the siRNA.<sup>15</sup>

The functionalization of UCNPs with proteins or peptides *via* EDC/NHS chemistry is a simple way to obtain luminescent cell labels. Transferrin receptors, especially TfR1, and integrins are present in the membrane of all cell types and are a favored target for bioimaging. Transferrin and (cyclic) peptides with the amino acid sequence arginine/glycine/aspartic acid (RGD) are bound to UCNPs for *in vitro* or *in vivo* imaging.<sup>26,167</sup> By linking an LRET donor and acceptor *via* a peptide that contains a cleavage site for an enzyme, the presence and the concentration of the enzyme can be determined. The feasibility of this system was shown for matrix metalloproteinase-2 (MMP-2) using an UCNPs as the donor and a carbon nanoparticle as the acceptor (Fig. 18).<sup>39</sup>

Lectins are proteins that selectively bind to carbohydrates. UCNPs modified either with lectins or the respective carbohydrate can be employed for bioimaging, heterogeneous or LRET-based homogeneous assays. Lectins can be attached to the surface of UCNPs according to standard protocols for protein labeling, most commonly by EDC/NHS activation.<sup>19,60</sup> Carbohydrates are bound

to the UCNPs surface either by EDC/NHS activation, in some cases after converting the amines on the surface of the UCNPs to carboxylic acids,<sup>34</sup> or by using amine-reactive isothiocyanates.<sup>32</sup> As the expression of certain surface glycoproteins is cell-specific, glycoproteins are important cell markers. UCNPs modified with respective lectins can thus be used as a target-specific luminescent probe for *in vitro* bioimaging.<sup>19</sup> UCNPs functionalized with carbohydrates or lectins have enabled the design of homogeneous assays. In these LRET-based assays, an UCNPs serves as the donor and either a dye-labeled lectin<sup>32</sup> or a graphene-labeled carbohydrate<sup>60</sup> as the acceptor. Another type of assays exploits the increased aggregation of carbohydrate-modified UCNPs after binding to lectins either in solution or on the surface of cancer cells.<sup>34</sup>

Although folic acid can be bound to the UCNPs surface by a simple ligand exchange reaction as described in Section 4.1, a covalent attachment avoids desorption processes during applications. Folic acid can be linked to amine-modified UCNPs *via* the established EDC/NHS method *via* its two carboxylic groups.<sup>12,15,25,102</sup> The UCNPs functionalized with folic acid can then be employed for *in vitro* bioimaging of various tumor cell lines including HeLa,<sup>25</sup> HT-29,<sup>15</sup> or KB<sup>12,102</sup> cells.

Streptavidin and biotin<sup>28</sup> are mainly bound to the UCNPs surface *via* an amine/carboxylic acid coupling with an EDC/NHS activation<sup>28,36,115,168</sup> but also epoxides are employed as a binding site for the amine groups in avidin.<sup>105</sup> Since dissociation of biotin/(strept)avidin ( $K_d = 10^{-15}$  M) is almost absent over a wide pH range, this binding pair enables a modular surface modification of UCNPs without additional coupling agents. For instance, surface-bound streptavidin enables the detection of biotinylated biomolecules such as RNA<sup>28</sup> or antibodies<sup>115</sup> or biotinylated nanostructures such as gold nanoparticles.<sup>105</sup> Traces of (strept)avidin can be detected by using biotin-coated UCNPs. (Strept)avidin binds to both the biotinylated surface of UCNPs and a biotinylated acceptor molecule or gold nanoparticles, which results in increased LRET.<sup>36</sup>

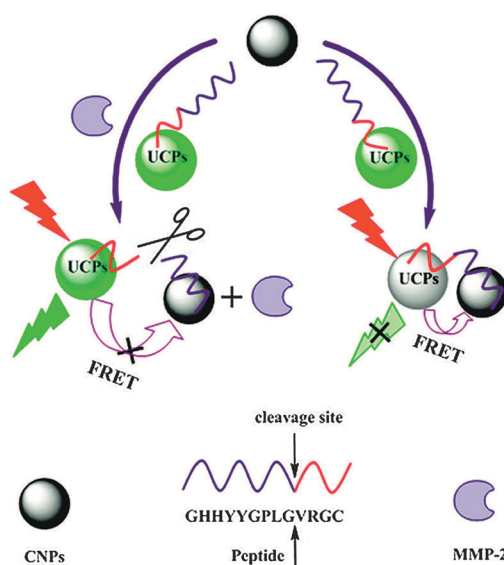


Fig. 18 Matrix metalloproteinase-2 (MMP-2) sensor based on UCNPs. The peptide bound to the UCNPs surface contains the cleavage site for MMP-2 and a  $\pi$ -rich domain for the attachment of CNPs by  $\pi-\pi$  interactions and connects the two nanoparticles. The resulting LRET leads to a quenching of the upconversion emission (left side). After the cleavage of the peptide by MMP-2 (right side) the CNP is released from the system leading to an increase of the upconversion emission. Reprinted with permission from ref. 39. Copyright © 2012, American Chemical Society.

## 5. Hybrid materials

The combination of UCNPs with other nanomaterials leads to the formation of hybrid materials, which can be used, for example, as multimodal probes in bioanalytical applications. In some cases, the generation of hybrid UCNPs can even have favorable effects on the upconversion luminescence. Nanostructures are the most popular materials for generating hybrid UCNPs (Table 7).

For example, sheets of manganese(IV) oxide can be deposited on the UCNPs surface by the reduction of potassium permanganate in 2-(*N*-morpholino)ethanesulfonic acid (MES) buffer to prepare probes for reductive biomolecules.<sup>37</sup> Such metal oxide nanostructures quench the upconversion luminescence resulting in nearly no emission at 20 mol% of  $\text{MnO}_2$ . The luminescence is restored by the reduction of these sheets to manganese(II) ions, for example by the antioxidant glutathione (Fig. 19). In *in vitro* measurements, UCNPs covered with  $\text{MnO}_2$  sheets can be employed



Table 7 Nanostructures employed for creating hybrid UCNPs

Nanomaterial	Type of UCNP	Application	Ref.
MnO <sub>2</sub> sheets	NaYF <sub>4</sub> :Yb,Tm	Probe for biomolecules	37
Fe <sub>3</sub> O <sub>4</sub> nanoparticle	NaYF <sub>4</sub> :Yb,Er	Magnetism	121, 167
Silver shell	NaYF <sub>4</sub> :Yb,Er	Photothermal treatment	123
Gold nanoparticle	NaYF <sub>4</sub> :Yb,Tm	Luminescence enhancement	125, 180
Silver nanoparticle	NaYF <sub>4</sub> :Yb,Er	Proof of principle	136, 178
Silver nanoparticle	NaYF <sub>4</sub> :Yb,Er	Luminescence enhancement	170

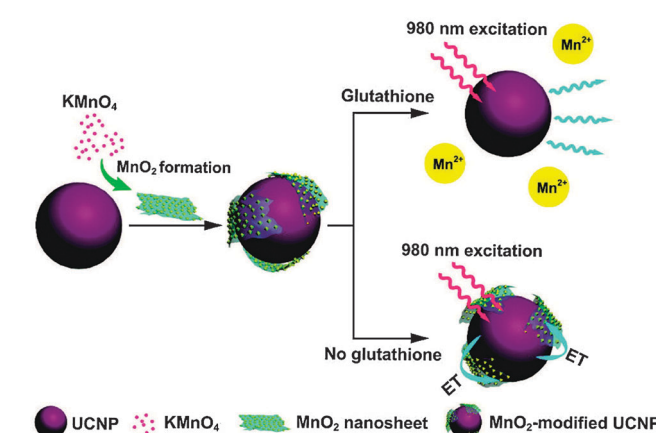


Fig. 19 Design and function of a glutathione (GSH) sensitive probe based on UCNPs. The emission of the UCNPs is quenched by the manganese oxide ( $MnO_2$ ) nanosheets formed on the nanoparticle surface. The analyte GHS reduces  $MnO_2$ , removes the nanosheets, and restores the emission of the UCNPs. Reprinted with permission from ref. 37. Copyright © 2011, American Chemical Society.

as a glutathione-sensitive probe without cross reactivity with other biological compounds.<sup>37</sup>

Luminescent and magnetic materials are of great interest for multimodal applications. Magnetic UCNPs can be prepared by a paramagnetic codopant, in particular  $Gd^{3+}$ , or in combination with superparamagnetic  $Fe_3O_4$  nanoparticles. These hybrid nanoparticles can be employed for the separation of cells or biomolecules<sup>167</sup> or as a bimodal probe for bioimaging. Magnetic nanoparticles can either be bound to the UCNP surface *e.g.* *via* EDC/NHS activation,<sup>167</sup> or  $Fe_3O_4$  can be immobilized on the surface of carboxyl- or thiol-modified UCNPs. Thiol-modified UCNPs result in smaller magnetic nanoparticles due to their high affinity to  $Fe_3O_4$ .<sup>121</sup>

A silver shell on the UCNP surface yields a multimodal hybrid material that can be employed *e.g.* in photothermal therapy.<sup>123</sup> The wavelength of surface plasmon resonance can be tuned to 980 nm by adjusting the thickness of the silver layer. Thereby, heating and bioimaging *via* the upconversion emission can be performed simultaneously under single wavelength irradiation. Similar to magnetite nanoparticles, thiol groups on the surface of UCNPs can serve as the nucleation point for silver nanoparticles. The elongation of the reaction time and an increased amount of the precursor  $AgNO_3$  cause the fusion of the preliminary formed silver nanoparticles to a homogeneous silver shell.<sup>123</sup> Hybrid UCNPs with gold or silver nanoparticles bound to the surface can enhance the upconversion luminescence by surface-plasmon-coupled emission (SPCE).

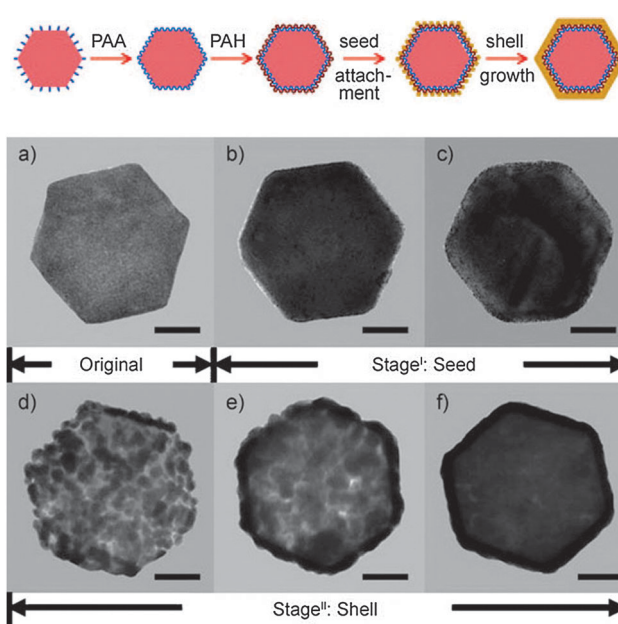


Fig. 20 Upper scheme: surface functionalization, attachment of gold nanoparticles, and growth of a gold nanoshell on an UCNP. Lower TEM images of UCNPs during gold seed attachment and shell growth, (a) original, (b and c) with increasing number of attached gold nanoparticles and (d–f) with growing gold nanoshells (scale bar: 50 nm). Reprinted with permission from ref. 125 Copyright © 2010, Wiley.

The interaction of the plasmon resonance of the noble metal nanostructures and the upconversion emission results in an increased decay rate of radiative and non-radiative processes.<sup>125,170</sup> The enhancement depends on the size of the metal nanoparticles, their distance to the UCNP surface, and the emission wavelength. Small nanoparticles cause a stronger enhancement,<sup>170</sup> and the emission of short wavelength light is more strongly enhanced than longer wavelengths.<sup>125,181</sup>

However, an emission enhancement by SPCE can only be observed for noble metal nanoparticles bound to the UCNP surface, whereas noble metal shells on the UCNP surface actually reduce the overall upconversion emission due to quenching effects.<sup>125</sup> The deposition of the noble metal shell can be performed either by *in situ* formation in presence of the UCNPs with thiols as the binding site<sup>123</sup> or by binding separately synthesized nanoparticles to the UCNP surface. Poly(allylamine hydrochloride) (PAH) can be deposited on PAA-coated UCNPs *via* electrostatic interactions to generate UCNPs with a positively charged surface. The PAH layer then serves as an electrostatic attachment site for negatively charged gold nanoparticles (Fig. 20).<sup>125</sup>



Table 8 UCNPs functionalized with dyes/quenchers

Application	Type of UCNP	$\lambda_{\text{em}}^a$ [nm]	Dye/Quencher	$\lambda_{\text{ex}}^b$ [nm]	$\lambda_{\text{em}}^b$ [nm]	Ref.
<i>In vivo</i> imaging	NaYF <sub>4</sub> :Yb,Er	545	Rhodamine B (RhB)	540	625	138
	NaYF <sub>4</sub> :Yb,Er	545	Rhodamine 6G (R6G)	526	555	
	NaYF <sub>4</sub> :Yb,Er	545	Tide Quencher 1 (TQ1)	490	—	
	NaYF <sub>4</sub> :Yb,Tm	—	d-Luciferin (caged)	365	560	171
	Y <sub>2</sub> O <sub>3</sub> :Yb,Er	—	Carbocyanine derivative	750	797	128
<i>In vitro</i> imaging	NaYF <sub>4</sub> :Yb,Tm	—	d-Luciferin	365	560	171
Color tuning	NaYF <sub>4</sub> :Yb,Er	545	Rhodamine B (RhB)	540	625	138
	NaYF <sub>4</sub> :Yb,Er	545	Rhodamine 6G (R6G)	526	555	
	NaYF <sub>4</sub> :Yb,Er	545	Tide Quencher 1 (TQ1)	490	—	
Self-referenced nanosensor	NaYF <sub>4</sub> :Yb,Er	—	2-(4-Aminophenylethyl)-5-methoxy-2-(2-pyridyl)thiazole (MPTEA)	350	430	136
Proof of principle	NaYF <sub>4</sub> :Yb,Er	540	Rhodamine B	540	625	18
	NaYF <sub>4</sub> :Yb,Er/NaYF <sub>4</sub> :Tm,Yb	—	BODIPY derivative	520	535	101
	NaYF <sub>4</sub> :Yb,Er/NaYF <sub>4</sub> :Yb,Tm	—	Phenoxazine derivative	590	625	

<sup>a</sup> UCNP emission wavelength absorbed by dye/quencher. <sup>b</sup> Excitation/emission wavelength of dye/quencher.

## 6. Tuning the emission of UCNPs

Organic fluorophores, gold nanoparticles and quantum dots that are bound to the nanoparticle surface can modulate the emission color of UCNPs.<sup>8,17,91,136,138</sup> There are two phenomena that account for the changes in the emission spectrum of UCNPs by surface-bound dyes: the inner filter effect<sup>105,182,183</sup> and luminescence resonance energy transfer (LRET).<sup>36,60,94</sup> An inner filter effect can be observed if the emission light of the UCNPs is reabsorbed by the surface-bound dye. By contrast, LRET relies on a non-radiative energy transfer. However, an unambiguous assignment of the emission spectra modulations is still a subject of controversy. The modified spectra of UCNPs by surface-bound dyes can be used for encoding which requires several spectrally distinct colors for the multiplexed detection of analytes.<sup>9</sup>

Also the design of sensors based on UCNPs and an analyte-specific dye relies on changes in the emission spectra. For example, a pH-sensitive dye such as bromothymol blue or phenol red on the surface of UCNPs can be used for sensing acids,<sup>182,183</sup> carbon dioxide,<sup>184</sup> or bases *e.g.* ammonia.<sup>185</sup> The color change of the pH-sensitive dye alters the emission spectra of the UCNPs by screening off one emission band while the other emission band remains unaffected and serves as a reference signal for ratiometric measurements.<sup>185</sup> For other sensor applications, the UCNPs can act as a nanolamp to excite the analyte-sensitive fluorophore. Oxygen is a strong quencher of fluorescence and can be detected in this way.<sup>186</sup> For example, the luminescence of an iridium(III) coumarin complex is strongly quenched by oxygen. Its absorbance spectrum overlaps with the blue emission of Tm<sup>3+</sup>-doped UCNPs and its emission spectrum does not overlap with the UCNPs emissions. The range of applications for dye-modified UCNPs is quite broad as shown in Table 8.

The attachment of organic dyes to the nanoparticle surface is an easy method to adjust the emission spectra. Organic dyes can

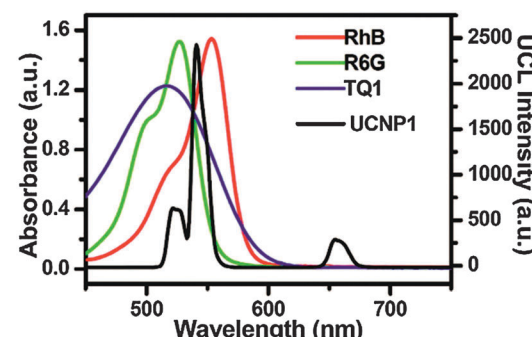


Fig. 21 Comparison of the UV-VIS absorption spectra of rhodamine B (RhB), rhodamine 6G (R6G), and Tide Quencher 1 (TQ1) and the emission spectra of NaYF<sub>4</sub>:Yb,Er. The overlapping spectra in the green range enable a luminescence energy transfer (LRET) from the UCNPs to the respective dye resulting in a decrease of the green emission of the UCNPs with rising dye concentration and an increase of the dye emission in the case of RhB and R6G. Reprinted with permission from ref. 138. Copyright © 2011, American Chemical Society.

be either bound covalently *via* appropriate functional groups<sup>136,171</sup> or non-covalently by enclosing the dye in a hydrophobic layer that also shields the dye from water.<sup>138</sup> The emission colors of UCNPs can be tuned by the absorption of one upconversion emission band by the dye to obtain several luminescent labels for bioanalytical applications. Also fluorescent dyes can be used to add emission bands to the spectrum (Fig. 21).<sup>138</sup>

Photoswitchable dyes can change the emission spectra of UCNPs. Photoswitchable dyes have two isomeric forms that show different absorption spectra and are transformed into each other by the excitation at a specific wavelength. For example, only the ring-closed isomer of a dithienylethenes derivative can absorb and thus decrease the green emission intensity of Er<sup>3+</sup>-doped UCNPs while the open isomer has no effect on the upconversion luminescence.<sup>187</sup>

Bioluminescent reagents can be bound to the UCNPs surface *via* established amine–carboxylic acid coupling reactions, both

in their natural and photocaged form. In photocaged d-luciferin, a photosensitive component blocks the bioluminescent reaction. Tm<sup>3+</sup>-doped UCNPs irradiated with NIR light emit UV light which uncages d-luciferin bound to the UCNPs surface. Free d-luciferin can then undergo a bioluminescent reaction with firefly luciferase. This technique is amenable to *in vivo* and *in vitro* applications<sup>171</sup>

Fluorescent dyes that are quenched by heavy metal ions can also be bound to UCNPs. While the fluorescence signal of the dye under UV excitation indicates the heavy metal concentration, the UCNPs luminescence under NIR irradiation remains nearly unchanged and thus serves as a reference signal.<sup>136</sup> It should be noted, however, that certain heavy metals can also quench the upconversion emission.<sup>188</sup>

## 7. Methods for the characterization of UCNPs

In particular for bioanalytical applications, it is important to confirm (1) that the surface of UCNPs has been successfully modified with a shell, functional groups and/or biomolecules and (2) that the upconversion efficiency and the colloidal stability in aqueous dispersions are not negatively affected by the modification. Depending on the type of functionalization, there are several techniques available. Some features of UCNPs can be monitored directly while others rely on indirect methods.

After synthesis, UCNPs typically display a homogeneous size and shape as spherical nanoparticles,<sup>100,101,118,163</sup> hexagonal plates<sup>18,71,73,116</sup> or nanocubes<sup>28</sup> observable by transmission electron microscopy (TEM). The morphology of UCNPs can be determined by X-ray diffraction (XRD).<sup>69,77</sup> According to the Scherrer equation, the peak width of the XRD diffractogram indicates the size of nanocrystals. XRD also provides information on the purity of the crystal phase of UCNPs.<sup>33,129,148</sup> For example, a complete conversion from a cubic to a hexagonal phase is necessary to enhance the upconversion efficiency of UCNPs. Similar information on the crystallinity of UCNPs can be gained by electron diffraction (ED).<sup>119,130</sup> High resolution transmission electron microscopy (HRTEM) can depict the spacing between crystallographic planes of the UCNPs and thus the crystal phase can be derived from this distance by comparison to crystallographic data.<sup>68,70,121,127</sup>

### 7.1 Size, shape and composition of core–shell UCNPs

While UCNPs can be synthesized in different sizes, a uniform size and shape in a single batch is essential because irregularly shaped UCNPs typically lead to a broad variability of functionalization accompanied by hindered target recognition or a loss of activity. The size and shape of UCNPs can change after growing a shell on the surface of UCNPs.<sup>23,66,136,143</sup> Transmission electron microscopy (TEM) is mainly used to determine the growth of a shell of silica, gold, or undoped host material since these materials are electron dense and provide a high TEM contrast.<sup>126,134,157,175</sup> TEM also provides information on the thickness and the composition of the shell provided that the core and the shell display a different contrast.<sup>31,125,152</sup> For very thin shells of less than 3 nm, high resolution TEM (HRTEM) is required. In

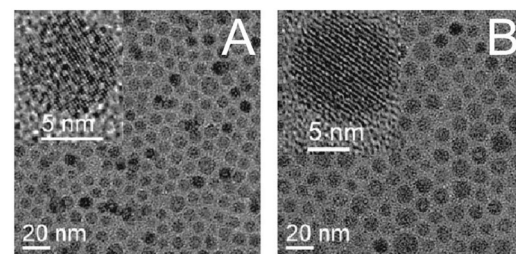


Fig. 22 TEM images of (A) core-only NaYF<sub>4</sub>:Yb,Er UCNPs and (B) core-shell UCNPs NaYF<sub>4</sub>:Yb,Er@NaYF<sub>4</sub>. The increase in diameter is attributed to the growth of an undoped host material shell on the surface of the core-only UCNPs. Reprinted with permission from ref. 70. Copyright © 2007, American Chemical Society.

contrast, an additional shell of host material is only visible by a size increase (Fig. 22) as the low lanthanide dopant concentration in the core material has a negligible influence on the electron density.

Scanning electron microscopy (SEM) and atomic force microscopy (AFM) can also be employed to determine the size and shape after growing a shell on UCNPs.<sup>128,129,171</sup> These techniques, however, only provide information on the surface structure but not on the shell thickness or composition.

A variation of TEM, high-angle annular dark-field imaging (HAADF), uses a special kind of scattered electron detector to distinguish between core and shell materials that differ in at least one type of atom.<sup>67,82</sup> TEM or SEM can also be combined with energy-dispersive X-ray spectrometry (EDS, EDXA) to simultaneously obtain information about the size, shape and composition of the shell as long as it has a different material composition as the core.<sup>68,127</sup> For example, a shell of silica displays a distinct EDS spectrum.<sup>3,13</sup> While it is possible to readily distinguish a shell of NaGdF<sub>4</sub> from a core of NaYF<sub>4</sub><sup>67,77,82</sup> (Fig. 23), coating with the same host material is only indicated by the ratio of two elements that are present in different concentration in the core and shell.<sup>65,70</sup>

Alternatively, TEM and electron energy loss spectroscopy (EELS) can be combined to differentiate between the material compositions of core and shell.<sup>67,75</sup> X-ray photoelectron spectroscopy (XPS) has a limited penetration depth and, thus, can be used for investigating the dopant composition of the shell only.<sup>31,84</sup>

While silica,<sup>12</sup> or silver<sup>123</sup> are easily detectable by XRD, coating with host material can only be detected reliably if core and shell have a different morphology.<sup>65</sup> The growth of a silica shell is also confirmed by the formation of distinct absorption bands in Fourier transform infrared (FTIR) or Raman spectroscopy.<sup>23,31,100,152,163</sup> The pore size of mesoporous silica can be determined by N<sub>2</sub> adsorption–desorption isotherms according to the Brunauer–Emmett–Teller (BET) theory.<sup>20</sup> This technique can also determine the amount of cargo load in mesoporous silica, which *e.g.* is important for drug delivery or photodynamic therapy.<sup>153</sup>

### 7.2 Analysis of surface ligands and biomolecules

In principle, the different types of elemental analysis are applicable to analyze modified silanes,<sup>101</sup> nanoparticles,<sup>121</sup> lanthanide-containing complexes<sup>147</sup> or the amount of complexed

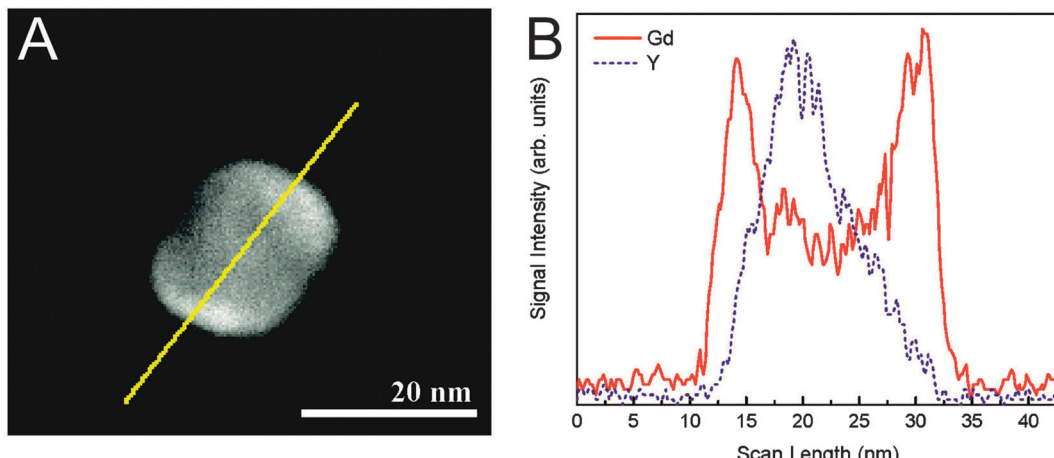


Fig. 23 (A) TEM image and (B) EDS scan of a  $\text{NaYF}_4$ @ $\text{NaGdF}_4$  nanoparticle. The yellow line represents the scan line. The EDS scan clearly shows the different material compositions of core and shell. Reprinted with permission from ref. 67. Copyright © 2011, American Chemical society.

ions on UCNPs, but the elementary composition of most organic compounds is too similar to distinguish them reliably. As the structure of UCNPs is not affected at high temperatures, the presence of ligands on the surface of UCNPs can be analyzed by thermogravimetric analysis (TGA). Weight changes at specific temperatures can indicate the amount and type of ligands on the UCNPs surface (Fig. 24).<sup>69,91,105,115,135,138</sup> However, a comparison with reference materials is required to identify the surface ligands. The density of the newly introduced surface ligands can also be assessed by TGA.<sup>33</sup>

A more accurate and specific determination of organic ligands and functional groups on the surface of UCNPs is achieved by Fourier transform infrared (FTIR) spectroscopy<sup>68,91,105,106,116,127</sup> or diffuse reflectance infrared (DRIFT) spectroscopy.<sup>21,101</sup> The surface functionalization can be confirmed either by the appearance of new absorption bands in the IR spectra<sup>33,64,93,128,129,136</sup> (Fig. 25) or the disappearance of absorption bands of former

surface ligands.<sup>12,23,31,64,136,139</sup> A difference spectrum derived from the FTIR spectra before and after the surface modification shows both types of information and allows for a simplified spectra evaluation.<sup>101</sup>

FTIR spectra are especially important for analyzing (multiple) ligand exchange reactions.<sup>32,100</sup> If the FTIR-peaks of the ligands before and after the modification overlap or are only slightly shifted, it is difficult to identify the ligand unambiguously (e.g. both ligands contain a carboxylate group).<sup>20,126</sup> However, since most surface ligands show more than one IR-absorption band, band shifts or overlapping peaks in combination with new or disappearing bands can still be used to proof the presence of a new surface ligand. Additionally, surface modifications can be analyzed by Raman spectroscopy<sup>71</sup> albeit with similar limitations as FTIR such as overlapping signals.

Nuclear magnetic resonance (NMR) can identify changes in the type and composition of surface ligands. However, since the  $^1\text{H}$  NMR spectra of the ligands are influenced by the lanthanide dopants (e.g.  $\text{Yb}^{3+}$ ,  $\text{Er}^{3+}$ , and  $\text{Tm}^{3+}$ ) in UCNPs,<sup>122</sup> typically undoped

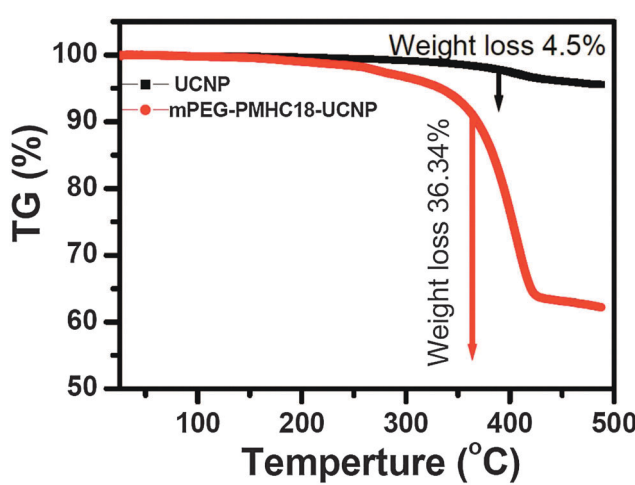


Fig. 24 Thermogravimetric analysis (TGA) curves of UCNPs coated with oleic acid (black curve) or PEG-PMHC<sub>18</sub> (red curve). The expected larger weight loss of PEG-coated UCNPs with 36.34% compared to unmodified UCNPs with only 4.5% is clearly observable. Reprinted with permission from ref. 138. Copyright © 2011, American Chemical Society.

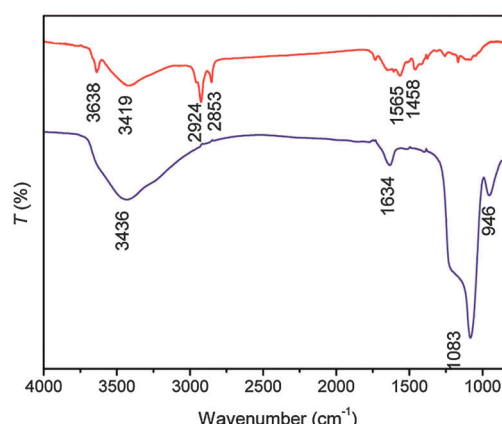


Fig. 25 FTIR spectra of unmodified  $\text{NaYbF}_4$ : $\text{Er}$  UCNPs (upper red curve) and silica-coated  $\text{NaYbF}_4$ : $\text{Er}$  UCNPs (lower blue curve). The strong new band at  $1083\text{ cm}^{-1}$  is assigned to stretching vibration of  $\text{Si}-\text{O}$ . Reprinted with permission from ref. 163. Copyright © 2009, American Chemical Society.



UCNPs are used to investigate the surface modification.<sup>10,28,122</sup> NMR can also differentiate between bound and unbound surface ligands due to a broadening of NMR signals after surface attachment.<sup>10,122</sup> This phenomenon has been attributed to a reduction of rotational freedom and to differing binding sites of the ligands on the nanoparticle surface, which influences the magnetic environment.<sup>28</sup> More sophisticated NMR techniques such as diffusion ordered spectroscopy (DOSY) and nuclear Overhauser effect spectroscopy (NOESY) enable a more refined distinction of bound and unbound surface ligands and a more precise determination of the surface coating of nanoparticles such as quantum dots or UCNPs.<sup>189–191</sup> While <sup>1</sup>H NMR<sup>28,116,122</sup> and <sup>13</sup>C NMR<sup>136</sup> spectra can be recorded for all ligands, the investigation of certain heteroatoms such as <sup>31</sup>P by NMR allows for a more specific recognition of surface ligands.<sup>10</sup>

As UCNPs are excited with NIR light, they do not interfere with the conventional optical detection of functional groups and biomolecules on their surface. Consequently, the surface modification with folic acid,<sup>15</sup> antibodies,<sup>164</sup> or oligonucleotides<sup>18</sup> can be identified by comparing the intrinsic UV absorption spectra of these biomolecules to unmodified UCNPs. Alternatively, functional groups on the UCNPs surface can be detected and quantified by using chromogenic reagents or fluorescent labels. For example, the amount of protein on the UCNPs surface can be determined by the micro bicinchoninic acid (BCA) assay.<sup>33</sup> A carbohydrate-modified UCNPs surface can be detected by using phenol sulfuric acid, which yields a yellow product ( $\lambda_{\text{max}} = 490$  nm).<sup>32</sup> The functionalization with azides or alkynes can be analyzed with high selectivity by using respective clickable fluorescent dyes.<sup>101</sup> Primary amines on the surface of UCNPs can be detected by ninhydrin (color change from blue to purple,  $\lambda_{\text{max}} = 565$  nm)<sup>12,22</sup> or trinitrobenzene sulfonic acid (TNBS, colored product,  $\lambda_{\text{max}} = 401$  nm).<sup>164</sup> Most of these detection reactions result in permanent modification of the functional groups, which is then not available for subsequent reactions or applications. By contrast, fluorenylmethoxycarbonyl (Fmoc) chloride, which is a standard protecting group in peptide

synthesis, is a reversible label for amines that can be removed to restore the free amine. The released Fmoc can then be quantified (Fig. 26).<sup>26,122</sup> The quantification of surface ligands by spectrometric methods, however, typically relies on a calibration with standard solutions, which may add some fluctuations to the measurements.<sup>22,32</sup>

### 7.3 Dispersibility and aggregation

The sensitivity and accuracy of bioanalytical measurements critically depend on the availability of non-aggregated and monodisperse UCNPs that are well dispersible in aqueous buffers. While TEM, SEM and AFM provide a detailed image of the UCNPs structure, these microscopic techniques require time-consuming sample preparation and measurements. Furthermore, images can be taken only after removing the dispersant and/or after attachment to the grid surface. Thus, it is essentially not possible to determine if clusters of UCNPs in the images are aggregates that were already present in dispersion or if they are an artifact that formed after drying or surface immobilization. In contrast to the real size and shape given by electron microscopy, dynamic light scattering (DLS)<sup>1,82,104,121</sup> can determine the hydrodynamic diameter,<sup>33,69,96,139</sup> which additionally includes the layer of surface ligands and/or solvent molecules on UCNPs. Another difference relates to the indirect size determination based on the Stokes–Einstein equation. Only if the dispersant viscosity, the refractive index of the UCNPs surface and the temperature are well defined it is possible to calculate the hydrodynamic diameter accurately. In addition to UCNPs, all nanoparticulate materials such as dust or proteins contribute to the size distribution of the sample and can lead to strong fluctuations. Thus, a careful sample handling and repeated measurements under well-defined conditions are crucial to obtain reliable results. It is also advisable to control the result of the DLS measurement for example by taking a TEM image of the sample.

Any type of surface modification can change the surface characteristics of UCNPs and thus lead to enhanced aggregation. While severe aggregation is typically observable by eye as a

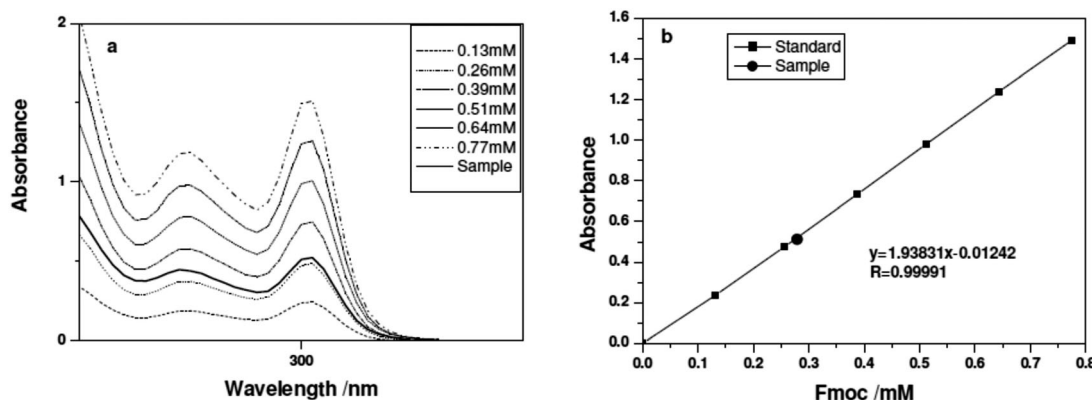


Fig. 26 Quantitative analysis of amine groups on the UCNPs surface via Fmoc labeling. After labeling the amines bound to the UCNPs surface with Fmoc and a washing step to remove excess Fmoc, the Fmoc group is cleaved from the amines. The Fmoc concentration of the sample is determined via UV spectroscopy (left) and the amine content can be calculated using calibration solutions (right). Reprinted with permission from ref. 122. Copyright © 2011, American Chemical Society.



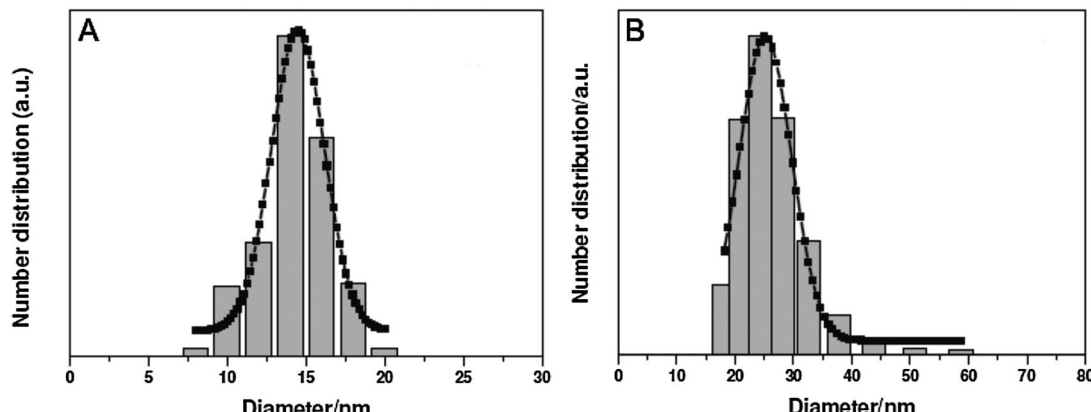


Fig. 27 DLS of UCNPs coated with oleylamine (A) and 6-aminohexanoic acid (B). The increase of the hydrodynamic diameter can be attributed to ligand change on the UCNPs surface from hydrophobic (low hydrodynamic diameter) to hydrophilic (high hydrodynamic diameter). Also the size distribution remains nearly unaffected indicating a surface modification without aggregation. Reprinted with permission from ref. 122. Copyright © 2011, American Chemical Society.

change in the sample's transparency<sup>14,16,17,64,70</sup> DLS is a much more sensitive method that can also analyze the size distribution of small aggregates. DLS is typically used to determine the long-time colloidal stability of UCNPs as well as the dispersibility after surface modification<sup>113,129,147,171</sup> (Fig. 27) or a change of the dispersant,<sup>33,96,139</sup> e.g. from water to buffer or serum.

The surface charge of UCNPs is one of the most decisive parameters for the colloidal stability that is strongly influenced by any surface modification step. The surface charge can be assessed indirectly and easily by measuring the zeta potential<sup>10,104</sup> – conveniently on the same instruments as DLS. Typically, a high negative or positive zeta potential is indicative of good colloidal stability. A reversal of the zeta potential is a strong indicator of a successful surface modification. In particular, layer-by-layer deposition is accompanied by a reversal of the surface charge and can thus be readily analyzed by zeta potential measurements.<sup>36</sup> A reversal of the zeta potential is also observed e.g. if uncoated UCNPs that expose positively charged lanthanide ions on their surface bind negatively charged ligands such as PAA<sup>70,93</sup> or if a silica shell is modified with neutral or positively charged silanes.<sup>71,164</sup> Also, the attachment of ions, e.g. Gd<sup>3+</sup>, to the UCNPs surface by either binding in a complex or cation exchange with surface lanthanide ions leads to a strongly increased positive zeta potential.<sup>113,122</sup> In many cases, however, zeta potential changes are less distinct because they can be influenced by variations in the experimental conditions.

The range of methods available for analyzing UCNPs – and nanoparticles in general – in dispersion is fairly limited and typically do not allow for purifying a polydisperse sample after surface modification. Agarose gel electrophoresis can be used for the separation of UCNPs exposing charged functional groups that cannot be easily stripped from the surface. For example, silica-coated UCNPs expose a negative surface charge due to the dissociation of silanol groups. The separation is also possible after performing a silanization reaction, e.g. with a carboxyl silane. Single silica-coated UCNPs can be separated from small nanoparticle clusters or larger aggregates, which

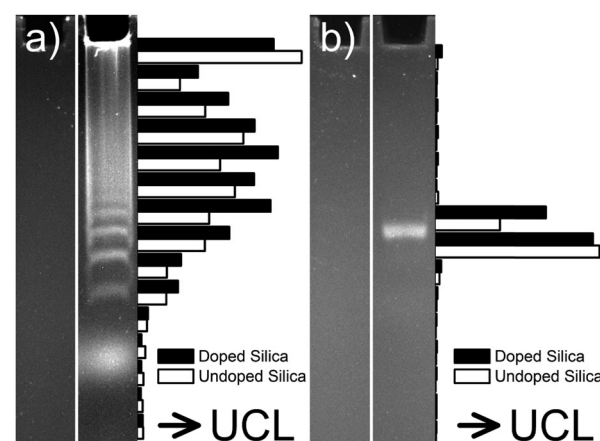


Fig. 28 Agarose gel electrophoresis reveals nanoparticle aggregation. (a) UCNPs coated with a bare silica shell are separated in several distinct bands, which can be attributed to discrete clusters of UCNPs. (b) Silica-coated UCNPs functionalized with carboxylic groups form only a single well-defined band of monodisperse UCNPs. Each panel shows silica-coated UCNPs without (left lane) and with (right lane) fluorescein that are directly visible in the gel under UV illumination. The UCNPs were recovered in suspension from separate gel sections to determine the upconversion luminescence (UCL). Essentially the same electrophoretic separation is observed for fluorescently doped UCNPs (full bars) and non-doped UCNPs (empty bars). Reprinted with permission from ref. 177. Copyright © 2014, American Chemical Society.

allows for analyzing aggregation in dispersion but also for the purification of the sample (Fig. 28).<sup>177</sup> After redispersion of the purified sample, monodisperse UCNPs can be used directly for bioanalytical applications or for subsequent modification steps.

#### 7.4 Characterization of hybrid nanoparticles

The surface modification of UCNPs by other nanoparticles or nanosheets and thus the formation of hybrid materials can be detected by TEM, XRD, or EDS<sup>121</sup> as described for core–shell structures. The exact size and position of these nanomaterials relative to the UCNPs can be determined by TEM. Silver,<sup>170</sup>

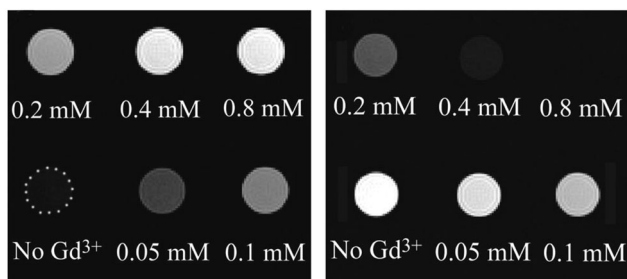


Fig. 29 MR images of  $\text{NaYF}_4@\text{SiO}_2$  functionalized with a  $\text{Gd}^{3+}$ -coordinating complex with varying gadolinium concentrations (left:  $T_1$ -weighted; right:  $T_2$ -weighted). The reference solution ("No  $\text{Gd}^{3+}$ ") contains the  $\text{NaYF}_4@\text{SiO}_2$  functionalized with the complex but without any coordinated  $\text{Gd}^{3+}$ . The  $\text{Gd}^{3+}$ -functionalized UCNPs are more applicable for  $T_1$ -weighted MRI. Reprinted with permission from ref. 147. Copyright © 2009, American Chemical Society.

gold<sup>125,136</sup> or magnetite ( $\text{Fe}_3\text{O}_4$ )<sup>121,167</sup> nanoparticles as well as nanosheets consisting of manganese dioxide ( $\text{MnO}_2$ )<sup>37</sup> are clearly observable in TEM images and also their composition can be determined by HR-TEM.<sup>121,136</sup> Furthermore, shells<sup>125</sup> or nanoparticles<sup>18,170</sup> of noble metals and deposited sheets of manganese dioxide<sup>37</sup> on the surface of UCNPs can be identified by UV/VIS spectroscopy.

UCNPs can also be rendered magnetic either by binding ferromagnetic materials to the surface or by using the intrinsically paramagnetic  $\text{Gd}^{3+}$  as a co-dopant. In the first case, typically the hysteresis curve and the concomitant changes in the magnetic saturation values are analyzed.<sup>63,128</sup> In the second case, the longitudinal (R1) and the transverse (R2) relaxivity of the paramagnetic UCNPs are investigated by magnetic resonance imaging (MRI) (Fig. 29).<sup>77,113,122,147,192</sup>

UCNPs labeled with radioactive isotopes constitute another type of hybrid nanoparticle that allows for a multimodal readout.<sup>117,122</sup> For example, thin-layer chromatography with autoradiography has been used to confirm the surface modification of UCNPs with the radioisotope  $^{18}\text{F}$ .<sup>122</sup>

## 7.5 Cytotoxicity

UCNPs of low cytotoxicity are especially important for *in vitro* or *in vivo* applications. UCNPs show only low toxic effects on cells or organisms. Their cytotoxicity rather depends on the surface modification. The MTT assay<sup>22,26,113,117,122</sup> and MTS assay<sup>14,128,170</sup> are similar techniques for measuring the cell viability in the presence of UCNPs. In the MTS assay, living cells reduce a colorless thiazolyl tetrazolium salt to insoluble formazan that absorbs light of 500–600 nm. Dead cells, by contrast, are not metabolic active and show no color change. The result of these assays also depends on the cell type, their growth rate and the assay conditions. Proliferating cells yield larger amounts of formazan than resting cells and the assay conditions can lead to fluctuations in the reductive reaction. Therefore, both the cell type and the assay conditions have to be chosen well in order to obtain reproducible results.

In contrast to the MTT/MTS assay, the sulforhodamine B (SRB) assay<sup>96</sup> is independent of the cell activity, since this dye

binds to basic amino acids in proteins located in the cytoplasm of cells. The cytotoxicity can also be determined by testing the integrity of the cell membrane with the lactate dehydrogenase (LDH) assay.<sup>14</sup> After membrane damage, the enzyme lactate dehydrogenase is released from the cells and leads to a consumption of NADH after adding pyruvate as a substrate. The decrease of the NADH concentration can be observed by photometry (absorption:  $\lambda = 340$  nm). In addition to the cytotoxicity assays, the toxicity of UCNPs on whole organisms can be investigated. For example, the biodistribution of UCNPs was analyzed by imaging the upconversion luminescence in the nematode worm *Caenorhabditis elegans*.<sup>139</sup> Furthermore, the distribution of UCNPs in small animals and their potential accumulation in organs is an important indicator of their toxicity. When UCNPs coated with citrate,<sup>117</sup> 6-hexanoic acid,<sup>122</sup> or PAA<sup>124</sup> are used for bioimaging studies in mice, larger amounts of UCNPs were found in the liver and spleen since these organs are major elimination routes of the circulatory system.

## 8. Conclusion

UCNPs have attracted much interest in the field of bioanalysis because they can be excited without background interference from biological materials and thus are a valuable alternative for conventional fluorescent labels. The background luminescence, however, is only one part of the overall background. The reduction of non-specific binding, aggregation and precipitation is at least equally important for the successful implementation of bioanalytical applications. The key to reducing these interferences lies in the optimized surface design of UCNPs.

Silanization of silica-coated UCNPs, ligand exchange reactions, and ligand interaction are currently the most prominent methods for generating UCNPs that form stable dispersions and can be further functionalized. Silanization yields a stable covalent attachment of functional groups that can be subsequently conjugated to various biomolecules, but silica entails aggregation over time. In a ligand exchange reaction, hydrophilic ligands typically compete with the densely packed oleic acid on the UCNPs surface. Hydrophilic ligands in their solvated form, however, have a higher surface energy and are more loosely packed than hydrophobic ligands. Consequently, ligand exchange reactions depend on a strong coordination to lanthanide ions to efficiently compete for the lanthanide binding sites on the surface of UCNPs. This thermodynamically unfavored reaction can be avoided if oleic acid is stripped from the surface in a first step to obtain "naked" UCNPs. However, also the long-term stability after ligand binding crucially depends on the stability of the surface coordination. Furthermore, the choice of an optimal surface ligand depends on its ability to reduce the surface quenching of the upconversion luminescence, its biocompatibility and cytotoxicity.

Another parameter that should be carefully selected is the dispersant. For example, the electrostatic repulsion conferred by partially deprotonated silanol ( $\text{pK}_a = 7.0$ ) has a strong influence on the colloidal stability of silica-coated UCNPs. At a high pH aggregation is reduced because the silanol groups are mainly deprotonated. Similarly, a buffer of high ionic strength can



interfere with the electrostatic repulsion and lead to faster aggregation. The same considerations also hold for UCNPs that are coated with ligands exposing ionic groups on the surface.

Great progress has been made in the design of highly luminescent UCNPs over recent years. There are, however, several reasons why UCNPs are not more widely applied in bioanalysis, yet, despite their obvious advantages. First, there are no commercial instruments specifically adapted for the characterization and readout of the upconversion luminescence. But equally important, there are no standardized protocols for the surface functionalization and characterization of UCNPs as discussed in this Review. Thus, collaborations between researchers working in different fields of the upconversion technology as well as industry are essential before UCNPs can find a wider distribution. A step into this direction has recently been made by implementing “The European Upconversion Network: From the design of photon-upconverting nanoparticles to biomedical applications”.

## Acknowledgements

We acknowledge the COST Action CM1403 funded by the European Union.

## References

- 1 F. Auzel, Upconversion Processes in Coupled Ion Systems, *J. Lumin.*, 1990, **45**(1–6), 341–345.
- 2 S. Heer, K. Kompe, H. U. Gudel and M. Haase, Highly efficient multicolour upconversion emission in transparent colloids of lanthanide-doped  $\text{NaYF}_4$  nanocrystals, *Adv. Mater.*, 2004, **16**(23–24), 2102–2105.
- 3 C. T. Xu, P. Svenmarker, H. C. Liu, X. Wu, M. E. Messing, L. R. Wallenberg and S. Andersson-Engels, High-Resolution Fluorescence Diffuse Optical Tomography Developed with Nonlinear Upconverting Nanoparticles, *ACS Nano*, 2012, **6**(6), 4788–4795.
- 4 J. C. Boyer and F. C. J. M. van Veggel, Absolute quantum yield measurements of colloidal  $\text{NaYF}_4:\text{Er}^{3+},\text{Yb}^{3+}$  upconverting nanoparticles, *Nanoscale*, 2010, **2**(8), 1417–1419.
- 5 A. D. Ostrowski, E. M. Chan, D. J. Gargas, E. M. Katz, G. Han, P. J. Schuck, D. J. Milliron and B. E. Cohen, Controlled Synthesis and Single-Particle Imaging of Bright, Sub-10 nm Lanthanide-Doped Upconverting Nanocrystals, *ACS Nano*, 2012, **6**(3), 2686–2692.
- 6 B. Dong, B. S. Cao, Y. Y. He, Z. Liu, Z. P. Li and Z. Q. Feng, Temperature Sensing and In Vivo Imaging by Molybdenum Sensitized Visible Upconversion Luminescence of Rare-Earth Oxides, *Adv. Mater.*, 2012, **24**(15), 1987–1993.
- 7 N. C. Dyck, F. C. J. M. van Veggel and G. P. Demopoulos, Size-Dependent Maximization of Upconversion Efficiency of Citrate-Stabilized ss-phase  $\text{NaYF}_4:\text{Yb}^{3+},\text{Er}^{3+}$  Crystals via Annealing, *ACS Appl. Mater. Interfaces*, 2013, **5**(22), 11661–11667.
- 8 M. Haase and H. Schafer, Upconverting Nanoparticles, *Angew. Chem., Int. Ed.*, 2011, **50**(26), 5808–5829.
- 9 H. H. Gorris and O. S. Wolfbeis, Photon-upconverting nanoparticles for optical encoding and multiplexing of cells, biomolecules, and microspheres, *Angew. Chem., Int. Ed.*, 2013, **52**(13), 3584–3600.
- 10 J. C. Boyer, M. P. Manseau, J. I. Murray and F. C. J. M. van Veggel, Surface Modification of Upconverting  $\text{NaYF}_4$  Nanoparticles with PEG-Phosphate Ligands for NIR (800 nm) Biolabeling within the Biological Window, *Langmuir*, 2010, **26**(2), 1157–1164.
- 11 D. K. Chatterjee, A. J. Rufalhah and Y. Zhang, Upconversion fluorescence imaging of cells and small animals using lanthanide doped nanocrystals, *Biomaterials*, 2008, **29**(7), 937–943.
- 12 H. Hu, L. Q. Xiong, J. Zhou, F. Y. Li, T. Y. Cao and C. H. Huang, Multimodal-Luminescence Core-Shell Nanocomposites for Targeted Imaging of Tumor Cells, *Chem. – Eur. J.*, 2009, **15**(14), 3577–3584.
- 13 N. M. Idris, Z. Q. Li, L. Ye, E. K. W. Sim, R. Mahendran, P. C. L. Ho and Y. Zhang, Tracking transplanted cells in live animal using upconversion fluorescent nanoparticles, *Biomaterials*, 2009, **30**(28), 5104–5113.
- 14 R. A. Jalil and Y. Zhang, Biocompatibility of silica coated  $\text{NaYF}_4$  upconversion fluorescent nanocrystals, *Biomaterials*, 2008, **29**(30), 4122–4128.
- 15 S. Jiang, Y. Zhang, K. M. Lim, E. K. W. Sim and L. Ye, NIR-to-visible upconversion nanoparticles for fluorescent labeling and targeted delivery of siRNA, *Nanotechnology*, 2009, **20**, 155101.
- 16 R. Kumar, M. Nyk, T. Y. Ohulchanskyy, C. A. Flask and P. N. Prasad, Combined Optical and MR Bioimaging Using Rare Earth Ion Doped  $\text{NaYF}_4$  Nanocrystals, *Adv. Funct. Mater.*, 2009, **19**(6), 853–859.
- 17 Z. Q. Li, Y. Zhang and S. Jiang, Multicolor Core/Shell-Structured Upconversion Fluorescent Nanoparticles, *Adv. Mater.*, 2008, **20**(24), 4765–4769.
- 18 L. L. Li, R. B. Zhang, L. L. Yin, K. Z. Zheng, W. P. Qin, P. R. Selvin and Y. Lu, Biomimetic Surface Engineering of Lanthanide-Doped Upconversion Nanoparticles as Versatile Bioprobes, *Angew. Chem., Int. Ed.*, 2012, **51**(25), 6121–6125.
- 19 F. Y. Liu, Q. Zhao, H. P. You and Z. X. Wang, Synthesis of stable carboxy-terminated  $\text{NaYF}_4:\text{Yb}^{3+},\text{Er}^{3+}$  @  $\text{SiO}_2$  nanoparticles with ultrathin shell for biolabeling applications, *Nanoscale*, 2013, **5**(3), 1047–1053.
- 20 H. S. Qian, H. C. Guo, P. C. L. Ho, R. Mahendran and Y. Zhang, Mesoporous-Silica-Coated Up-Conversion Fluorescent Nanoparticles for Photodynamic Therapy, *Small*, 2009, **5**(20), 2285–2290.
- 21 M. M. Rubner, D. E. Achatz, H. S. Mader, J. A. Stolwijk, J. Wegener, G. S. Harms, O. S. Wolfbeis and H. A. Wagenknecht, DNA “Nanolamps”: “Clicked” DNA Conjugates with Photon Upconverting Nanoparticles as Highly Emissive Biomaterial, *ChemPlusChem*, 2012, **77**(2), 129–134.
- 22 J. N. Shan, J. B. Chen, J. Meng, J. Collins, W. Soboyejo, J. S. Friedberg and Y. G. Ju, Biofunctionalization,

cytotoxicity, and cell uptake of lanthanide doped hydrophobically ligated  $\text{NaYF}_4$  upconversion nanophosphors, *J. Appl. Phys.*, 2008, **104**, 094308.

23 M. Wang, C. C. Mi, W. X. Wang, C. H. Liu, Y. F. Wu, Z. R. Xu, C. B. Mao and S. K. Xu, Immunolabeling and NIR-Excited Fluorescent Imaging of HeLa Cells by Using  $\text{NaYF}_4:\text{Yb},\text{Er}$  Upconversion Nanoparticles, *ACS Nano*, 2009, **3**(6), 1580–1586.

24 S. W. Wu, G. Han, D. J. Milliron, S. Aloni, V. Alton, D. V. Talapin, B. E. Cohen and P. J. Schuck, Non-blinking and photostable upconverted luminescence from single lanthanide-doped nanocrystals, *Proc. Natl. Acad. Sci. U. S. A.*, 2009, **106**(27), 10917–10921.

25 L. Q. Xiong, Z. G. Chen, M. X. Yu, F. Y. Li, C. Liu and C. H. Huang, Synthesis, characterization, and in vivo targeted imaging of amine-functionalized rare-earth up-converting nanophosphors, *Biomaterials*, 2009, **30**(29), 5592–5600.

26 L. Q. Xiong, Z. G. Chen, Q. W. Tian, T. Y. Cao, C. J. Xu and F. Y. Li, High Contrast Upconversion Luminescence Targeted Imaging in Vivo Using Peptide-Labeled Nanophosphors, *Anal. Chem.*, 2009, **81**(21), 8687–8694.

27 M. X. Yu, F. Y. Li, Z. G. Chen, H. Hu, C. Zhan, H. Yang and C. H. Huang, Laser Scanning Up-Conversion Luminescence Microscopy for Imaging Cells Labeled with Rare-Earth Nanophosphors, *Anal. Chem.*, 2009, **81**(3), 930–935.

28 Z. G. Chen, H. L. Chen, H. Hu, M. X. Yu, F. Y. Li, Q. Zhang, Z. G. Zhou, T. Yi and C. H. Huang, Versatile synthesis strategy for carboxylic acid-functionalized upconverting nanophosphors as biological labels, *J. Am. Chem. Soc.*, 2008, **130**(10), 3023–3029.

29 M. Kumar, Y. Guo and P. Zhang, Highly sensitive and selective oligonucleotide sensor for sickle cell disease gene using photon upconverting nanoparticles, *Biosens. Bioelectron.*, 2009, **24**(5), 1522–1526.

30 T. Rantanen, M. L. Jarvenpaa, J. Vuojola, R. Arppe, K. Kuningas and T. Soukka, Upconverting phosphors in a dual-parameter LRET-based hybridization assay, *Analyst*, 2009, **134**(8), 1713–1716.

31 M. Wang, W. Hou, C. C. Mi, W. X. Wang, Z. R. Xu, H. H. Teng, C. B. Mao and S. K. Xu, Immunoassay of Goat Antihuman Immunoglobulin G Antibody Based on Luminescence Resonance Energy Transfer between Near-Infrared Responsive  $\text{NaYF}_4:\text{Yb},\text{Er}$  Upconversion Fluorescent Nanoparticles and Gold Nanoparticles, *Anal. Chem.*, 2009, **81**(21), 8783–8789.

32 N. Bogdan, F. Vetrone, R. Roy and J. A. Capobianco, Carbohydrate-coated lanthanide-doped upconverting nanoparticles for lectin recognition, *J. Mater. Chem.*, 2010, **20**(35), 7543–7550.

33 M. Kamimura, D. Miyamoto, Y. Saito, K. Soga and Y. Nagasaki, Design of poly(ethylene glycol)/streptavidin coimmobilized upconversion nanophosphors and their application to fluorescence biolabeling, *Langmuir*, 2008, **24**(16), 8864–8870.

34 Y. Liu, T. Kobayashi, M. Iizuka, T. Tanaka, I. Sotokawa, A. Shimoyama, Y. Murayama, E. Otsuji, S. Ogura and H. Yuasa, Sugar-attached upconversion lanthanide nanoparticles: a novel tool for high-throughput lectin assay, *Bioorg. Med. Chem.*, 2013, **21**(11), 2832–2842.

35 M. Kumar and P. Zhang, Highly Sensitive and Selective Label-Free Optical Detection of DNA Hybridization Based on Photon Upconverting Nanoparticles, *Langmuir*, 2009, **25**(11), 6024–6027.

36 L. Y. Wang, R. X. Yan, Z. Y. Hao, L. Wang, J. H. Zeng, H. Bao, X. Wang, Q. Peng and Y. D. Li, Fluorescence resonant energy transfer biosensor based on upconversion-luminescent nanoparticles, *Angew. Chem., Int. Ed.*, 2005, **44**(37), 6054–6057.

37 R. R. Deng, X. J. Xie, M. Vendrell, Y. T. Chang and X. G. Liu, Intracellular Glutathione Detection Using  $\text{MnO}_2$ -Nanosheet-Modified Upconversion Nanoparticles, *J. Am. Chem. Soc.*, 2011, **133**(50), 20168–20171.

38 Y. H. Wang, L. Bao, Z. H. Liu and D. W. Pang, Aptamer Biosensor Based on Fluorescence Resonance Energy Transfer from Upconverting Phosphors to Carbon Nanoparticles for Thrombin Detection in Human Plasma, *Anal. Chem.*, 2011, **83**(21), 8130–8137.

39 Y. H. Wang, P. Shen, C. Y. Li, Y. Y. Wang and Z. H. Liu, Upconversion Fluorescence Resonance Energy Transfer Based Biosensor for Ultrasensitive Detection of Matrix Metalloproteinase-2 in Blood, *Anal. Chem.*, 2012, **84**(3), 1466–1473.

40 H. S. Mader, P. Kele, S. M. Saleh and O. S. Wolfbeis, Upconverting luminescent nanoparticles for use in bioconjugation and bioimaging, *Curr. Opin. Chem. Biol.*, 2010, **14**(5), 582–596.

41 P. Y. Qiu, N. Zhou, H. Y. Chen, C. L. Zhang, G. Gao and D. X. Cui, Recent advances in lanthanide-doped upconversion nanomaterials: synthesis, nanostructures and surface modification, *Nanoscale*, 2013, **5**(23), 11512–11525.

42 G. Y. Chen, H. L. Qiu, P. N. Prasad and X. Y. Chen, Upconversion Nanoparticles: Design, Nanochemistry, and Applications in Theranostics, *Chem. Rev.*, 2014, **114**(10), 5161–5214.

43 S. L. Gai, C. X. Li, P. P. Yang and J. Lin, Recent Progress in Rare Earth Micro/Nanocrystals: Soft Chemical Synthesis, Luminescent Properties, and Biomedical Applications, *Chem. Rev.*, 2014, **114**(4), 2343–2389.

44 Z. J. Gu, L. Yan, G. Tian, S. J. Li, Z. F. Chai and Y. L. Zhao, Recent Advances in Design and Fabrication of Upconversion Nanoparticles and Their Safe Theranostic Applications, *Adv. Mater.*, 2013, **25**(28), 3758–3779.

45 G. S. Yi, H. C. Lu, S. Y. Zhao, G. Yue, W. J. Yang, D. P. Chen and L. H. Guo, Synthesis, characterization, and biological application of size-controlled nanocrystalline  $\text{NaYF}_4:\text{Yb},\text{Er}$  infrared-to-visible up-conversion phosphors, *Nano Lett.*, 2004, **4**(11), 2191–2196.

46 Y. Wei, F. Q. Lu, X. R. Zhang and D. P. Chen, Synthesis and characterization of efficient near-infrared upconversion Yb and Tm codoped  $\text{NaYF}_4$  nanocrystal reporter, *J. Alloys Compd.*, 2007, **427**(1–2), 333–340.

47 Z. Q. Li and Y. Zhang, An efficient and user-friendly method for the synthesis of hexagonal-phase  $\text{NaYF}_4:\text{Yb},\text{Er}/\text{Tm}$

nanocrystals with controllable shape and upconversion fluorescence, *Nanotechnology*, 2008, **19**, 345606.

48 J. C. Boyer, F. Vetrone, L. A. Cuccia and J. A. Capobianco, Synthesis of colloidal upconverting  $\text{NaYF}_4$  nanocrystals doped with  $\text{Er}^{3+}$ ,  $\text{Yb}^{3+}$  and  $\text{Tm}^{3+}$ ,  $\text{Yb}^{3+}$  via thermal decomposition of lanthanide trifluoroacetate precursors, *J. Am. Chem. Soc.*, 2006, **128**(23), 7444–7445.

49 J. Shan, X. Qin, N. Yao and Y. Ju, Synthesis of monodisperse hexagonal  $\text{NaYF}_4:\text{Yb},\text{Ln}$  ( $\text{Ln} = \text{Er}$ ,  $\text{Ho}$  and  $\text{Tm}$ ) upconversion nanocrystals in TOPO, *Nanotechnology*, 2007, **18**, 445607.

50 H. Q. Wang and T. Nann, Monodisperse Upconverting Nanocrystals by Microwave-Assisted Synthesis, *ACS Nano*, 2009, **3**(11), 3804–3808.

51 H. W. Rhee, C. R. Lee, S. H. Cho, M. R. Song, M. Cashel, H. E. Choy, Y. J. Seok and J. I. Hong, Selective fluorescent chemosensor for the bacterial alarmone (p)ppGpp, *J. Am. Chem. Soc.*, 2008, **130**(3), 784–785.

52 O. Ehler, R. Thomann, M. Darbandi and T. Nann, A four-color colloidal multiplexing nanoparticle system, *ACS Nano*, 2008, **2**(1), 120–124.

53 G. F. Wang, Q. Peng and Y. D. Li, Upconversion Luminescence of Monodisperse  $\text{CaF}_2:\text{Yb}^{3+}/\text{Er}^{3+}$  Nanocrystals, *J. Am. Chem. Soc.*, 2009, **131**(40), 14200–14201.

54 J. Yang, C. M. Zhang, C. Peng, C. X. Li, L. L. Wang, R. T. Chai and J. Lin, Controllable Red, Green, Blue (RGB) and Bright White Upconversion Luminescence of  $\text{Lu}_2\text{O}_3:\text{Yb}^{3+}/\text{Er}^{3+}/\text{Tm}^{3+}$  Nanocrystals through Single Laser Excitation at 980 nm, *Chem. – Eur. J.*, 2009, **15**(18), 4649–4655.

55 Y. S. Liu, D. T. Tu, H. M. Zhu and X. Y. Chen, Lanthanide-doped luminescent nanoprobe: controlled synthesis, optical spectroscopy, and bioapplications, *Chem. Soc. Rev.*, 2013, **42**(16), 6924–6958.

56 L. W. Yang, H. L. Han, Y. Y. Zhang and J. X. Zhong, White Emission by Frequency Up-Conversion in  $\text{Yb}^{3+}-\text{Ho}^{3+}-\text{Tm}^{3+}$  Triply Doped Hexagonal  $\text{NaYF}_4$  Nanorods, *J. Phys. Chem. C*, 2009, **113**(44), 18995–18999.

57 G. Y. Chen, H. C. Liu, G. Somesfalean, H. J. Liang and Z. G. Zhang, Upconversion emission tuning from green to red in  $\text{Yb}^{3+}/\text{Ho}^{3+}$ -codoped  $\text{NaYF}_4$  nanocrystals by tridoping with  $\text{Ce}^{3+}$  ions, *Nanotechnology*, 2009, **20**, 385704.

58 H. J. Liang, G. Y. Chen, L. Li, Y. Liu, F. Qin and Z. G. Zhang, Upconversion luminescence in  $\text{Yb}^{3+}/\text{Tb}^{3+}$ -codoped monodisperse  $\text{NaYF}_4$  nanocrystals, *Opt. Commun.*, 2009, **282**(14), 3028–3031.

59 X. Wang, J. Zhuang, Q. Peng and Y. D. Li, Hydrothermal synthesis of rare-earth fluoride nanocrystals, *Inorg. Chem.*, 2006, **45**(17), 6661–6665.

60 C. L. Zhang, Y. X. Yuan, S. M. Zhang, Y. H. Wang and Z. H. Liu, Biosensing Platform Based on Fluorescence Resonance Energy Transfer from Upconverting Nanocrystals to Graphene Oxide, *Angew. Chem., Int. Ed.*, 2011, **50**(30), 6851–6854.

61 A. Patra, C. S. Friend, R. Kapoor and P. N. Prasad, Upconversion in  $\text{Er}^{3+}:\text{ZrO}_2$  nanocrystals, *J. Phys. Chem. B*, 2002, **106**(8), 1909–1912.

62 Y. X. Liu, W. A. Pisarski, S. J. Zeng, C. F. Xu and Q. B. Yang, Tri-color upconversion luminescence of Rare earth doped  $\text{BaTiO}_3$  nanocrystals and lowered color separation, *Opt. Express*, 2009, **17**(11), 9089–9098.

63 G. GlasPELL, J. Anderson, J. R. Wilkins and M. S. Ei-Shall, Vapor phase synthesis of upconverting  $\text{Y}_2\text{O}_3$  nanocrystals doped with  $\text{Yb}^{3+}$ ,  $\text{Er}^{3+}$ ,  $\text{Ho}^{3+}$ , and  $\text{Tm}^{3+}$  to generate red, green, blue, and white light, *J. Phys. Chem. C*, 2008, **112**(30), 11527–11531.

64 C. Liu, H. Wang, X. Li and D. Chen, Monodisperse, size-tunable and highly efficient  $\beta\text{-NaYF}_4:\text{Yb},\text{Er}(\text{Tm})$  upconversion luminescent nanospheres: controllable synthesis and their surface modifications, *J. Mater. Chem.*, 2009, **19**(21), 3546–3553.

65 H. X. Mai, Y. W. Zhang, L. D. Sun and C. H. Yan, Highly efficient multicolor up-conversion emissions and their mechanisms of monodisperse  $\text{NaYF}_4:\text{Yb},\text{Er}$  core and core/shell-structured nanocrystals, *J. Phys. Chem. C*, 2007, **111**(37), 13721–13729.

66 Y. Wang, L. P. Tu, J. W. Zhao, Y. J. Sun, X. G. Kong and H. Zhang, Upconversion Luminescence of  $\beta\text{-NaYF}_4:\text{Yb}^{3+},\text{Er}^{3+}$  @ $\beta\text{-NaYF}_4$  Core/Shell Nanoparticles: Excitation Power, Density and Surface Dependence, *J. Phys. Chem. C*, 2009, **113**(17), 7164–7169.

67 K. A. Abel, J. C. Boyer, C. M. Andrei and F. C. J. M. van Veggel, Analysis of the Shell Thickness Distribution on  $\text{NaYF}_4/\text{NaGdF}_4$  Core/Shell Nanocrystals by EELS and EDS, *J. Phys. Chem. Lett.*, 2011, **2**(3), 185–189.

68 D. Q. Chen, Y. L. Yu, F. Huang, H. Lin, P. Huang, A. P. Yang, Z. X. Wang and Y. S. Wang, Lanthanide dopant-induced formation of uniform sub-10 nm active-core/active-shell nanocrystals with near-infrared to near-infrared dual-modal luminescence, *J. Mater. Chem.*, 2012, **22**(6), 2632–2640.

69 H. Schäfer, P. Ptacek, K. Kompe and M. Haase, Lanthanide-doped  $\text{NaYF}_4$  nanocrystals in aqueous solution displaying strong up-conversion emission, *Chem. Mater.*, 2007, **19**(6), 1396–1400.

70 G. S. Yi and G. M. Chow, Water-soluble  $\text{NaYF}_4:\text{Yb},\text{Er}(\text{Tm})/\text{NaYF}_4/\text{polymer}$  core/shell/shell nanoparticles with significant enhancement of upconversion fluorescence, *Chem. Mater.*, 2007, **19**(3), 341–343.

71 R. B. Liebherr, T. Soukka, O. S. Wolfbeis and H. H. Gorris, Maleimide activation of photon upconverting nanoparticles for bioconjugation, *Nanotechnology*, 2012, **23**, 485103.

72 F. Wang, J. A. Wang and X. G. Liu, Direct Evidence of a Surface Quenching Effect on Size-Dependent Luminescence of Upconversion Nanoparticles, *Angew. Chem., Int. Ed.*, 2010, **49**(41), 7456–7460.

73 D. Q. Chen, L. Lei, A. P. Yang, Z. X. Wang and Y. S. Wang, Ultra-broadband near-infrared excitable upconversion core/shell nanocrystals, *Chem. Commun.*, 2012, **48**(47), 5898–5900.

74 F. Vetrone, R. Naccache, V. Mahalingam, C. G. Morgan and J. A. Capobianco, The Active-Core/Active-Shell Approach: A Strategy to Enhance the Upconversion Luminescence in



Lanthanide-Doped Nanoparticles, *Adv. Funct. Mater.*, 2009, **19**(18), 2924–2929.

75 F. Wang, R. R. Deng, J. Wang, Q. X. Wang, Y. Han, H. M. Zhu, X. Y. Chen and X. G. Liu, Tuning upconversion through energy migration in core-shell nanoparticles, *Nat. Mater.*, 2011, **10**(12), 968–973.

76 D. M. Yang, C. X. Li, G. G. Li, M. M. Shang, X. J. Kang and J. Lin, Colloidal synthesis and remarkable enhancement of the upconversion luminescence of  $\text{BaGdF}_5:\text{Yb}^{3+}/\text{Er}^{3+}$  nanoparticles by active-shell modification, *J. Mater. Chem.*, 2011, **21**(16), 5923–5927.

77 H. Guo, Z. Q. Li, H. S. Qian, Y. Hu and I. N. Muhammad, Seed-mediated synthesis of  $\text{NaYF}_4:\text{Yb},\text{Er}/\text{NaGdF}_4$  nanocrystals with improved upconversion fluorescence and MR relaxivity, *Nanotechnology*, 2010, **21**, 125602.

78 X. X. Cui, J. B. She, C. Gao, K. Cui, C. Q. Hou, W. Wei and B. Peng, Luminescent properties of  $\text{Nd}^{3+}$ -doped  $\text{LaF}_3$  core/shell nanoparticles with enhanced near infrared (NIR) emission, *Chem. Phys. Lett.*, 2010, **494**(1–3), 60–63.

79 X. B. Chen, Y. B. Lou, A. C. Samia and C. Burda, Coherency strain effects on the optical response of core/shell hetero-nanostructures, *Nano Lett.*, 2003, **3**(6), 799–803.

80 G. C. Jiang, J. Pichaandi, N. J. J. Johnson, R. D. Burke and F. C. J. M. van Veggel, An Effective Polymer Cross-Linking Strategy To Obtain Stable Dispersions of Upconverting  $\text{NaYF}_4$  Nanoparticles in Buffers and Biological Growth Media for Biolabeling Applications, *Langmuir*, 2012, **28**(6), 3239–3247.

81 C. J. Carling, F. Nourmohammadian, J. C. Boyer and N. R. Branda, Remote-Control Photorelease of Caged Compounds Using Near-Infrared Light and Upconverting Nanoparticles, *Angew. Chem., Int. Ed.*, 2010, **49**(22), 3782–3785.

82 G. Y. Chen, J. Shen, T. Y. Ohulchanskyy, N. J. Patel, A. Kutikov, Z. P. Li, J. Song, R. K. Pandey, H. Agren, P. N. Prasad and G. Han,  $\alpha\text{-NaYbF}_4:\text{Tm}^{3+}/\text{CaF}_2$  Core/Shell Nanoparticles with Efficient Near-Infrared to Near-Infrared Upconversion for High-Contrast Deep Tissue Bioimaging, *ACS Nano*, 2012, **6**(9), 8280–8287.

83 H. Schäfer, P. Ptacek, O. Zerzouf and M. Haase, Synthesis and Optical Properties of  $\text{KYF}_4/\text{Yb},\text{Er}$  Nanocrystals, and their Surface Modification with Undoped  $\text{KYF}_4$ , *Adv. Funct. Mater.*, 2008, **18**(19), 2913–2918.

84 H. S. Qian and Y. Zhang, Synthesis of Hexagonal-Phase Core-Shell  $\text{NaYF}_4$  Nanocrystals with Tunable Upconversion Fluorescence, *Langmuir*, 2008, **24**(21), 12123–12125.

85 J. C. Boyer, C. J. Carling, B. D. Gates and N. R. Branda, Two-Way Photoswitching Using One Type of Near-Infrared Light, Upconverting Nanoparticles, and Changing Only the Light Intensity, *J. Am. Chem. Soc.*, 2010, **132**(44), 15766–15772.

86 F. Vetrone, J. C. Boyer, J. A. Capobianco, A. Speghini and M. Bettinelli, Effect of  $\text{Yb}^{3+}$  codoping on the upconversion emission in nanocrystalline  $\text{Y}_2\text{O}_3:\text{Er}^{3+}$ , *J. Phys. Chem. B*, 2003, **107**(5), 1107–1112.

87 F. Vetrone, J. C. Boyer, J. A. Capobianco, A. Speghini and M. Bettinelli, Significance of  $\text{Yb}^{3+}$  concentration on the upconversion mechanisms in codoped  $\text{Y}_2\text{O}_3:\text{Er}^{3+},\text{Yb}^{3+}$  nanocrystals, *J. Appl. Phys.*, 2004, **96**(1), 661–667.

88 X. J. Xie, N. Y. Gao, R. R. Deng, Q. Sun, Q. H. Xu and X. G. Liu, Mechanistic Investigation of Photon Upconversion in  $\text{Nd}^{3+}$ -Sensitized Core-Shell Nanoparticles, *J. Am. Chem. Soc.*, 2013, **135**(34), 12608–12611.

89 J. Shen, G. Y. Chen, A. M. Vu, W. Fan, O. S. Bilsel, C. C. Chang and G. Han, Engineering the Upconversion Nanoparticle Excitation Wavelength: Cascade Sensitization of Tri-doped Upconversion Colloidal Nanoparticles at 800 nm, *Adv. Opt. Mater.*, 2013, **1**(9), 644–650.

90 Q. Q. Zhan, J. Qian, H. J. Liang, G. Somesfalean, D. Wang, S. L. He, Z. G. Zhang and S. Andersson-Engels, Using 915 nm Laser Excited  $\text{Tm}^{3+}/\text{Er}^{3+}/\text{Ho}^{3+}$ -Doped  $\text{NaYbF}_4$  Upconversion Nanoparticles for in Vitro and Deeper in Vivo Bioimaging without Overheating Irradiation, *ACS Nano*, 2011, **5**(5), 3744–3757.

91 H. H. Gorris, R. Ali, S. M. Saleh and O. S. Wolfbeis, Tuning the Dual Emission of Photon-Upconverting Nanoparticles for Ratiometric Multiplexed Encoding, *Adv. Mater.*, 2011, **23**(14), 1652–1655.

92 F. Wang and X. G. Liu, Upconversion multicolor fine-tuning: visible to near-infrared emission from lanthanide-doped  $\text{NaYF}_4$  nanoparticles, *J. Am. Chem. Soc.*, 2008, **130**(17), 5642–5643.

93 T. Konishi, M. Yamada, K. Soga, D. Matsuura and Y. Nagasaki, PEG-based surface modification on upconversion nanophosphors for bio-imaging under IR excitation, *J. Photopolym. Sci. Technol.*, 2006, **19**(2), 145–149.

94 K. Kuningas, T. Ukonaho, H. Pakkila, T. Rantanen, J. Rosenberg, T. Lovgren and T. Soukka, Upconversion fluorescence resonance energy transfer in a homogeneous immunoassay for estradiol, *Anal. Chem.*, 2006, **78**(13), 4690–4696.

95 S. Liang, X. Zhang, Z. N. Wu, Y. Liu, H. Zhang, H. Z. Sun, H. C. Sun and B. Yang, Decoration of up-converting  $\text{NaYF}_4:\text{Yb},\text{Er}(\text{Tm})$  nanoparticles with surfactant bilayer. A versatile strategy to perform oil-to-water phase transfer and subsequently surface silication, *CrystEngComm*, 2012, **14**(10), 3484–3489.

96 J. N. Shan, S. J. Budijono, G. H. Hu, N. Yao, Y. B. Kang, Y. G. Ju and R. K. Prud'homme, Pegylated Composite Nanoparticles Containing Upconverting Phosphors and meso-Tetraphenyl porphine (TPP) for Photodynamic Therapy, *Adv. Funct. Mater.*, 2011, **21**(13), 2488–2495.

97 T. Soukka, T. Rantanen and K. Kuningas, Photon upconversion in homogeneous fluorescence-based bioanalytical assays, *Fluorescence Methods and Applications: Spectroscopy, Imaging, and Probes*, 2008, **1130**, 188–200.

98 Y. Wei, F. Q. Lu, X. R. Zhang and D. P. Chen, Polyol-mediated synthesis and luminescence of lanthanide-doped  $\text{NaYF}_4$  nanocrystal upconversion phosphors, *J. Alloys Compd.*, 2008, **455**(1–2), 376–384.

99 R. Naccache, F. Vetrone, V. Mahalingam, L. A. Cuccia and J. A. Capobianco, Controlled Synthesis and Water Dispersibility of Hexagonal Phase  $\text{NaGdF}_4:\text{Ho}^{3+}/\text{Yb}^{3+}$  Nanoparticles, *Chem. Mater.*, 2009, **21**(4), 717–723.

100 N. J. J. Johnson, N. M. Sangeetha, J. C. Boyer and F. C. J. M. van Veggel, Facile ligand-exchange with polyvinylpyrrolidone and subsequent silica coating of hydrophobic upconverting  $\beta$ -NaYF<sub>4</sub>:Yb<sup>3+</sup>/Er<sup>3+</sup> nanoparticles, *Nanoscale*, 2010, **2**(5), 771–777.

101 H. S. Mader, M. Link, D. E. Achatz, K. Uhlmann, X. H. Li and O. S. Wolfbeis, Surface-Modified Upconverting Micro-particles and Nanoparticles for Use in Click Chemistries, *Chem. – Eur. J.*, 2010, **16**(18), 5416–5424.

102 T. Y. Cao, Y. Yang, Y. A. Gao, J. Zhou, Z. Q. Li and F. Y. Li, High-quality water-soluble and surface-functionalized upconversion nanocrystals as luminescent probes for bio-imaging, *Biomaterials*, 2011, **32**(11), 2959–2968.

103 Z. Tian, G. Y. Chen, X. Li, H. J. Liang, Y. S. Li, Z. G. Zhang and Y. Tian, Autofluorescence-free *in vivo* multicolor imaging using upconversion fluoride nanocrystals, *Laser Med. Sci.*, 2010, **25**(4), 479–484.

104 J. W. Zhao, Y. J. Sun, X. G. Kong, L. J. Tian, Y. Wang, L. P. Tu, J. L. Zhao and H. Zhang, Controlled Synthesis, Formation Mechanism, and Great Enhancement of Red Upconversion Luminescence of NaYF<sub>4</sub>:Yb<sup>3+</sup>,Er<sup>3+</sup> Nanocrystals/Submicroplates at Low Doping Level, *J. Phys. Chem. B*, 2008, **112**(49), 15666–15672.

105 S. M. Saleh, R. Ali, T. Hirsch and O. S. Wolfbeis, Detection of biotin-avidin affinity binding by exploiting a self-referenced system composed of upconverting luminescent nanoparticles and gold nanoparticles, *J. Nanopart. Res.*, 2011, **13**(10), 4603–4611.

106 H. L. Qiu, G. Y. Chen, L. Sun, S. W. Hao, G. Han and C. H. Yang, Ethylenediaminetetraacetic acid (EDTA)-controlled synthesis of multicolor lanthanide doped BaYF<sub>5</sub> upconversion nanocrystals, *J. Mater. Chem.*, 2011, **21**(43), 17202–17208.

107 Z. Q. Li and Y. Zhang, Monodisperse silica-coated polyvinylpyrrolidone/NaYF<sub>4</sub> nanocrystals with multicolor upconversion fluorescence emission, *Angew. Chem., Int. Ed.*, 2006, **45**(46), 7732–7735.

108 J. H. Zeng, J. Su, Z. H. Li, R. X. Yan and Y. D. Li, Synthesis and upconversion luminescence of hexagonal-phase NaYF<sub>4</sub>:Yb<sup>3+</sup>,Er<sup>3+</sup>, phosphors of controlled size and morphology, *Adv. Mater.*, 2005, **17**(17), 2119–2123.

109 F. Wang, D. K. Chatterjee, Z. Q. Li, Y. Zhang, X. P. Fan and M. Q. Wang, Synthesis of polyethylenimine/NaYF<sub>4</sub> nanoparticles with upconversion fluorescence, *Nanotechnology*, 2006, **17**(23), 5786–5791.

110 M. Kumar and P. Zhang, Highly sensitive and selective label-free optical detection of mercuric ions using photon upconverting nanoparticles, *Biosens. Bioelectron.*, 2010, **25**(11), 2431–2435.

111 L. Y. Wang, Y. Zhang and Y. Y. Zhu, One-Pot Synthesis and Strong Near-Infrared Upconversion Luminescence of Poly(acrylic acid)-Functionalized YF<sub>3</sub>:Yb<sup>3+</sup>/Er<sup>3+</sup> Nanocrystals, *Nano Res.*, 2010, **3**(5), 317–325.

112 X. F. Yu, M. Li, M. Y. Xie, L. D. Chen, Y. Li and Q. Q. Wang, Dopant-Controlled Synthesis of Water-Soluble Hexagonal NaYF<sub>4</sub> Nanorods with Efficient Upconversion Fluorescence for Multicolor Bioimaging, *Nano Res.*, 2010, **3**(1), 51–60.

113 Y. Wang, L. Ji, B. B. Zhang, P. H. Yin, Y. Y. Qiu, D. Q. Song, J. Y. Zhou and Q. Li, Upconverting rare-earth nanoparticles with a paramagnetic lanthanide complex shell for upconversion fluorescent and magnetic resonance dual-modality imaging, *Nanotechnology*, 2013, **24**, 175101.

114 C. Brunot, L. Ponsonnet, C. Lagneau, P. Farge, C. Picart and B. Grosgogeat, Cytotoxicity of polyethyleneimine (PEI), precursor base layer of polyelectrolyte multilayer films, *Biomaterials*, 2007, **28**(4), 632–640.

115 Q. B. Zhang, K. Song, J. W. Zhao, X. G. Kong, Y. J. Sun, X. M. Liu, Y. L. Zhang, Q. H. Zeng and H. Zhang, Hexanedioic acid mediated surface-ligand-exchange process for transferring NaYF<sub>4</sub>:Yb/Er(or Yb/Tm) up-converting nanoparticles from hydrophobic to hydrophilic, *J. Colloid Interface Sci.*, 2009, **336**(1), 171–175.

116 N. Bogdan, F. Vetrone, G. A. Ozin and J. A. Capobianco, Synthesis of Ligand-Free Colloidally Stable Water Dispersible Brightly Luminescent Lanthanide-Doped Upconverting Nanoparticles, *Nano Lett.*, 2011, **11**(2), 835–840.

117 J. Zhou, M. X. Yu, Y. Sun, X. Z. Zhang, X. J. Zhu, Z. H. Wu, D. M. Wu and F. Y. Li, Fluorine-18-labeled Gd<sup>3+</sup>/Yb<sup>3+</sup>/Er<sup>3+</sup> co-doped NaYF<sub>4</sub> nanophosphors for multimodality PET/MR/UCL imaging, *Biomaterials*, 2011, **32**(4), 1148–1156.

118 T. Y. Cao, T. S. Yang, Y. Gao, Y. Yang, H. Hu and F. Y. Li, Water-soluble NaYF<sub>4</sub>:Yb/Erupconversion nanophosphors: Synthesis, characteristics and application in bioimaging, *Inorg. Chem. Commun.*, 2010, **13**(3), 392–394.

119 Q. Liu, Y. Sun, T. S. Yang, W. Feng, C. G. Li and F. Y. Li, Sub-10 nm Hexagonal Lanthanide-Doped NaLuF<sub>4</sub> Upconversion Nanocrystals for Sensitive Bioimaging in Vivo, *J. Am. Chem. Soc.*, 2011, **133**(43), 17122–17125.

120 Y. Bao, Q. A. N. Luu, C. K. Lin, J. M. Schloss, P. S. May and C. Y. Jiang, Layer-by-layer assembly of freestanding thin films with homogeneously distributed upconversion nanocrystals, *J. Mater. Chem.*, 2010, **20**(38), 8356–8361.

121 J. Shen, L. D. Sun, Y. W. Zhang and C. H. Yan, Superparamagnetic and upconversion emitting Fe<sub>3</sub>O<sub>4</sub>/NaYF<sub>4</sub>:Yb,Er hetero-nanoparticles *via* a crosslinker anchoring strategy, *Chem. Commun.*, 2010, **46**(31), 5731–5733.

122 Q. Liu, Y. Sun, C. G. Li, J. Zhou, C. Y. Li, T. S. Yang, X. Z. Zhang, T. Yi, D. M. Wu and F. Y. Li, F-18-Labeled Magnetic-Upconversion Nanophosphors *via* Rare-Earth Cation-Assisted Ligand Assembly, *ACS Nano*, 2011, **5**(4), 3146–3157.

123 B. A. Dong, S. Xu, J. A. Sun, S. Bi, D. Li, X. Bai, Y. Wang, L. P. Wang and H. W. Song, Multifunctional NaYF<sub>4</sub>:Yb<sup>3+</sup>,Er<sup>3+</sup>@Agcore/shell nanocomposites: integration of upconversion imaging and photothermal therapy, *J. Mater. Chem.*, 2011, **21**(17), 6193–6200.

124 L. Q. Xiong, T. S. Yang, Y. Yang, C. J. Xu and F. Y. Li, Long-term *in vivo* biodistribution imaging and toxicity of polyacrylic acid-coated upconversion nanophosphors, *Biomaterials*, 2010, **31**(27), 7078–7085.

125 H. Zhang, Y. J. Li, I. A. Ivanov, Y. Q. Qu, Y. Huang and X. F. Duan, Plasmonic Modulation of the Upconversion Fluorescence in NaYF<sub>4</sub>:Yb/Tm Hexaplate Nanocrystals

Using Gold Nanoparticles or Nanoshells, *Angew. Chem., Int. Ed.*, 2010, **49**(16), 2865–2868.

126 C. Vinegoni, D. Razansky, S. A. Hilderbrand, F. W. Shao, V. Ntziachristos and R. Weissleder, Transillumination fluorescence imaging in mice using biocompatible upconverting nanoparticles, *Opt. Lett.*, 2009, **34**(17), 2566–2568.

127 Y. S. Liu, D. T. Tu, H. M. Zhu, R. F. Li, W. Q. Luo and X. Y. Chen, A Strategy to Achieve Efficient Dual-Mode Luminescence of  $\text{Eu}^{3+}$  in Lanthanides Doped Multifunctional  $\text{NaGdF}_4$  Nanocrystals, *Adv. Mater.*, 2010, **22**(30), 3266–3271.

128 S. A. Hilderbrand, F. W. Shao, C. Salthouse, U. Mahmood and R. Weissleder, Upconverting luminescent nanomaterials: application to in vivo bioimaging, *Chem. Commun.*, 2009, (28), 4188–4190.

129 S. J. Budijono, J. N. Shan, N. Yao, Y. Miura, T. Hoye, R. H. Austin, Y. G. Ju and R. K. Prud'homme, Synthesis of Stable Block-Copolymer-Protected  $\text{NaYF}_4:\text{Yb}^{3+},\text{Er}^{3+}$  Up-Converting Phosphor Nanoparticles, *Chem. Mater.*, 2010, **22**(2), 311–318.

130 G. S. Yi and G. M. Chow, Synthesis of hexagonal-phase  $\text{NaYF}_4:\text{Yb},\text{Er}$  and  $\text{NaYF}_4:\text{Yb},\text{Tm}$  nanocrystals with efficient up-conversion fluorescence, *Adv. Funct. Mater.*, 2006, **16**(18), 2324–2329.

131 T. V. Esipova, X. C. Ye, J. E. Collins, S. Sakadzic, E. T. Mandeville, C. B. Murray and S. A. Vinogradov, Dendritic upconverting nanoparticles enable in vivo multiphoton microscopy with low-power continuous wave sources, *Proc. Natl. Acad. Sci. U. S. A.*, 2012, **109**(51), 20826–20831.

132 J. M. Harris and R. B. Chess, Effect of pegylation on pharmaceuticals, *Nat. Rev. Drug Discovery*, 2003, **2**(3), 214–221.

133 J. Lee, J. Kim, E. Park, S. Jo and R. Song, PEG-ylated cationic  $\text{CdSe}/\text{ZnS}$  QDs as an efficient intracellular labeling agent, *Phys. Chem. Chem. Phys.*, 2008, **10**(13), 1739–1742.

134 E. L. Bentzen, I. D. Tomlinson, J. Mason, P. Gresch, M. R. Warnement, D. Wright, E. Sanders-Bush, R. Blakely and S. J. Rosenthal, Surface modification to reduce non-specific binding of quantum dots in live cell assays, *Bioconjugate Chem.*, 2005, **16**(6), 1488–1494.

135 A. G. Dong, X. C. Ye, J. Chen, Y. J. Kang, T. Gordon, J. M. Kikkawa and C. B. Murray, A Generalized Ligand-Exchange Strategy Enabling Sequential Surface Functionalization of Colloidal Nanocrystals, *J. Am. Chem. Soc.*, 2011, **133**(4), 998–1006.

136 H. P. Zhou, C. H. Xu, W. Sun and C. H. Yan, Clean and Flexible Modification Strategy for Carboxyl/Aldehyde-Functionalized Upconversion Nanoparticles and Their Optical Applications, *Adv. Funct. Mater.*, 2009, **19**(24), 3892–3900.

137 C. Luccardini, C. Tribet, F. Vial, V. Marchi-Artzner and M. Dahan, Size, charge, and interactions with giant lipid vesicles of quantum dots coated with an amphiphilic macromolecule, *Langmuir*, 2006, **22**(5), 2304–2310.

138 L. A. Cheng, K. Yang, M. W. Shao, S. T. Lee and Z. A. Liu, Multicolor In Vivo Imaging of Upconversion Nanoparticles with Emissions Tuned by Luminescence Resonance Energy Transfer, *J. Phys. Chem. C*, 2011, **115**(6), 2686–2692.

139 Z. N. Wu, C. R. Guo, S. Liang, H. Zhang, L. P. Wang, H. C. Sun and B. Yang, A pluronic F127 coating strategy to produce stable up-conversion  $\text{NaYF}_4:\text{Yb},\text{Er}(\text{Tm})$  nanoparticles in culture media for bioimaging, *J. Mater. Chem.*, 2012, **22**(35), 18596–18602.

140 B. Ungun, R. K. Prud'homme, S. J. Budijono, J. N. Shan, S. F. Lim, Y. G. Ju and R. Austin, Nanofabricated upconversion nanoparticles for photodynamic therapy, *Opt. Express*, 2009, **17**(1), 80–86.

141 H. Shen, S. Y. Hong, R. K. Prud'homme and Y. Liu, Self-assembling process of flash nanoprecipitation in a multi-inlet vortex mixer to produce drug-loaded polymeric nanoparticles, *J. Nanopart. Res.*, 2011, **13**(9), 4109–4120.

142 Z. X. Zhu, K. Margulis-Goshen, S. Magdassi, Y. Talmon and C. W. Macosko, Polyelectrolyte Stabilized Drug Nanoparticles via Flash Nanoprecipitation: A Model Study With  $\beta$ -Carotene, *J. Pharm. Sci.*, 2010, **99**(10), 4295–4306.

143 K. M. Pustulka, A. R. Wohl, H. S. Lee, A. R. Michel, J. Han, T. R. Hoye, A. V. McCormick, J. Panyam and C. W. Macosko, Flash Nanoprecipitation: Particle Structure and Stability, *Mol. Pharmaceutics*, 2013, **10**(11), 4367–4377.

144 K. W. Ferrara, M. A. Borden and H. Zhang, Lipid-Shelled Vehicles: Engineering for Ultrasound Molecular Imaging and Drug Delivery, *Acc. Chem. Res.*, 2009, **42**(7), 881–892.

145 A. Wagner, M. Platzgummer, G. Kreismayr, H. Quendler, G. Stiegler, B. Ferko, G. Vecera, K. Vorauer-Uhl and H. K. Prof, GMP production of liposomes – A new industrial approach, *J. Liposome Res.*, 2006, **16**(3), 311–319.

146 G. Decher, Fuzzy nanoassemblies: toward layered polymeric multicomposites, *Science*, 1997, **277**(5330), 1232–1237.

147 Z. Q. Li, Y. Zhang, B. Shuter and N. M. Idris, Hybrid Lanthanide Nanoparticles with Paramagnetic Shell Coated on Upconversion Fluorescent Nanocrystals, *Langmuir*, 2009, **25**(20), 12015–12018.

148 J. N. Shan and Y. G. Ju, Controlled synthesis of lanthanide-doped  $\text{NaYF}_4$  upconversion nanocrystals via ligand induced crystal phase transition and silica coating, *Appl. Phys. Lett.*, 2007, **91**, 123103.

149 T. Nann and P. Mulvaney, Single quantum dots in spherical silica particles, *Angew. Chem., Int. Ed.*, 2004, **43**(40), 5393–5396.

150 Z. Y. Lu, J. Dai, X. N. Song, G. Wang and W. S. Yang, Facile synthesis of  $\text{Fe}_3\text{O}_4/\text{SiO}_2$  composite nanoparticles from primary silica particles, *Colloids Surf., A*, 2008, **317**(1–3), 450–456.

151 A. L. Morel, S. I. Nikitenko, K. Gionnet, A. Wattiaux, J. Lai-Kee-Him, C. Labrugere, B. Chevalier, G. Deleris, C. Petibois, A. Brisson and M. Simonoff, Sonochemical approach to the synthesis of  $\text{Fe}_3\text{O}_4@\text{SiO}_2$  core-shell nanoparticles with tunable properties, *ACS Nano*, 2008, **2**(5), 847–856.

152 S. Wilhelm, T. Hirsch, W. M. Patterson, E. Scheucher, T. Mayr and O. S. Wolfbeis, Multicolor Upconversion Nanoparticles for Protein Conjugation, *Theranostics*, 2013, **3**(4), 239–248.

153 Z. Y. Hou, C. X. Li, P. A. Ma, G. G. Li, Z. Y. Cheng, C. Peng, D. M. Yang, P. P. Yang and J. Lin, Electrospinning Preparation and Drug-Delivery Properties of an Up-conversion Luminescent Porous  $\text{NaYF}_4:\text{Yb}^{3+},\text{Er}^{3+}$ @Silica Fiber Nanocomposite, *Adv. Funct. Mater.*, 2011, **21**(12), 2356–2365.

154 S. L. Gai, P. P. Yang, C. X. Li, W. X. Wang, Y. L. Dai, N. Niu and J. Lin, Synthesis of Magnetic, Up-Conversion Luminescent, and Mesoporous Core-Shell-Structured Nanocomposites as Drug Carriers, *Adv. Funct. Mater.*, 2010, **20**(7), 1166–1172.

155 W. Stöber, A. Fink and E. Bohn, Controlled Growth of Monodisperse Silica Spheres in Micron Size Range, *J. Colloid Interface Sci.*, 1968, **26**(1), 62–69.

156 C. Graf, D. L. J. Vossen, A. Imhof and A. van Blaaderen, A general method to coat colloidal particles with silica, *Langmuir*, 2003, **19**(17), 6693–6700.

157 M. Darbandi and T. Nann, One-pot synthesis of  $\text{YF}_3$ @silica core/shell nanoparticles, *Chem. Commun.*, 2006(7), 776–778.

158 P. Zhang, W. Steelant, M. Kumar and M. Scholfield, Versatile photosensitizers for photodynamic therapy at infrared excitation, *J. Am. Chem. Soc.*, 2007, **129**(15), 4526–4527.

159 Z. L. Lei, X. L. Pang, N. Li, L. Lin and Y. L. Li, A novel two-step modifying process for preparation of chitosan-coated  $\text{Fe}_3\text{O}_4/\text{SiO}_2$  microspheres, *J. Mater. Process. Technol.*, 2009, **209**(7), 3218–3225.

160 H. C. Lu, G. S. Yi, S. Y. Zhao, D. P. Chen, L. H. Guo and J. Cheng, Synthesis and characterization of multi-functional nanoparticles possessing magnetic, up-conversion fluorescence and bio-affinity properties, *J. Mater. Chem.*, 2004, **14**(8), 1336–1341.

161 R. P. Bagwe, L. R. Hilliard and W. H. Tan, Surface modification of silica nanoparticles to reduce aggregation and nonspecific binding, *Langmuir*, 2006, **22**(9), 4357–4362.

162 M. Kobayashi, F. Juillerat, P. Galletto, P. Bowen and M. Borkovec, Aggregation and charging of colloidal silica particles: effect of particle size, *Langmuir*, 2005, **21**(13), 5761–5769.

163 M. Wang, C. C. Mi, Y. X. Zhang, J. L. Liu, F. Li, C. B. Mao and S. K. Xu, NIR-Responsive Silica-Coated  $\text{NaYbF}_4:\text{Er}/\text{Tm}/\text{Ho}$  Upconversion Fluorescent Nanoparticles with Tunable Emission Colors and Their Applications in Immunolabeling and Fluorescent Imaging of Cancer Cells, *J. Phys. Chem. C*, 2009, **113**(44), 19021–19027.

164 S. Nagarajan, Z. Q. Li, V. Marchi-Artzner, F. Grasset and Y. Zhang, Imaging gap junctions with silica-coated upconversion nanoparticles, *Med. Biol. Eng. Comput.*, 2010, **48**(10), 1033–1041.

165 J. Hampl, M. Hall, N. A. Mufti, Y. M. M. Yao, D. B. MacQueen, W. H. Wright and D. E. Cooper, Upconverting phosphor reporters in immunochromatographic assays, *Anal. Biochem.*, 2001, **288**(2), 176–187.

166 S. Jiang and Y. Zhang, Upconversion Nanoparticle-Based FRET System for Study of siRNA in Live Cells, *Langmuir*, 2010, **26**(9), 6689–6694.

167 C. C. Mi, J. P. Zhang, H. Y. Gao, X. L. Wu, M. Wang, Y. F. Wu, Y. Q. Di, Z. R. Xu, C. B. Mao and S. K. Xu, Multifunctional nanocomposites of superparamagnetic ( $\text{Fe}_3\text{O}_4$ ) and NIR-responsive rare earth-doped up-conversion fluorescent ( $\text{NaYF}_4:\text{Yb},\text{Er}$ ) nanoparticles and their applications in biolabeling and fluorescent imaging of cancer cells, *Nanoscale*, 2010, **2**(7), 1141–1148.

168 F. van de Rijke, H. Zijlmans, S. Li, T. Vail, A. K. Raap, R. S. Niedbala and H. J. Tanke, Up-converting phosphor reporters for nucleic acid microarrays, *Nat. Biotechnol.*, 2001, **19**(3), 273–276.

169 R. S. Niedbala, H. Feindt, K. Kardos, T. Vail, J. Burton, B. Bielska, S. Li, D. Milunic, P. Bourdelle and R. Vallejo, Detection of analytes by immunoassay using up-converting phosphor technology, *Anal. Biochem.*, 2001, **293**(1), 22–30.

170 P. Y. Yuan, Y. H. Lee, M. K. Gnanasammandhan, Z. P. Guan, Y. Zhang and Q. H. Xu, Plasmon enhanced upconversion luminescence of  $\text{NaYF}_4:\text{Yb},\text{Er}$ @ $\text{SiO}_2$ @Ag core-shell nanocomposites for cell imaging, *Nanoscale*, 2012, **4**(16), 5132–5137.

171 Y. M. Yang, Q. Shao, R. R. Deng, C. Wang, X. Teng, K. Cheng, Z. Cheng, L. Huang, Z. Liu, X. G. Liu and B. G. Xing, In Vitro and In Vivo Uncaging and Bioluminescence Imaging by Using Photocaged Upconversion Nanoparticles, *Angew. Chem., Int. Ed.*, 2012, **51**(13), 3125–3129.

172 E. M. Sletten and C. R. Bertozzi, From Mechanism to Mouse: A Tale of Two Bioorthogonal Reactions, *Acc. Chem. Res.*, 2011, **44**(9), 666–676.

173 H. C. Kolb, M. G. Finn and K. B. Sharpless, Click chemistry: diverse chemical function from a few good reactions, *Angew. Chem., Int. Ed.*, 2001, **40**(11), 2004–2021.

174 E. M. Sletten and C. R. Bertozzi, Bioorthogonal Chemistry: Fishing for Selectivity in a Sea of Functionality, *Angew. Chem., Int. Ed.*, 2009, **48**(38), 6974–6998.

175 J. R. Acharya, H. T. Zhang, X. Li and E. E. Nesterov, Chemically Controlled Amplified Ratiometric Fluorescence in Surface-Immobilized End-Capped Oligo(p-phenylene ethynylene)s, *J. Am. Chem. Soc.*, 2009, **131**(3), 880–881.

176 K. M. L. Taylor, J. S. Kim, W. J. Rieter, H. An, W. L. Lin and W. B. Lin, Mesoporous silica nanospheres as highly efficient MRI contrast agents, *J. Am. Chem. Soc.*, 2008, **130**(7), 2154–2155.

177 A. Hlavacek, A. Sedlmeier, P. Skladal and H. H. Gorris, Electrophoretic characterization and purification of silica-coated photon-upconverting nanoparticles and their bioconjugates, *ACS Appl. Mater. Interfaces*, 2014, **6**(9), 6930–6935.

178 L. L. Li, P. W. Wu, K. Hwang and Y. Lu, An Exceptionally Simple Strategy for DNA-Functionalized Up-Conversion Nanoparticles as Biocompatible Agents for Nanoassembly, DNA Delivery, and Imaging, *J. Am. Chem. Soc.*, 2013, **135**(7), 2411–2414.

179 H. H. Gorris, S. Bade, N. Rockendorf, M. Franek and A. Frey, Pushing Antibody-Based Labeling Systems to Higher Sensitivity by Linker-Assisted Affinity Enhancement, *Bioconjugate Chem.*, 2011, **22**(8), 1619–1624.

180 N. Liu, W. P. Qin, G. S. Qin, T. Jiang and D. Zhao, Highly plasmon-enhanced upconversion emissions from  $\text{Au}$ @ $\beta$ - $\text{NaYF}_4:\text{Yb},\text{Tm}$  hybrid nanostructures, *Chem. Commun.*, 2011, **47**(27), 7671–7673.

181 S. Schietinger, T. Aichele, H. Q. Wang, T. Nann and O. Benson, Plasmon-Enhanced Upconversion in Single  $\text{NaYF}_4:\text{Yb}^{3+}/\text{Er}^{3+}$  Codoped Nanocrystals, *Nano Lett.*, 2010, **10**(1), 134–138.

182 R. J. Meier, J. M. B. Simbürger, T. Soukka and M. Schäferling, Background-Free Referenced Luminescence Sensing and Imaging of pH Using Upconverting Phosphors and Color Camera Read-out, *Anal. Chem.*, 2014, **86**(11), 5535–5540.

183 L. N. Sun, H. S. Peng, M. I. J. Stich, D. Achatz and O. S. Wolfbeis, pH sensor based on upconverting luminescent lanthanide nanorods, *Chem. Commun.*, 2009, (33), 5000–5002.

184 R. Ali, S. M. Saleh, R. J. Meier, H. A. Azab, I. I. Abdelgawad and O. S. Wolfbeis, Upconverting nanoparticle based optical sensor for carbon dioxide, *Sens. Actuators, B*, 2010, **150**(1), 126–131.

185 H. S. Mader and O. S. Wolfbeis, Optical Ammonia Sensor Based on Upconverting Luminescent Nanoparticles, *Anal. Chem.*, 2010, **82**(12), 5002–5004.

186 D. E. Achatz, R. J. Meier, L. H. Fischer and O. S. Wolfbeis, Luminescent Sensing of Oxygen Using a Quenchable Probe and Upconverting Nanoparticles, *Angew. Chem., Int. Ed.*, 2011, **50**(1), 260–263.

187 J. C. Boyer, C. J. Carling, S. Y. Chua, D. Wilson, B. Johnsen, D. Baillie and N. R. Branda, Photomodulation of Fluorescent Upconverting Nanoparticle Markers in Live Organisms by Using Molecular Switches, *Chem. – Eur. J.*, 2012, **18**(11), 3122–3126.

188 S. M. Saleh, R. Ali and O. S. Wolfbeis, Quenching of the Luminescence of Upconverting Luminescent Nanoparticles by Heavy Metal Ions, *Chem. – Eur. J.*, 2011, **17**(51), 14611–14617.

189 R. Gomes, A. Hassinen, A. Szczygiel, Q. A. Zhao, A. Vantomme, J. C. Martins and Z. Hens, Binding of Phosphonic Acids to CdSe Quantum Dots: A Solution NMR Study, *J. Phys. Chem. Lett.*, 2011, **2**(3), 145–152.

190 B. Fritzinger, I. Moreels, P. Lommens, R. Koole, Z. Hens and J. C. Martins, In Situ Observation of Rapid Ligand Exchange in Colloidal Nanocrystal Suspensions Using Transfer NOE Nuclear Magnetic Resonance Spectroscopy, *J. Am. Chem. Soc.*, 2009, **131**(8), 3024–3032.

191 I. Moreels, B. Fritzinger, J. C. Martins and Z. Hens, Surface Chemistry of Colloidal PbSe Nanocrystals, *J. Am. Chem. Soc.*, 2008, **130**(45), 15081–15086.

192 K. A. Abel, J. C. Boyer and F. C. J. M. van Veggel, Hard Proof of the  $\text{NaYF}_4/\text{NaGdF}_4$  Nanocrystal Core/Shell Structure, *J. Am. Chem. Soc.*, 2009, **131**(41), 14644–14645.

